

Modeling, Simulation, and Design of Hybrid EV-Battery Charger for Optimum Grid Utilization

by

Laith Alkhawaldeh

A Thesis

Submitted to the School of Graduate and Postdoctoral Studies

in Partial Fulfillment of the Requirements

for the Degree of

Master of Applied Science

in

Electrical, Computer, and Software Engineering

Faculty of Engineering and Applied Science

University of Ontario Institute of Technology (Ontario Tech University)

Oshawa, Ontario, Canada

December 2020

© Laith Alkhawaldeh, 2020

THESIS EXAMINATION INFORMATION

Submitted by: **Laith Alkhawaldeh**

MASc in Electrical, Computer, and Software Engineering Program

Thesis title: Modeling, Simulation, and Design of Hybrid EV-Battery Charger for Optimum Grid Utilization

An oral defense of this thesis took place on December 09, 2020 in front of the following examining committee:

Examining Committee:

Chair of Examining Committee	Dr. Ying Wang
Research Supervisor	Dr. Mohamed Youssef
Examining Committee Member	Dr. Jing Ren
Thesis Examiner	Dr. Moustafa El-Gindy

The above committee determined that the thesis is acceptable in form and content and that a satisfactory knowledge of the field covered by the thesis was demonstrated by the candidate during an oral examination. A signed copy of the Certificate of Approval is available from the School of Graduate and Postdoctoral Studies.

ABSTRACT

The rapid recent development of electric vehicles (EVs) charging system, is changing the future of the transportation sector. Thanks to Photovoltaics solar energy (PV), the EV charging operating cost is reduced, and an environmentally friendly EV is promoted to the public. In this thesis, an EV-PV-Grid charging system is modelled and simulated under PSIM software while considering and detailing the necessary control for each part in the system concerned to manage the energy coming from two different sources. The PSIM simulation and proof of concept prototype results of the developed model illustrate the performance of the realized model while indicating the battery charging state as well as the power flow between the grid, battery and PV for different irradiation.

Keywords: Electric Vehicles; Energy; Solar Energy; Bidirectional Charger; Modeling, Energy storage, Electric vehicle, Power electronics, Energy management systems, Electric vehicles charging, Solar energy, Photovoltaic system, Distributed energy resources.

AUTHOR'S DECLARATION

I hereby declare that this thesis consists of original work of which I have authored. This is a true copy of the thesis, including any required final revisions, as accepted by my examiners.

I authorize the University of Ontario institute of Technology (Ontario Tech University)

to lend this thesis to other institutions or individuals for the purpose of scholarly research. I

further authorize University of Ontario institute of Technology (Ontario Tech University)

to reproduce this thesis by photocopying or by other means, in total or in part, at the request of other institutions or individuals for the purpose of scholarly research. I understand that my thesis will be made electronically available to the public.

Laith Alkhawaldeh

STATEMENT OF CONTRIBUTIONS

I hereby certify that I am the sole author of this thesis and that no part of this thesis has been published or submitted for publication. I have used standard referencing practices to acknowledge ideas, research techniques, or other materials that belong to others. Furthermore, I hereby certify that I am the sole source of the creative works and/or inventive knowledge described in this thesis.

ACKNOWLEDGEMENTS

It is with great honor that I would like to express my sincere thanks and to express my great gratitude to all those who have contributed directly or indirectly to the success of this research.

It is a pleasure for me to thank my supervisor:

Dr. Mohamed Youssef

For his encouragement and valuable advice during the Thesis period.

The support of my family is beyond words. I owe my life to my family, parents, and siblings.

Also, I am grateful for all my friends who supported the success of this thesis.

Finally, I would like to express my gratitude to the University of Ontario institute of Technology (Ontario Tech University) for the proper study environment that it provides

TABLE OF CONTANTS

Thesis Examination Information	ii
Abstract.....	iii
Author's Declaration	iv
Acknowledgements	vi
List of Tables	ix
List of Figures.....	x
List of Abbreviations and Symbols	xiii
Chapter 1. Introduction.....	1
1.1 Background and Motivation	1
1.2 Scope of the Thesis	2
1.3 Objectives of the Thesis	2
Chapter 2. Literature Review	3
2.1 Introduction	3
2.2 Solar photovoltaic system	3
2.2.1 History.....	3
2.2.2 Operating	4
2.2.3 Types of photovoltaic systems.....	5
2.2.4 Solar Panel Control MPPT	8
2.3 Electrical Vehicle Charged from PV and Grid	13
2.3.1 Sustainability and Economics	13
2.3.2 System Architecture for the EV-PV-Grid System	13
2.3.3 Comparison of system architecture:	17
2.3.4 EV-PV-Grid Power Flows	18
2.4 EV-PV-Grid Power Converter Topology.....	19
2.4.1 DC/DC conversion	20
2.4.2 DC/AC and AC/DC Conversion	23
Chapter 3. EV-PV Charging System Design	30
3.1 Introduction	30
3.2 EV-PV charging system structure under PSIM software	30
3.2.1 Model and Characteristics of EV Battery	31
3.2.2 Photovoltaic panel	33

3.2.3	Structure of DC/DC Boost Converter	34
3.2.4	Maximum Power Point Tracking Command	38
3.3	EV-PV Charging System Results	41
3.3.1	Case 1: Irradiation Equal to 1000 W/ m ²	41
3.3.2	Case 2: Irradiation equal to 700 W/ m ²	44
3.4	Conclusion	47
Chapter 4.	EV-PV-Grid Charging System Design	48
4.1	Introduction:	48
4.2	EV-PV-Grid charging system structure in PSIM software:	48
4.2.1	Simulation condition:	52
4.2.2	Battery charging method:	53
4.2.3	Energy management:	53
4.2.4	Dc link topology:	54
4.2.5	Grid converter side:	55
4.2.6	Battery converter side:	61
4.3	EV-PV-Grid charging system simulation results under PSIM software:	65
4.3.1	Case 1: Constant Irradiation 1000 W/m ²	65
4.3.2	Case 2: variable radiation:	74
4.3.3	Case 3: The Effect of Sudden Change of Grid voltage on the charger controller stability	80
4.4	Conclusion	81
Chapter 5.	The Experimental Test	82
5.1	The Experimental Setup	82
5.2	Experimental Results	84
Chapter 6.	Conclusions	87
6.1	General Conclusion	87
6.2	Research contributions	88
6.3	Future Work	88
REFERENCES.	89
Appendices	92
Appendices A:	Characteristics of the solar panel in PSIM software	92
Appendices B:	Characteristics of Lithium-ion battery	93
Appendices C:	Characteristics of 3-phase resistor-inductor branch filter	93

LIST OF TABLES

Table 2. 1: Table of comparison between the different architecture of the EV-PV-Grid system [13].	18
Table 3. 1: Table explaining the parameters of Li-ion battery in PSIM software [32].	32
Table 3. 2: Table explaining the parameters of the solar panel (physical model) in PSIM software [33].	34
Table 3. 3: Table explaining the parameters of the MOSFET used in the EV-PV system [34].	36
Table 3. 4: Table explaining the parameters of the capacitor used in the EV-PV system [34].	37
Table 3. 5: Table explaining the parameters of the inductor used in the EV-PV system [34].	37
Table 3. 6: Table explaining the parameters of the diode used in the EV-PV system [34].	38
Table 3. 7: Table translating the effects of changing the perturbation value on the system time stability and the extracted power ripples	40
Table 3. 8: Table explaining the different components of the MPPT system in PSIM Software [34].	40
Table 4. 1: Table explaining the simulation parameters in PSIM software.	51
Table 4. 2: Table explaining the parameters of a three-phase y-connected sinusoidal voltage source in PSIM software [34].	52
Table 4. 3: Table explaining the different control employed for the inverter.	60
Table 4. 4: The effect of the PI gain on the overshoot and time rise in DC-link controller	60
Table 4. 5: The effect of the PI time constant on the overshoot and time rise in DC-link controller	61
Table 4. 6: The effect of the PI gain on the overshoot and time rise in I_q and I_d controller	61
Table 4. 7: The effect of the PI time constant on the overshoot and time rise in I_q and I_d controller	61
Table 4. 8: Output Current and voltage PI controllers	64
Table 4. 9: The specification of each component in the experimental setup	83

LIST OF FIGURES

CHAPTER 2

Fig 2. 1: Operating of photovoltaic cells [4].	5
Fig 2. 2: Diagram block of Grid-connected PV system [15].	6
Fig 2. 3: Diagram block of a standalone system [15].	7
Fig 2. 4: Diagram block of the hybrid system [15].	8
Fig 2. 5: Power- voltage curve of the solar panel for different temperatures [19].	9
Fig 2. 6: Power-voltage curve of the solar panel for different irradiation [19].	9
Fig 2. 7: Flow chart of perturb and observe algorithm [6].	10
Fig 2. 8: Flow chart of the incremental conductance algorithm [6].	12
Fig 2. 9: Grid-PV-EV system interlinked on AC interconnection [13].	14
Fig 2. 10: Grid-PV-EV system interlinked on DC interconnection [13].	15
Fig 2. 11: MPC for PV and EV interlinked with the Grid on AC interconnection [13].	15
Fig 2. 12: Architecture of a multi-port-converter with AC interconnection [13].	16
Fig 2. 13: MPC for PV and EV interlinked with the Grid on DC interconnection [13].	16
Fig 2. 14: Architecture of multi-port-converter with DC interconnection [13].	17
Fig 2. 15: Figure translating the different modes of power flow [13].	19
Fig 2. 16: State of the switch for DC/DC converter [23].	20
Fig 2. 17: Electric circuit of boost converter [23].	21
Fig 2. 18: Electric circuit of the accumulation phase [9].	21
Fig 2. 19: Electric circuit of the restitution phase [9].	22
Fig 2. 20: Electric circuit of buck converter [25].	22
Fig 2. 21: Electric circuit of a buck converter with switch OFF [25].	22
Fig 2. 22: Electric circuit of buck-boost converter [26].	23
Fig 2. 23: Power flow through AC/DC and DC/AC converter [26].	24
Fig 2. 24: Electric circuit of an uncontrolled bridge rectifier [27].	25
Fig 2. 25: Electric circuit of an uncontrolled three-phase bridge rectifier [27].	25
Fig 2. 26: Electric circuit of phase-controlled single-phase rectifier [27].	26
Fig 2. 27: Electric circuit of phase-controlled three-phase rectifier [27].	26
Fig 2. 28: Electric circuit of PWM-controlled single-phase bridge rectifier [28].	27
Fig 2. 29: Electric circuit of PWM-controlled three-phase bridge rectifier [28].	27
Fig 2. 30: Electric circuit of a three-phase voltage source inverter [30].	28
Fig 2. 31: Electric circuit of a single-phase voltage source inverter [30].	29

CHAPTER 3

Fig 3. 1:Block diagram of EV-PV charging system	30
Fig 3. 2: Electric circuit of EV-PV system in PSIM software	31
Fig 3. 3: Model of Li-ion battery in PSIM software [32].	32
Fig 3. 4: Voltage-Capacity curve of Li-ion battery [32].	33
Fig 3. 5: Model of the photovoltaic panel in PSIM Software [33].	33

Fig 3. 6: Electric circuit of DC/DC boost converter connected to a solar panel in PSIM software	35
Fig 3. 7: Electric circuit of perturb and observe algorithm in PSIM software.....	39
Fig 3. 8: Battery state of charge, current and voltage curves during the charging period in a PV-EV charging system for irradiation equal to 1000W/m^2	42
Fig 3. 9: The evolution of PV voltage, current, maximum power and extracted power during the charging period in a PV-EV charging system for irradiation equal to 1000W/m^2	43
Fig 3. 10: The evolution of the duty cycle in perturb and observe algorithm employed in a PV-EV charging system for irradiation equal to 1000W/m^2	43
Fig 3. 11: Duty cycle, triangular wave and MPPT command curves translating the operating of PWM in a PV-EV charging system	44
Fig 3. 12: Battery state of charge, current and voltage curves during the charging period in a PV-EV charging system for irradiation equal to 700W/m^2	45
Fig 3. 13: The evolution of PV voltage, current, maximum power and extracted power during the charging period in a PV-EV charging system for irradiation equal to 700W/m^2	46
Fig 3. 14: The evolution of the duty cycle in perturb and observe algorithm employed in a PV-EV charging system for irradiation equal to 700W/m^2	46

CHAPTER 4

Fig 4. 1: Block diagram of EV-PV-Grid system.....	49
Fig 4. 2: Power circuit of EV-PV-Grid system in PSIM software.....	49
Fig 4. 3: Control circuit of EV-PV-Grid system in PSIM software (Current controller) .	50
Fig 4. 4: Control circuit of EV-PV-Grid system in PSIM software (MPPT controller) ...	50
Fig 4. 5: Control circuit of EV-PV-Grid system in PSIM software (Constant Current/ Constant voltage controller.	51
Fig 4. 6: A three-phase y-connected sinusoidal voltage source in PSIM software [34]..	52
Fig 4. 7: Current-time and voltage-time curve during the charging method [39].....	53
Fig 4. 8: Electric circuit of the grid converter side with a current control.....	56
Fig 4. 9: Electric circuit of the current control.....	58
Fig 4. 10: abc/dq transformation block.....	58
Fig 4. 11: Electric circuit of battery converter side	62
Fig 4. 12: Electric circuit of the control employed in battery converter side	64
Fig 4. 13: Battery state of charge, current and voltage curves during the charging period in a PV-EV-Grid charging system for a constant irradiation	66
Fig 4. 14: Zoomed part of battery current in EV-PV-Grid system showing the ripple for a constant irradiation.....	67
Fig 4. 15: Zoomed part of the battery voltage in EV-PV-Grid system showing the ripple for a constant irradiation.....	67
Fig 4. 16: The evolution of PV current during the charging period in a PV-EV-Grid charging system for a constant irradiation	68
Fig 4. 17: The evolution of PV voltage during the charging period in a PV-EV-Grid charging system for a constant irradiation	68

Fig 4. 18: The evolution of the maximum power delivered by the PV and the extracted power during the charging period in a PV-EV-Grid charging system for a constant irradiation	69
Fig 4. 19: Duty cycle, triangular wave and MPPT command curves translating the operating of PWM in a PV-EV-Grid charging system.....	69
Fig 4. 20: Curve translating the inverter input current during the different state of charge in EV-PV-Grid charging system for a constant irradiation	70
Fig 4. 21: Waveforms translating the input inverter, output boost and input buck current in EV-PV-Grid system for a constant irradiation	71
Fig 4. 22: The inverter AC current waveforms in EV-PV-Grid charging system for a constant irradiation.....	72
Fig 4. 23: Zoomed in for the inverter three-phase AC current during a SOC less than 80% in EV-PV-Grid charging system with a constant irradiation.....	72
Fig 4. 24: Zoomed in for the inverter three-phase AC current during a SOC greater than 80% in EV-PV-Grid charging system with a constant irradiation	73
Fig 4. 25: Curve translating the voltage across the DC-link in a PV-EV-Grid system for a constant irradiation.....	73
Fig 4. 26: Curve translating the variable irradiation in EV-PV-Grid charging system	74
Fig 4. 27: Battery state of charge, current and voltage curves during the charging period in a PV-EV-Grid charging system for a variable irradiation	75
Fig 4. 28: The evolution of PV voltage and current during the charging period in a PV-EV-Grid charging system for a variable irradiation	76
Fig 4. 29: The evolution of the power delivered by the PV and the extracted power in an EV-PV-Grid charging system for a variable irradiation	76
Fig 4. 30: Curve translating the inverter input current during the different state of charge in EV-PV-Grid system for a variable irradiation.....	77
Fig 4. 31: Waveforms translating the input inverter, output boost and input buck current in EV-PV-Grid system for a variable irradiation.....	78
Fig 4. 32: The inverter AC three-phase current waveforms in an EV-PV-Grid charging system for a variable irradiation.....	79
Fig 4. 33: Curve translating the voltage across the DC-link in a PV-EV-Grid system for a variable irradiation	80
Fig 4. 35: Battery state of charge, current and voltage curves during the charging period in a PV-EV-Grid charging system for variable irradiation for Under/Overvoltage conditions	81
Fig 4. 36: Off-grid system simplified block diagram	83
Fig 4. 37: Hardware implementation of single-phase inverter.	85
Fig 4. 38: The transient and steady-state behavior of the output voltages of the simulated circuit	85
Fig 4. 39 Output of the implemented single-phase off-grid inverter on the oscilloscope.	86
Fig 4. 40 Gate signals for the inverter switches on the oscilloscope.	86

LIST OF ABBREVIATIONS AND SYMBOLS

<i>AC</i>	Alternating Current
<i>DC</i>	Direct Current
<i>EV</i>	Electric Vehicle
<i>PV</i>	Photovoltaic
<i>EIS</i>	Electrochemical Impedance Spectroscopy
<i>GHG</i>	Greenhouse Gas
<i>MPP</i>	Maximum Power-Point
<i>PWM</i>	Pulse-Width-Modulation
<i>IGBT</i>	Insulated Gate Bipolar Transistor
<i>MOSFET</i>	Metal Oxide Semiconductor Field Effect Transistor
<i>MPPT</i>	Maximum Power Point Tracking
Θ	Angle
<i>AVEQ</i>	Association of Electric Vehicles in Quebec
<i>IEEE</i>	Institute of Electrical and Electronics Engineers
<i>MPC</i>	Multi-Port-Converter
<i>GTO</i>	Gate Turn-off Thyristor
<i>BJT</i>	Bipolar Junction Transistor
<i>CSI</i>	Current-Source Inverter
<i>VSI</i>	Voltage-Source Inverter
<i>C</i>	Capacitor
<i>L</i>	Inductor
<i>D</i>	Duty Cycle
<i>V_{in}</i>	Input Voltage across the Dc/Dc converter
<i>V_{out}</i>	Output Voltage across the Dc/Dc converter
<i>R</i>	Equivalent Resistance of the load
Δi_L	The Inductor current ripple
Δv	The Capacitor voltage ripple

I	Current
V	Voltage
P	Real Power
$PSIM$	Power Sim Software
N_s	No. of cells in series
N_p	No. of cells in parallel
K_s	Voltage Derating Factor
K_p	Capacity Derating Factor
E_{rated}	Rated Voltage
E_{cut}	Discharge Cut-off Voltage
E_{full}	Full voltage
E_{top}	Exponential Point Voltage
E_{nom}	Nominal Voltage
Q_{rated}	Rated Capacity
Q_{max}	Maximum Capacity
Q_{top}	Exponential Point Capacity
Q_{nom}	Nominal capacity
Q_0	Capacity at 0V
SOC	State of Charge
S	Light Intensity
S_0	Standard Light Intensity
T	Ambient Temperature Input
T_{ref}	Reference Temperature under standard conditions
I_a, I_b, I_c	Fundamental Current Components
R_{sh}	Shunt Resistance
I_d, I_q	Field Oriented Current Components
V_d, V_q	Field Oriented Voltage Components

R_s	Series Resistance
V_{th}	Threshold Voltage
I_{s0}	Short Circuit Current
E_g	Band Energy
C_t	Temperature Coefficient
PI	Proportional Integral
LQR	Linear-Quadratic Regulator
T_s	Periodic Time
f	Frequency
P_{IN}	Input Power
V_{PV}	Photovoltaic voltage
I_{PV}	Photovoltaic Current
L_{B0}	Boost inductor
C_{B0}	Boost Capacitor
L_B	Buck Inductor
C_B	Buck capacitor
V_g	Grid line voltage
V_{DC}	Direct Current link voltage
C_{DC}	Direct Current link capacitor
P_{EV}	Battery rated power
V_{BA}	Battery rated voltage
I_{BA}	Battery rated current

Chapter 1. Introduction

The transportation sector is one of the largest contributors to Green House Gas (GHG) emission in the world with fourteen percent and the second-largest contributor to GHG emission in Canada with 23.36 percent in 2014[1]. But this sector is irreplaceable since it is an integral part of our daily lives.

The movement that vehicles allow is essential to the realization of many activities, therefore in recent years the use of cars has increased. Thus, carbon emission and noise pollution have increased, and petroleum is running out soon.

In order to preserve the climate and natural resources, electrical vehicles technology is considered as the future mode of transportation and presents an enormous opportunity to decrease GHG emissions. Because of fears regarding the capacity of electric power distribution networks and the diminution of petroleum to produce electricity, we can admit that electric vehicles are only sustainable if the electricity used to charge them comes from clean and green energy that will never run out and will never cause harm for nature.

1.1 Background and Motivation

The electrical vehicles charging system by the solar panel have taken a significant leap forward and many researchers have been done in this area [2]–[11].

One of the significant problems of electrical vehicles charging by the solar panel is that the solar panel cannot always satisfy the demand of the EV because of the change of radiation and temperature. That is why it becomes necessary to use the grid while minimizing the energy exchange and maximizing PV energy for EV charging.

In this research, A bi-directional Hybrid charging system is constructed with a smaller number of components to charge an EV battery with high-efficiency output power, a low voltage and current ripple in each stage of the charger and to achieve the optimum grid utilization.

1.2 Scope of the Thesis

The concentrate of this thesis is employing different energy sources (i.e. the PV plant) to get a suitable output power and to design a reliable controller to manage the charging process for the battery from each source of power.

1.3 Objectives of the Thesis

1. The goal of this thesis is to realize a simulation of an electric vehicle charging system from the solar panel and the grid using PSIM to obtain an optimum grid utilization.
2. Studying the effect of changing the Radiation on the PV plant and how is the response of the system controller during these changes to ensure the reliability of using this controller.
3. Simulating the change in the grid power (over/under voltage) and its effect on the stability of the charging process.

Chapter 2. Literature Review

2.1 Introduction

Electric vehicles have existed since the nineteenth century, but they have not been for everyday practice until today[12]. According to statistics from the association of electric vehicles in Quebec (AVEQ), the number of electric vehicles in Canada reached 101 116 on March 31, 2019.

Many stations have been developed to charge that vehicle's battery using PV panels and the grid.

This chapter introduces the solar photovoltaic system (its history, operating, types, control), the EV-PV-Grid charging system (sustainability, architecture and comparison, mode of power flow) and the EV-PV-Grid converters topologies (DC/DC converters, AC/DC converters)

2.2 Solar photovoltaic system

Solar photovoltaic (PV) systems have gained immense popularity over the last decade as a means of distributed generation. By the end of 2016, the total installed capacity in the world reached 300GW with a record 75GW installed in 2016 alone[13].

In this section, a brief reminder of the solar photovoltaic system is presented: history, operating, and different types.

2.2.1 History

In 1839, a French physicist named Edmund Becquerel observed the photovoltaic effect, a physical phenomenon responsible for converting light to electricity. Becquerel

noted a voltage appeared when one of two identical electrodes in a weak conducting solution was illuminated[12].

In the 1870s, the photovoltaic effect was studied in solids, such as selenium. Soon afterward, selenium photovoltaic cells were converting light to electricity at 1% to 2% efficiency[12].

In 1905, Albert Einstein brought a theoretical explanation of the photoelectric effect on a quantum basis[12].

In the 1940s and early 1950s, major steps toward commercializing photovoltaic were taken when the first silicon crystalline solar cell was produced with an efficiency of up to 6%[12].

In 1985, the U.S. Vanguard space satellite carried a small array of PV cells to power its radio[12].

Today, photovoltaic systems are supplying a growing portion of the world demand for electricity. As this demand will increase in the coming years, the government, industry and research organizations are investing hundreds of millions of dollars in research, development and production to make photovoltaic systems more affordable and to improve their efficiency.

2.2.2 Operating

The photovoltaic effect is the basic physical process through which a photovoltaic cell converts sunlight into electricity.

A photovoltaic cell is composed of a semiconductor layer with a surplus of an electron, which is exposed to the sunlight and of a semiconductor layer with electron deficiency. Once the sunlight hits the solar panels, the absorbed photons provide the energy needed to free some electron from their bound condition and those electrons flow from the negative layer to the positive layer. Thus, electricity is produced [4].

This operation can be resumed in the picture below:

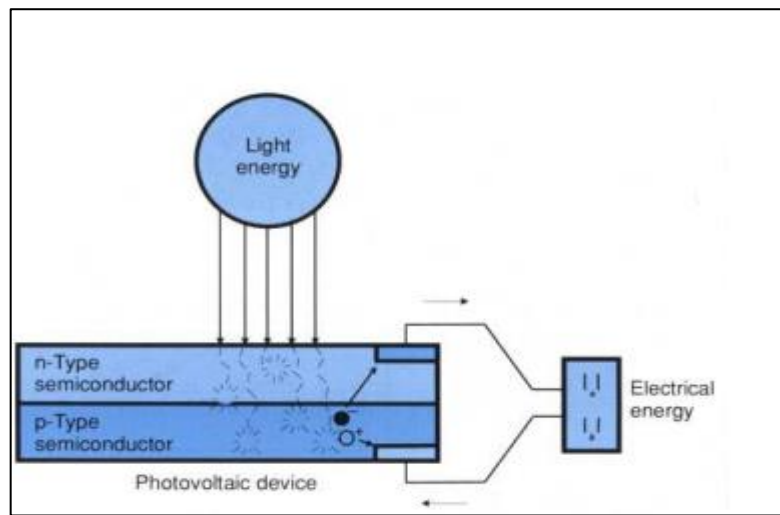


Fig 2. 1: Operating of photovoltaic cells [4].

2.2.3 Types of photovoltaic systems

Today photovoltaic systems are used to power anything on earth while operating in three primary forms[15]:

2.2.3.1 Grid-Connected PV systems

A grid-connected PV system consists of solar panels, inverter, distribution panel and grid. The inverter converts the DC power produced by the PV into AC power that conforms to the grid's electrical requirement. This AC power supply on-site electrical load or back-feed the grid when the PV system output is greater than the on-site load demand. When the

power required by the load is greater than the PV system output, it will be received from the electric utility [16].

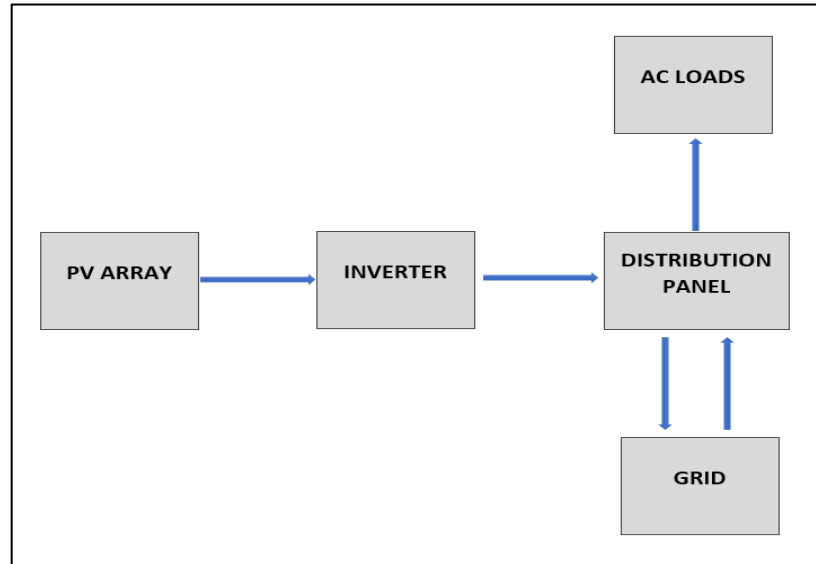


Fig 2. 2: Diagram block of Grid-connected PV system [15].

2.2.3.2 Standalone systems

Stand-alone PV systems also called off-Grid PV systems to operate independent of the electric utility grid. It consists of a charge controller, inverter, and storage battery [17].

The DC load uses the PV power immediately, and the AC loads are supplied by the AC power converted by the inverter. The battery is used to store energy that can be used at night or during cloudy weather. This system is suitable for many applications such as radio repeater stations, street lighting, water pumps...

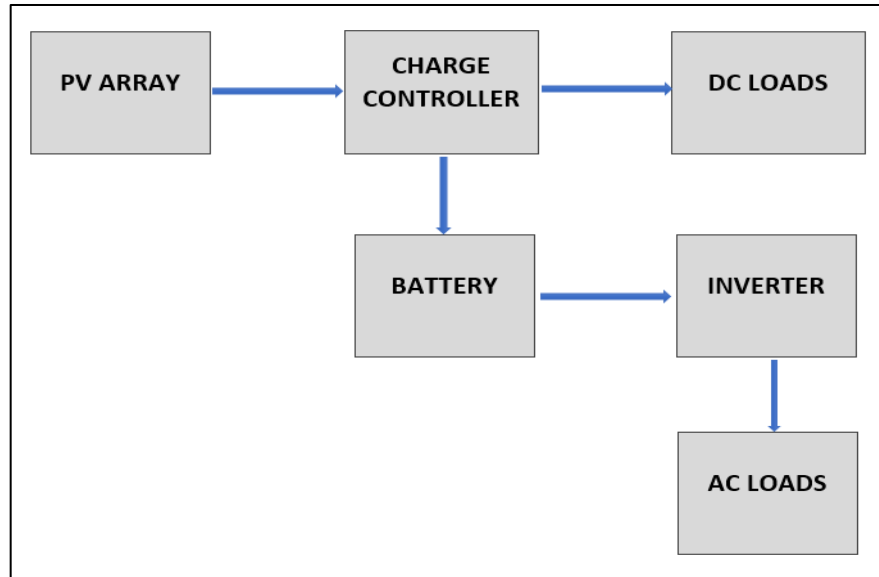


Fig 2. 3: Diagram block of a standalone system [15].

2.2.3.3 Hybrid Systems

A hybrid system combines PV with other forms of power generation, which can modulate power output as a function of demand [18].

The other form of power generation can be a diesel generator, wind turbine...

The photovoltaic power generation serves to reduce the consumption of non-renewable fuel.

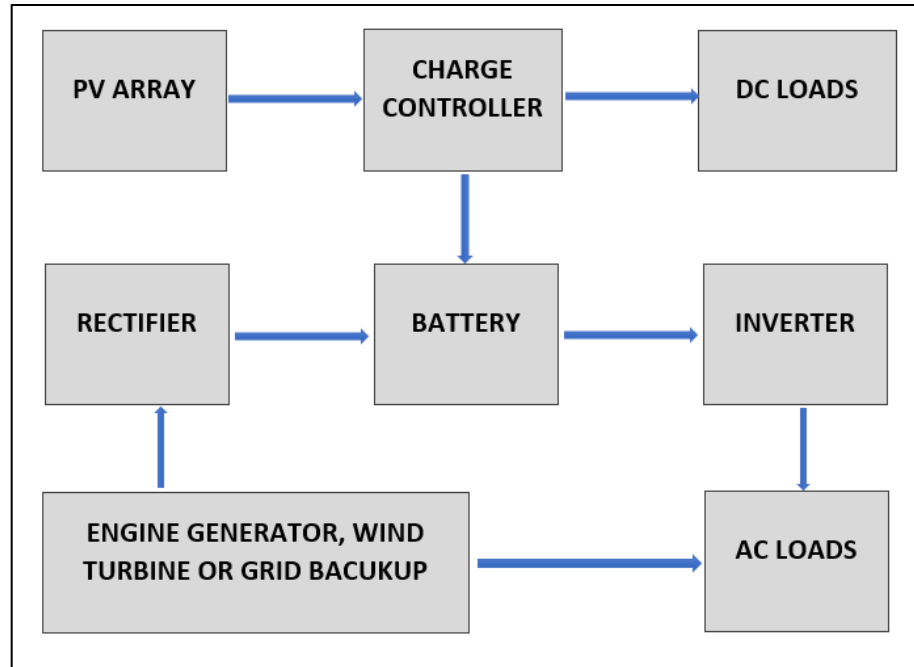


Fig 2. 4: Diagram block of the hybrid system [15].

2.2.4 Solar Panel Control MPPT

2.2.4.1 Role

Since the I-V and P-V characteristics of the solar panel are nonlinear, and the power generated depend on atmospheric conditions such as cell temperature and solar irradiation, the operating point of the photovoltaic panel does not always coincide with the maximum power-point.

Therefore, it has become essential to track the maximum power point and force the solar panel to be operated at a voltage that is consistent with this point [19].

The curve translating the P-V characteristics of the solar panel with different irradiation and temperature is the following.

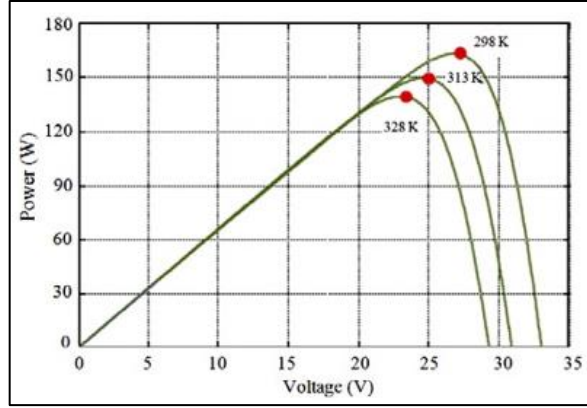


Fig 2. 5: Power- voltage curve of the solar panel for different temperatures [19].

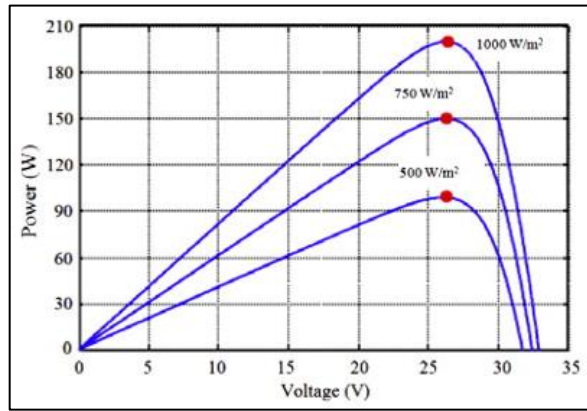


Fig 2. 6: Power-voltage curve of the solar panel for different irradiation [19].

2.2.4.2 Algorithm

There are many algorithms have been developed to extract the maximum energy converted by the panel and allows the optimal operation of the photovoltaic system.

The literature [6] contains algorithms based on the following methods such as: Hill climbing, perturb and observe, Incremental conductance...

A. Perturb and Observe Algorithm

The “perturb and observe” algorithm is the most commonly used in practice because of its ease of implementation.

This algorithm is based on comparing the actual value to the previous value of voltage and power generated by the solar panel.

The process followed to reach the maximum power point is:

If the power and the voltage increase or decrease at the same time, a perturbation step size X will be added to the duty cycle in order to force the operating point moving towards the maximum power-point.

If the power increase and the voltage decrease and vice versa, a perturbation step size X will be subtracted from the duty cycle in order to force the operating point moving towards the maximum power-point.

This process is resumed in a flow chart as shown in the figure bellow

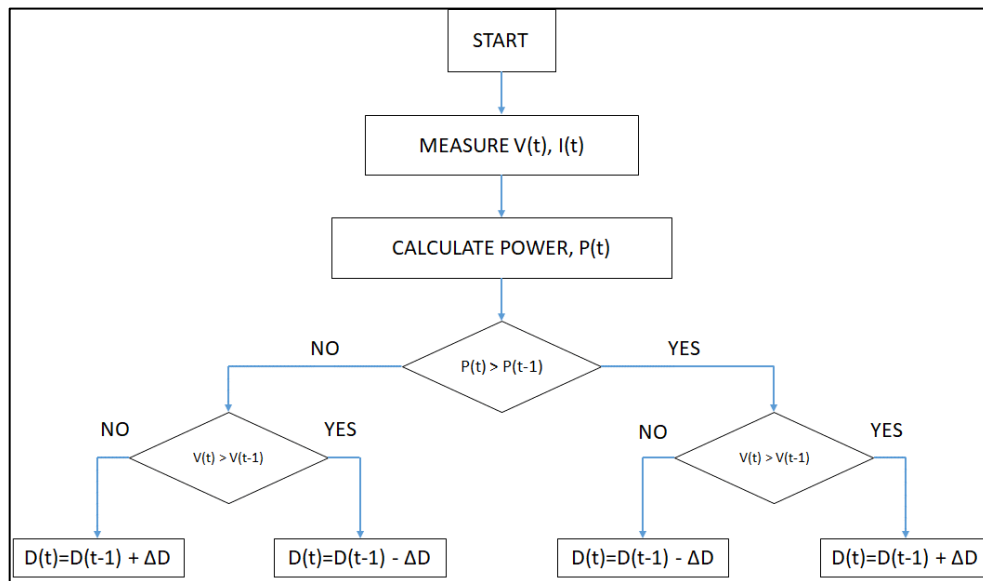


Fig 2. 7: Flow chart of perturb and observe algorithm [6].

B. Incremental Conductance

since the slope of the PV array power curve is zero at the MPP, positive on the left of the MPPT, and negative on the right [20]. This is shown in the following equations:

$$P = I * V \quad (1.1)$$

$$dP/dV = I + V * dI/dV = 0 \text{ at the MPP} \quad (1.2)$$

$$\frac{dI}{dV} = -\frac{I}{V} ; \left(\frac{dP}{dV} = 0 \right); \text{ at the MPP} \quad (1.3)$$

$$\frac{dI}{dV} > -\frac{I}{V} ; \left(\frac{dP}{dV} > 0 \right); \text{ left of MPP} \quad (1.4)$$

$$\frac{dI}{dV} < -\frac{I}{V} ; \left(\frac{dP}{dV} < 0 \right); \text{ right of MPP} \quad (1.5)$$

The process followed in this algorithm is:

If the actual and previous value of the voltage are not the same:

- If $\frac{dI}{dV} = -\frac{I}{V}$ then the previous values of voltage and current take the actual values
- If $\frac{dI}{dV} > -\frac{I}{V}$ then we increment the reference voltage
- If $\frac{dI}{dV} < -\frac{I}{V}$ then we decrement the reference voltage
- If the actual and previous value of the voltage are the same. The MPP was reached
- If the actual and previous values of the current are the same, then the atmospheric conditions have not changed and the MPPT is still operating at the MPP.

- If the actual value of the current is higher than the previous value, then the amount of sunlight has increased raising the MPP voltage. Therefore, we must decrement the reference voltage.
- If the previous value of current is higher than the actual value, then the amount of sunlight has decreased lowering the MPP voltage. Therefore, we must increment the reference voltage.

After every iteration, the previous values of current and voltage take the actual values.

This process is resumed in a flow chart as shown in the figure below:

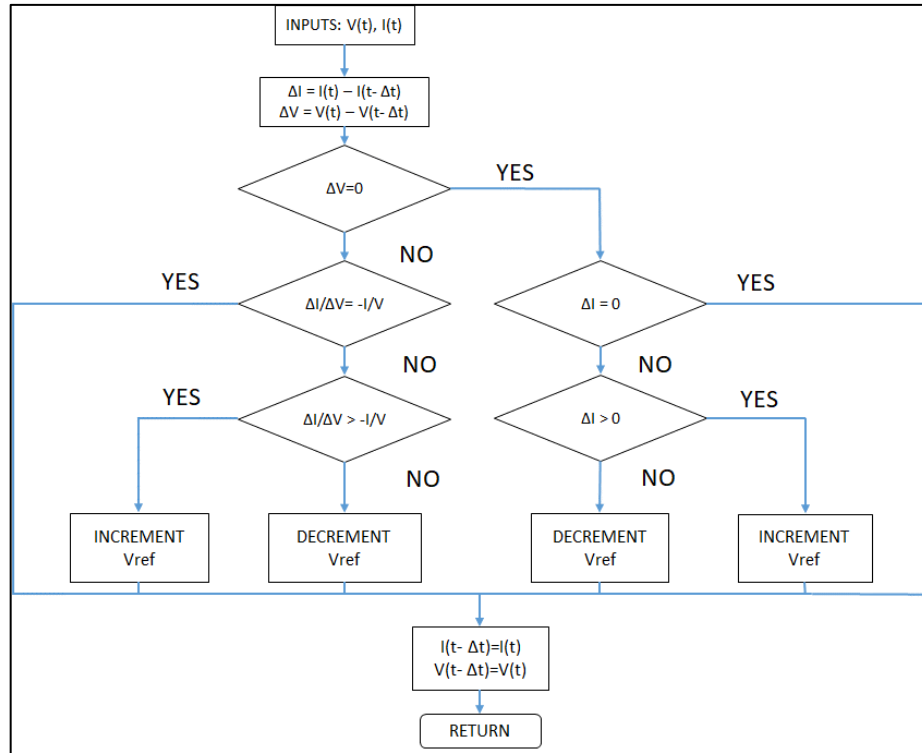


Fig 2. 8: Flow chart of the incremental conductance algorithm [6].

2.3 Electrical Vehicle Charged from PV and Grid

2.3.1 Sustainability and Economics

Charging EVs from solar photovoltaic panels and the grid (if the power of the PV cannot supply the demand) is an attractive option due to several reasons: first, the power demand on the grid will be reduced [21]. Thus, there will be less harmful exhaust emission. Second the PV panels are easy to implement and can be installed on roofs or as solar car parks, close to where EVs will be. Finally, the cost of charging the EV from both solar panels and the grid is cheaper than charging it from the grid only [22].

All these factors make EV charging from solar panels and grid attractive from an environment, sustainability and cost perspective.

2.3.2 System Architecture for the EV-PV-Grid System

To integrate the PV, EV and Grid, two different types of power converters can be used[13]:

A single multi-port-converter (MPC) that integrates PV, EV and Grid separate power converter for the grid, PV and EV which are interlinked on a common interconnection (AC or DC).

The electric vehicle can be charged from PV and grid according to four architectures[13]:

2.3.2.1 Architecture1: Separate power converter for the grid, PV and EV interlinked on AC interconnection:

The figure below shows architecture number 1, which uses an AC interconnection to connect the Grid and the converters for PV, EV.

In this architecture, a DC/AC converter is used for the PV side and an AC/DC converter is used for the EV side. All the power is passed via the grid; thus, it is the backbone of the architecture.

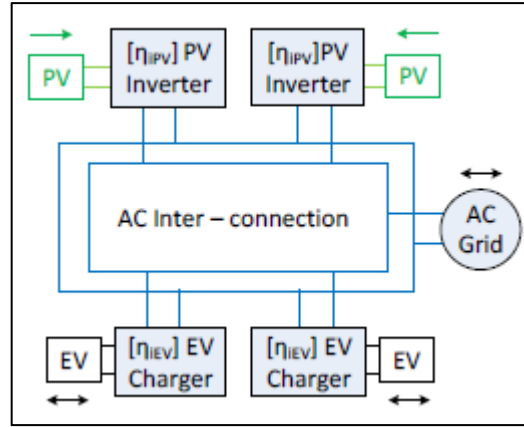


Fig 2. 9: Grid-PV-EV system interlinked on AC interconnection [13].

2.3.2.2 Architecture2: Separate power converter for the grid, PV and EV interlinked on DC interconnection:

The figure below shows architecture number two, which use a DC interconnection to connect the Grid and the converters for PV and EV.

In this architecture, a DC/DC converter is used for the PV and EV side and a bidirectional inverter used for the Grid side, which enables the feeding/drawing of the power due to the difference between PV generation, and EV charging demand.

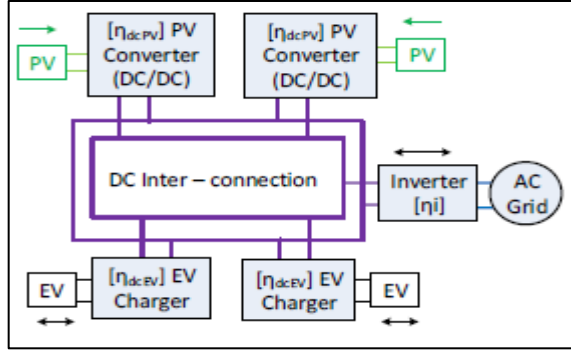


Fig 2. 10: Grid-PV-EV system interlinked on DC interconnection [13].

2.3.2.3 Architecture3: Multiport converter for PV, EV and Grid interlinked on AC:

The figure below shows architecture number three, which uses a multi-port converter for PV, EV and Grid interlinked on AC interconnection.

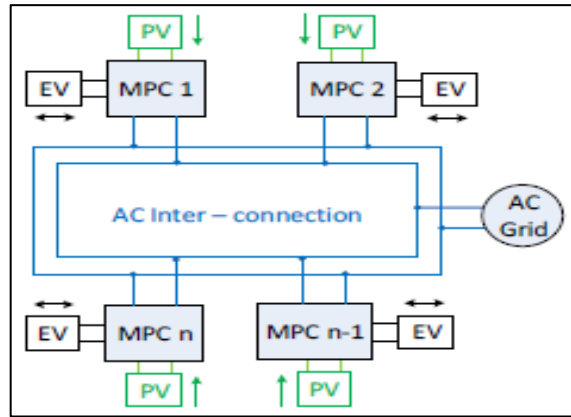


Fig 2. 11: MPC for PV and EV interlinked with the Grid on AC interconnection [13].

The multi-port converter is composed of a DC/DC converter for the PV side, a DC/DC converter for the EV side and an inverter for the AC interconnection as shown in the following figure.

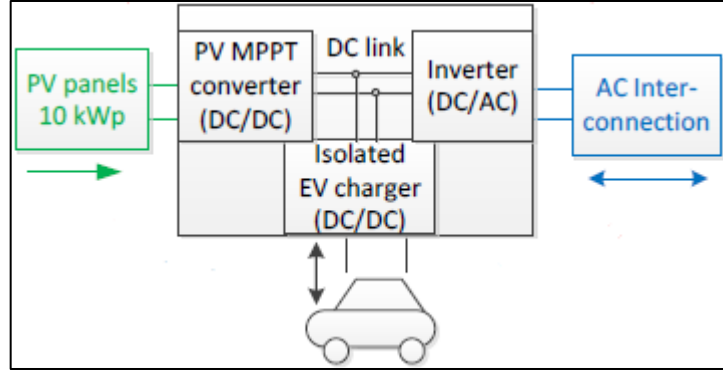


Fig 2. 12: Architecture of a multi-port-converter with AC interconnection [13].

2.3.2.4 Architecture4: Multiport converter for PV, EV and Grid interlinked on DC:

The figure below shows architecture number three, which uses a multi-port converter for PV, EV and an inverter for the Grid side, interlinked on DC interconnection.

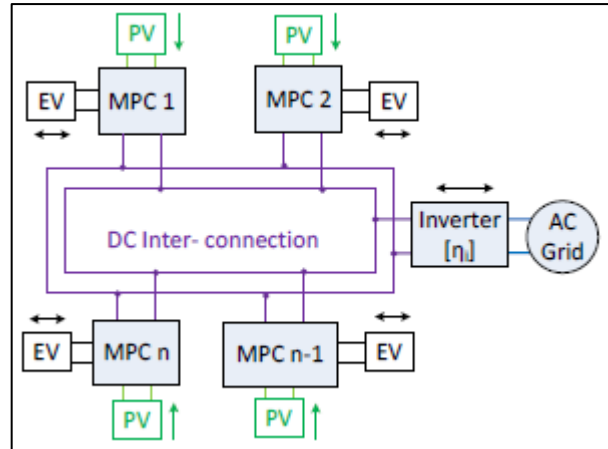


Fig 2. 13: MPC for PV and EV interlinked with the Grid on DC interconnection [13].

The multi-port converter is composed of a DC/DC converter for the PV side and a DC/DC converter for the EV side as shown in the following figure.

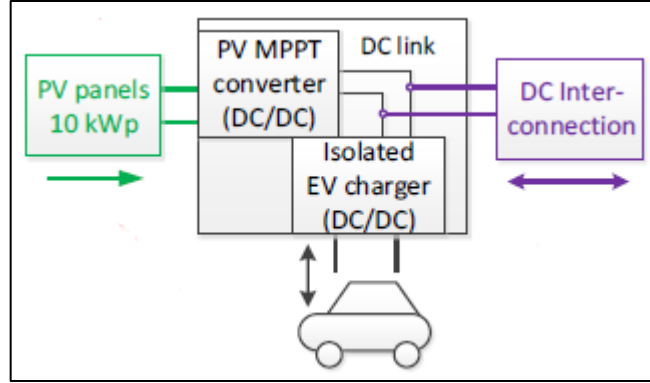


Fig 2. 14: Architecture of multi-port-converter with DC interconnection [13].

2.3.3 Comparison of system architecture:

The multi-port converter is characterized by the ease of controlling the individual EV, PV and Grid converters against controlling separate power converters using a communication infrastructure. In addition, a single inverter for both the EV and PV is used when a multi-port converter is used, which leads to lower component count, higher power density and lower losses. Those benefits of the multi-port converter are advantages for both architecture three and architecture four [13].

The build of DC interconnection instead of using the existing AC grid infrastructure requires protection and control, which is a disadvantage for architecture two and four.

The direct connection of DC power of EV and PV increases the efficiency gain. This is an advantage for architecture two, three and four [13].

The direct use of DC PV power to charge EV between multiple EV-PV chargers is an advantage for the architecture two and four.

The table below summarizes the comparison between the four architectures:

Table 2. 1: Table of comparison between the different architecture of the EV-PV-Grid system [13].

Criteria	Architectures			
	1	2	3	4
The ease of controlling the individual EV, PV and grid converters with minimal communication infrastructure.	No	No	Yes	Yes
Lower component count, higher power density and lower losses.	No	No	Yes	Yes
unnecessary protection and control are required due to the use of DC interconnection	Yes	No	Yes	No
High-efficiency gain thanks to the direct connection of DC power of EV and PV	No	Yes	Yes	Yes
The possibility of charging EV between multiple EV-PV chargers thanks to the direct use of DC PV power	No	Yes	No	Yes

From table 1 its clear that the third architecture is the architecture that has the most advantages.

2.3.4 EV-PV-Grid Power Flows

There are four possible power flow in the EV-PV-Grid system [13]:

A. Mode1:

In this mode, the PV power is directly used by the EV, which is the main objective of the system.

B. Mode2:

In this mode, the power flows from the grid to the EV. This mode is used when the PV cannot supply the demand for EV.

C. Mode3:

In this mode, the power flow from the EV to the grid.

D. Mode4:

In this mode, the power flows from the PV to the grid. This mode is used when there is no EV for charging, or the EV battery is full.

All those modes can be summarized in the following figure:

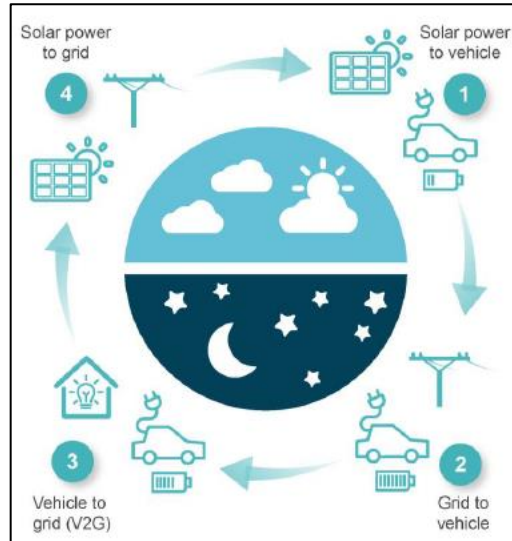


Fig 2. 15: Figure translating the different modes of power flow [13].

2.4 EV-PV-Grid Power Converter Topology

Since the PV delivers a DC voltage and the grid an AC voltage, the use of DC/DC and DC/AC converters is essential to obtain the necessary voltage that allows the battery charging.

In this section, the DC/DC and DC/AC converters are presented while explaining their role and operating.

2.4.1 DC/DC conversion

The DC/DC converter is used in EV-PV-Grid systems to convert a DC voltage to a different voltage level.

For power conversion, the key is to have high efficiency, so to avoid power dissipation and avoid overheating in electronic components, power conversion must be performed using storage components (inductor and capacitor) and switches (power switches).

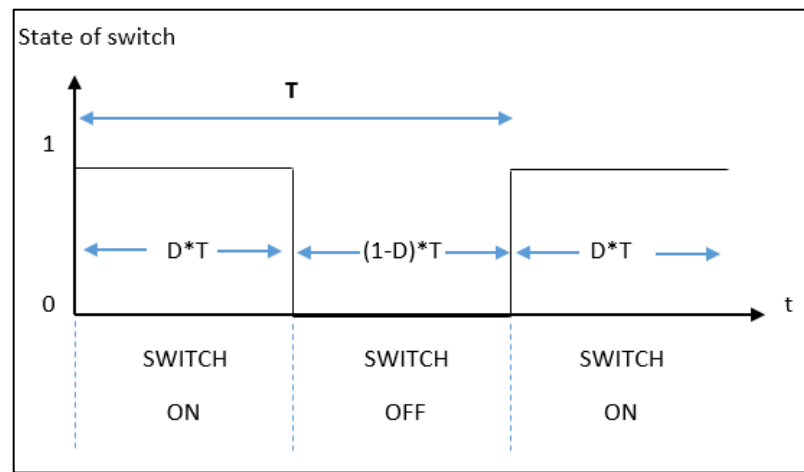


Fig 2. 16: State of the switch for DC/DC converter [23].

The circuits described in this section are classified as switched-mode DC/DC converters using a power bipolar junction transistor (BJT), a power metal-oxide-semiconductor field-effect transistor (MOSFET), a gate turn off thyristor (GTO), insulated gate bipolar transistor (IGBT) [23].

There are different types of DC/DC converters[24], which are detailed in this section.

2.4.1.1 Boost Converter

The DC-DC boost converter boosts up the output voltage to be greater than the input voltage.

The figure below shows the basic circuit topology of the DC-DC boost converter circuit consists of the power switch (M), switching control, inductor (L), capacitor (C), a diode (D) and load (R).

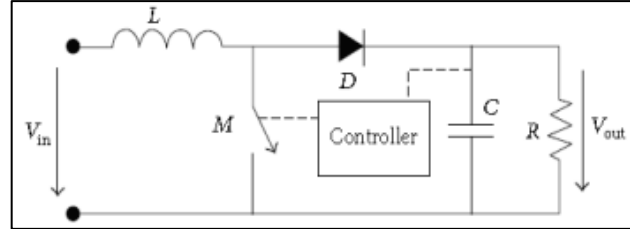


Fig 2. 17: Electric circuit of boost converter [23].

Depending on the state of the power switch (switch turn-on or switch turn-off), the operation of the DC-DC boost converter can be divided into two distinct phases[9]:

A. The accumulation phase:

When the switch is turn-on, the diode will be in reversed bias and the current in the inductor gradually increase so the inductor stores a quantity of energy in the form of magnetic energy. Thus, the capacitor will supply current to the load.

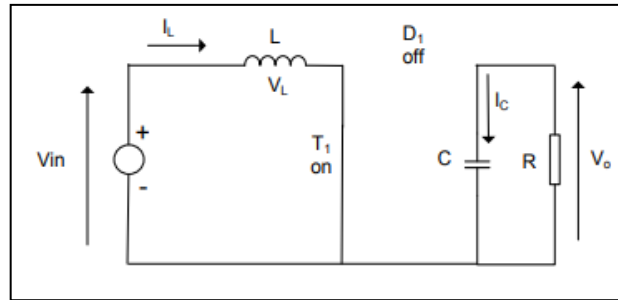


Fig 2. 18: Electric circuit of the accumulation phase [9].

B. The restitution phase:

When the switch is turn-off, the stored energy in the inductor will be transferred to the capacitor and load. Indeed, the decrease of the current in the inductor generates a voltage that is added to the supply voltage.

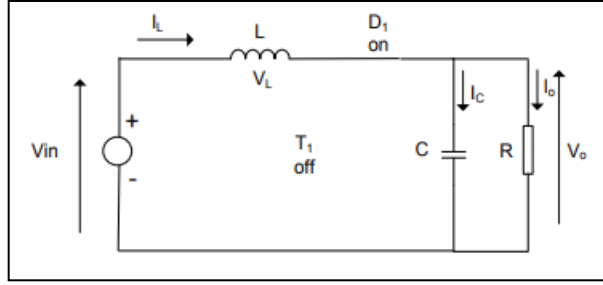


Fig 2. 19: Electric circuit of the restitution phase [9].

2.4.1.2 Buck Converter

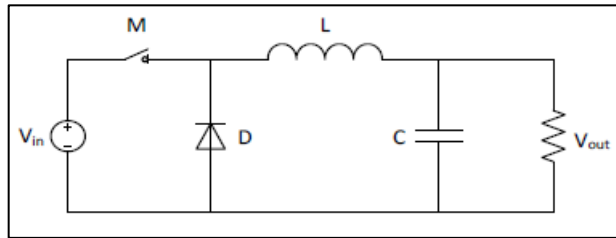


Fig 2. 20: Electric circuit of buck converter [25].

Depending on the state of the power switch (switch turn-on or switch turn-off), the operation of a DC-DC buck converter can be divided into two distinct phases[25]:

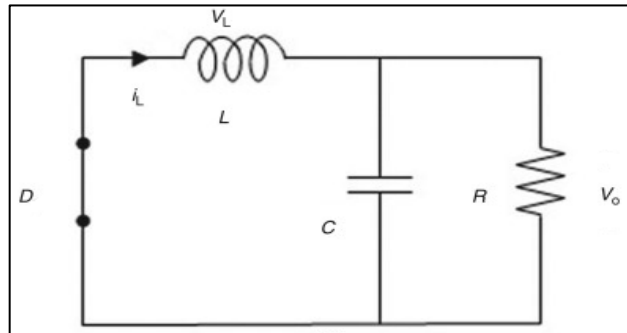


Fig 2. 21: Electric circuit of a buck converter with switch OFF [25].

2.4.1.3 Buck-Boost Converter

The DC-DC buck converter can step down or boost the output voltage level to be lower or greater than the output voltage.

The figure below shows the basic circuit topology of the DC-DC buck-boost converter circuit consists of the power switch (M), switching control, inductor (L), capacitor (C), a diode (D) and load (R).

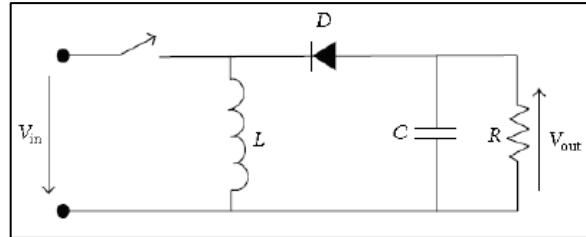


Fig 2. 22: Electric circuit of buck-boost converter [26].

Depending on the value of the duty cycle, the operating of the DC-DC buck-boost converter can be divided into three distinct operations [26]:

A. Duty cycle equal to 0.5:

The output voltage is equal to the input voltage.

B. Duty cycle less than 0.5:

The boost-buck converter operates in buck mode.

C. Duty cycle greater than 0.5:

The boost-buck converter operates in boost mode.

2.4.2 DC/AC and AC/DC Conversion

In the EV-PV-Grid system, the use of DC/AC and AC/DC conversion is needed to feed the EV with the necessary power if the PV cannot supply the demand or to extract the energy from PV in case the PV generates more than the demand or in case there is no vehicle to charge.

When the power flow is from DC to AC, the converter is an inverter and when the power flow is from AC to DC, the converter is a rectifier.

The power flow through the converter may be reversible, as shown in the figure below:

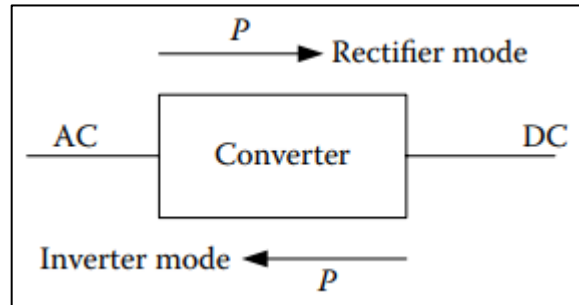


Fig 2. 23: Power flow through AC/DC and DC/AC converter [26].

2.4.2.1 AC/DC Conversion

In this case, the AC/DC converter is called a rectifier. It transforms the AC input to DC output.

Rectifiers can be divided into three types [27]: the uncontrolled rectifier with diode, the phase-controlled rectifier with thyristors and PWM-controlled rectifiers with IGBT or MOSFET.

A. Uncontrolled rectifier:

It's the simplest rectifier composed of diode which is manifested in 3 types: uncontrolled rectifier with diode, uncontrolled bridge rectifier and uncontrolled three-phase bridge rectifier.

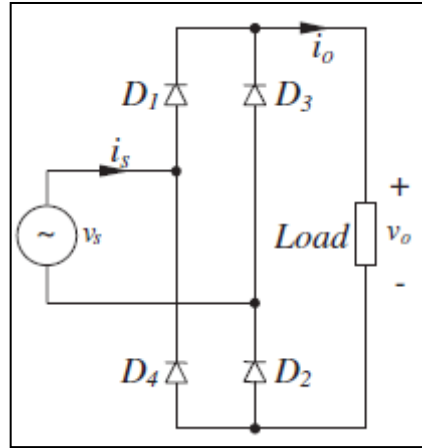


Fig 2. 24: Electric circuit of an uncontrolled bridge rectifier [27].

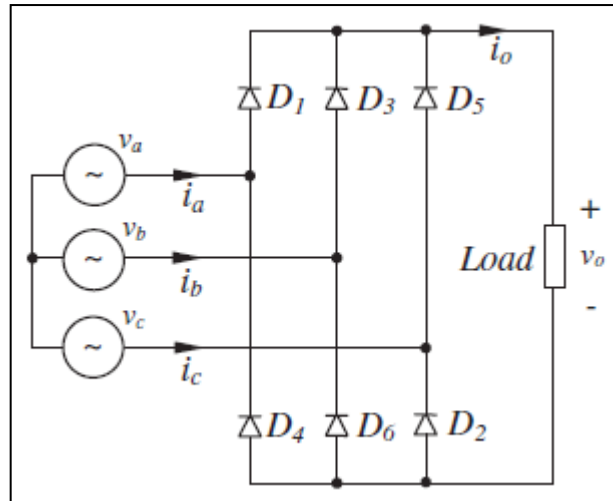


Fig 2. 25: Electric circuit of an uncontrolled three-phase bridge rectifier [27].

B. Phase-controlled rectifier:

Thyristors are adopted to form the phase-controlled rectifier, which allows controlling the output value by varying the firing angle of the thyristors. The possible topology of this rectifier is a phase-controlled single-phase rectifier and phase-controlled three-phase rectifier.

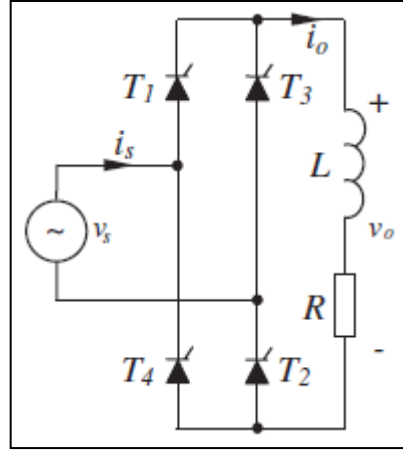


Fig 2. 26: Electric circuit of phase-controlled single-phase rectifier [27].

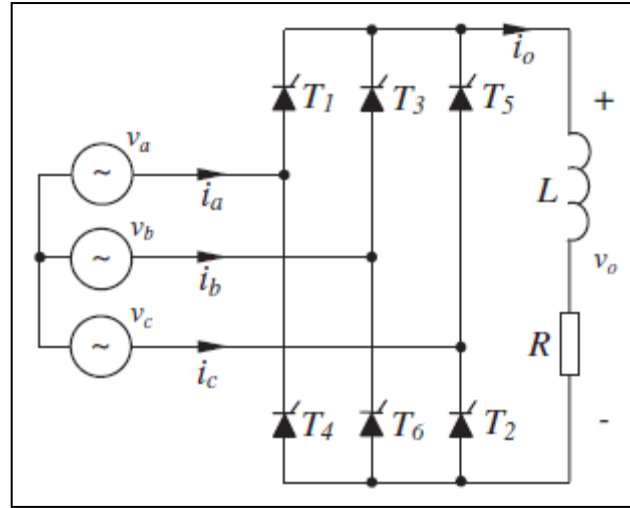


Fig 2. 27: Electric circuit of phase-controlled three-phase rectifier [27].

C. PWM-controlled rectifier:

The PWM-controlled rectifier is a bidirectional converter using PWM-controlled power switches. The power can flow from the AC side to the DC side (it is operating as a rectifier) or from the DC side to the AC side if there is energy available at the DC side (it is acting as an inverter) [28].

The topologies of the PWM-controlled rectifier are PWM-controlled single-phase bridge rectifier and PWM-controlled three-phase bridge rectifier

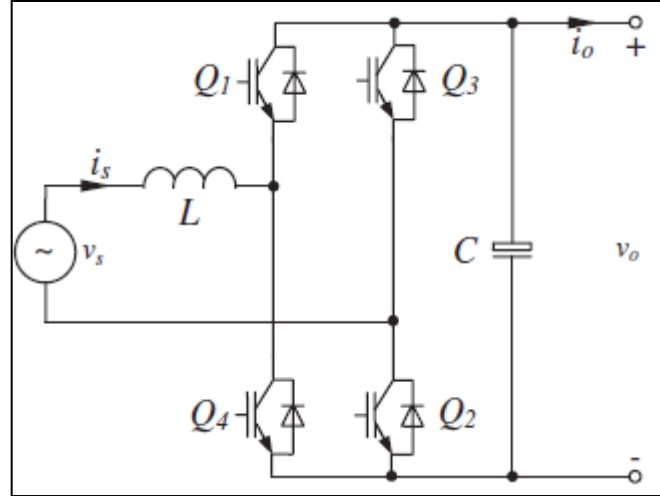


Fig 2. 28: Electric circuit of PWM-controlled single-phase bridge rectifier [28].

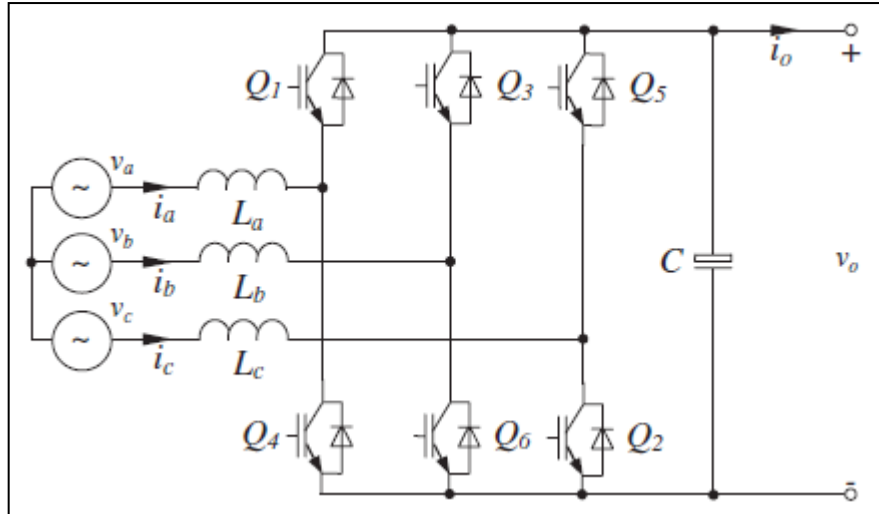


Fig 2. 29: Electric circuit of PWM-controlled three-phase bridge rectifier [28].

2.4.2.2 DC/AC Conversion

In this case, the DC/AC converter is called an inverter; it transforms the DC input to AC output.

Depending on the DC input, the inverter is a current-source inverter if the DC input is a current source (CSI) and the inverter is a voltage-source inverter if the DC input is a voltage-source (VSI). And depending on the AC output, the inverter is current-controlled

if the output is controlled to be a current source and the inverter is voltage-controlled if the output is controlled to be a voltage source [29].

The inverters can be line commutated (built with thyristor) or forced commutated (built with IGBT and MOSFET).

A. Line commutated inverters:

The line commutated inverter transforms the DC source to an AC source if the firing alpha is kept between 90 and 180 [30].

B. Forced commutated inverters:

A three-phase voltage source inverter and a single-phase voltage source inverter are presented in the figures below. The switching control can be achieved with pulse-width-modulation techniques and depending on the switching control, these converters can operate as an inverter or a rectifier.

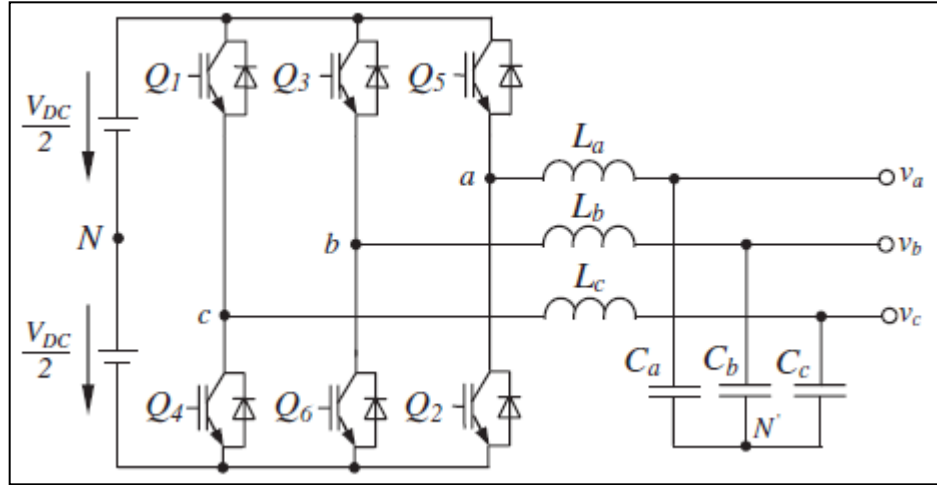


Fig 2. 30: Electric circuit of a three-phase voltage source inverter [30].

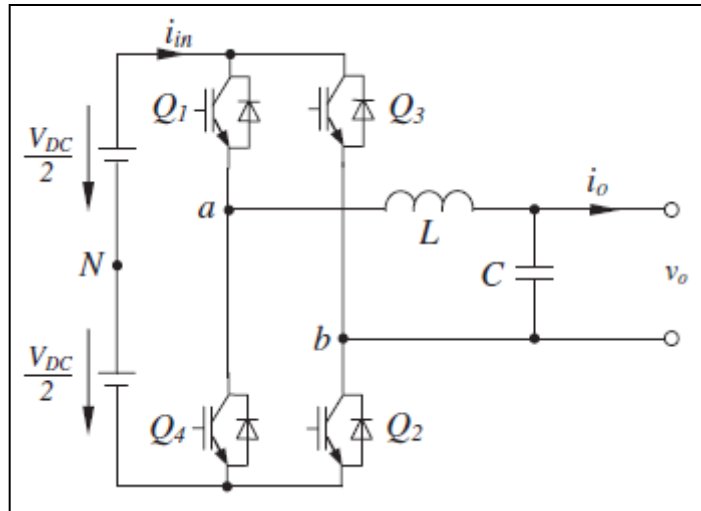


Fig 2. 31: Electric circuit of a single-phase voltage source inverter [30].

Chapter 3. EV-PV Charging System Design

3.1 Introduction

This chapter focus on the EV-PV-Grid charging system comprehension meaning simulations performed under PSIM software. In the first section, the system structure is presented, and the different components are detailed. Then in the second section, PSIM simulations results are presented, explained and discussed.

3.2 EV-PV charging system structure under PSIM software

The purpose is to realize a simulation in PSIM software allowing the charging of electric vehicle's battery from PV. The system is composed of a solar panel, the battery, DC/DC boost converter and maximum power point controller. The power delivered by the solar panel will pass by the DC/DC converter that is controlled by MPPT in order to extract the maximal power from the PV and to boost the voltage going to the battery to charge it.

The block diagram of the system is presented below:

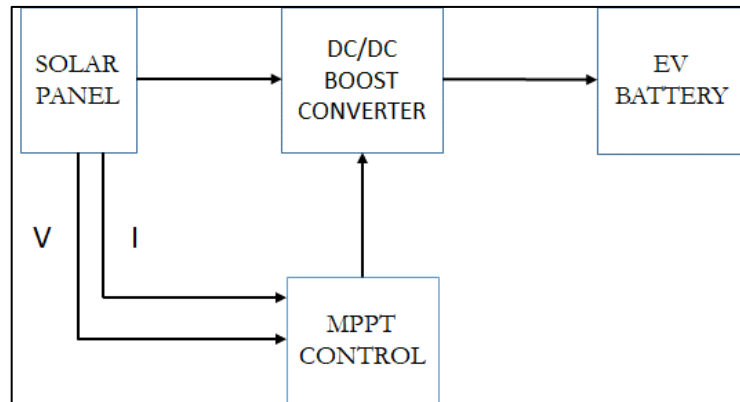


Fig 3. 1:Block diagram of EV-PV charging system

The electric circuit of the system in PSIM Software is presented and explained as follow:

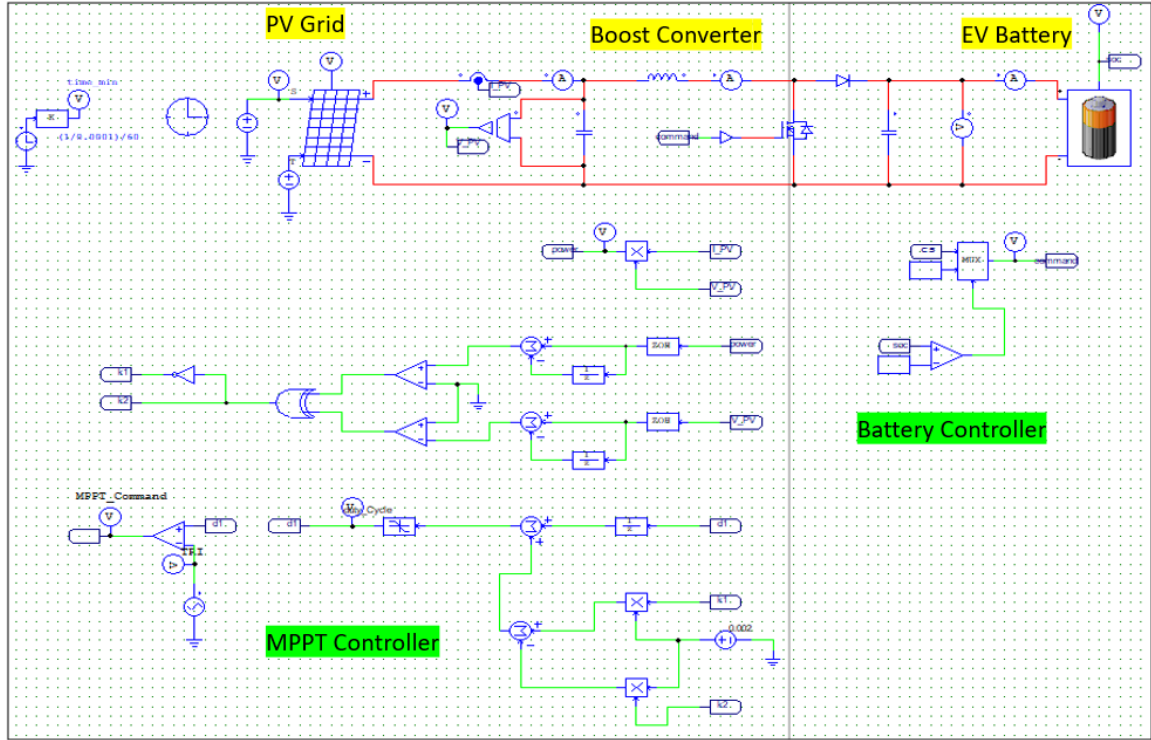


Fig 3. 2: Electric circuit of EV-PV system in PSIM software

3.2.1 Model and Characteristics of EV Battery

Since the Li-ion battery is the predominant battery energy storage technology for EVs[16], in the present simulation, a Li-ion battery of the Nissan Leaf electric vehicle which has a 427V as a maximal voltage and 360V as a nominal voltage is selected. The realized charging system is charging the Nissan Leaf battery with a power worth 19.3kW/h and capacity equal to 45Ah.

The Li-ion battery model is available in PSIM software as shown in the following figure [32]:

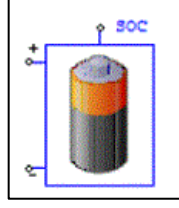


Fig 3. 3: Model of Li-ion battery in PSIM software [32].

The characteristics of the battery are as shown and explained in the figure and table below:

Table 3. 1: Table explaining the parameters of Li-ion battery in PSIM software [32].

PARAMETER	EXPLANATION
N_s	Number of cells in series in a battery pack
N_p	Number of cells in parallel in a battery pack
K_s	Voltage derating factor, from 0 (100% derating) to 1 (no derating)
K_p	Capacity derating factor, from 0 (100% derating) to 1 (no derating)
E_{rated}	Rated voltage of the battery cell, in V
E_{cut}	Battery voltage corresponding to the maximum capacity, in V
Q_{rated}	Rated capacity of the battery cell, in Ah
Internal resistance	Internal resistance of the battery cell, in Ohm
Discharge current	The discharge current of the curve under which model parameters are obtained, in A
Capacity factor	A factor that is roughly the ratio between the Q_0 (capacity at 0V) and Q_{max} (capacity at E_{cut}) on the discharge curve
E_{full}	Full voltage of the battery cell, in V
E_{top}	Battery voltage at the end of the exponential region in the discharge curve, in V
E_{nom}	Battery voltage at the end of the nominal region in the discharge curve, in V
Q_{max}	Maximum capacity of the battery cell corresponding to the E_{cut} , in Ah

Q_{top}	Battery capacity at the end of the exponential region in the discharge curve, in Ah
Q_{nom}	Battery capacity at the end of the nominal region in the discharge curve, in Ah
SOC	Initial battery state of charge (from 0 to 1)

Some characteristics can be extracted from the voltage-capacity curve as follow:

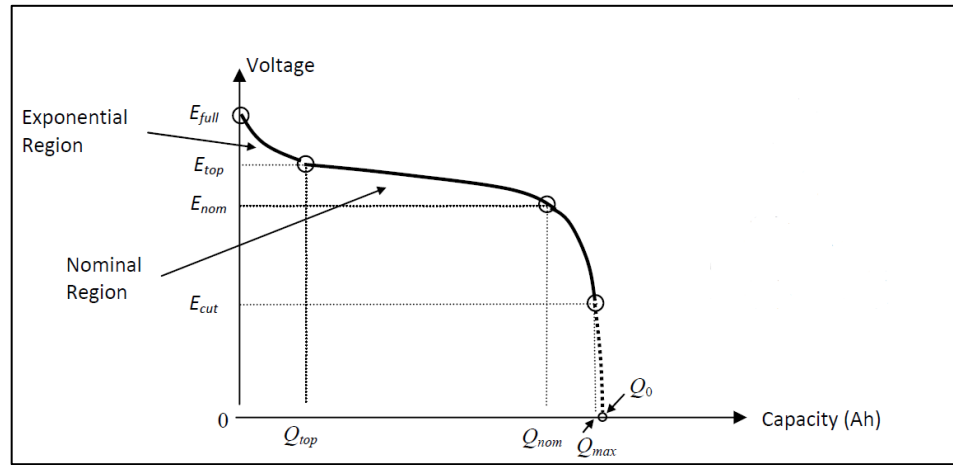


Fig 3. 4: Voltage-Capacity curve of Li-ion battery [32].

3.2.2 Photovoltaic panel

In our simulation, a physical solar panel model is chosen in PSIM Software as shown in the figure below, because it can consider variations of the light intensity and ambient temperature [33].

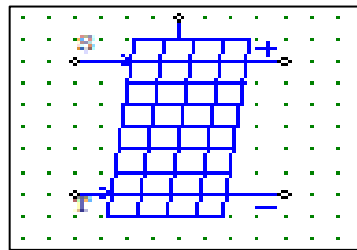


Fig 3. 5: Model of the photovoltaic panel in PSIM Software [33].

The node with the letter "S" refers to the light intensity input (in W/m^2) the node with the letter "T" refers to the ambient temperature input (in $^\circ\text{C}$), and the node on the top refers to the theoretical maximum power giving by the operating conditions.

The characteristics of the solar panel are detailed and explained in the figure and table below:

Table 3. 2: Table explaining the parameters of the solar panel (physical model) in PSIM software [33].

PARAMETER	EXPLANATION
N_s	The number of cells of the solar module. A solar module consists of N_s solar cells in series
S_0	Light intensity under the standard test conditions, in W/m^2 . The value usually is $1000 \text{ W}/\text{m}^2$ in the manufacturer datasheet.
T_{ref}	Temperature under the standard test conditions, in Celsius
R_s	Series resistance of each solar cell, in Ohm
R_{sh}	The shunt resistance of each solar cell, in Ohm
I_{s0}	Short circuit current of each solar cell at the reference temperature T_{ref} in A
Saturation Current	Diode saturation current of each solar cell at the reference temperature T_{ref} in A
E_g	Band energy of each solar cell, in eV. It is around 1.12 for crystalline silicon, and around 1.75 for amorphous silicon.
A	Ideality factor of each solar cell, also called the emission coefficient. It is around 2 for crystalline silicon and is less than 2 for amorphous silicon.
C_t	Temperature coefficient, in A/C or A/K

3.2.3 Structure of DC/DC Boost Converter

To connect the low solar panel array voltage to a high battery input voltage and achieve the most excellent possible power harvest, the use of a DC-DC boost converter is essential.

This converter with a switch controlled by the “maximum power point tracker” command will boost up the output voltage to be greater than the input voltage.

The electrical structure in PSIM software is as follows:

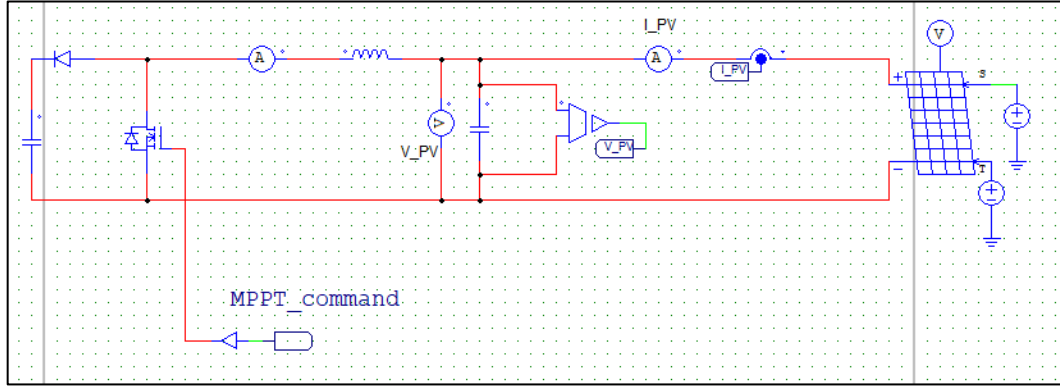


Fig 3. 6: Electric circuit of DC/DC boost converter connected to a solar panel in PSIM software

The output voltage and current switching ripple should be small in any well-designed converter. Therefore, the inductor and capacitor values must be chosen such that the desired ripple is obtained. In the presented system, the ripples are limited to 8% for the voltage and 5% for the current based on the IEEE Std 519-2014 [17].

The equations that can be used to choose the inductor and capacitor values are given below [35]:

$$D = 1 - \frac{V_{in}}{V_{out}} \quad (2.1)$$

$$L = \frac{V_{in} \cdot D \cdot T_s}{2 \Delta i_L} \quad (2.2)$$

$$C = \frac{V_{out} \cdot D \cdot T_s}{2 \Delta v \cdot R} \quad (2.3)$$

With:

D : duty cycle of the boost converter

$2\Delta i_L$: The inductor current ripple peak to peak

$2\Delta v$: The capacitor voltage ripple peak to peak

T_s : The inverse of the switching frequency

V_{in} : Voltage across the DC/DC boost converter input

V_{out} : Voltage across the DC/DC boost converter output

R : Equivalent resistance of the load.

The components of the DC/DC converter are detailed below:

3.2.3.1 MOSFET parameters:

An ideal MOSFET is used in the simulation with the parameters explained below:

Table 3. 3: Table explaining the parameters of the MOSFET used in the EV-PV system [34].

PARAMETER	EXPLANATION
Model-level	Ideal
On resistance	The resistance of the MOSFET transistor during the on state, in Ohm
Diode Forward Voltage	The forward threshold voltage of the anti-parallel diode, in V
Diode resistance	On resistance of the anti-parallel diode, in Ohm
Initial position	Flag for initial transistor position (0: off; 1: on)
Current Flag	Flag to save current data for SimView display (0: no display; 1: display)

3.2.3.2 Capacitor parameters:

An ideal capacitor with no parasitic components (level1) is used in the simulation with a 150uF as capacitance. The parameters of the capacitor are explained below:

Table 3. 4: Table explaining the parameters of the capacitor used in the EV-PV system [34].

PARAMETER	EXPLANATION
Model-level	The Level-1 model of the capacitor is an ideal capacitor with no parasitic components
Capacitance	Capacitance, in F
Initial capacitor voltage	Initial capacitor voltage, in V
Current flag	Flag for branch current output (1: current output; 0: no current output)

3.2.3.3 Inductor parameters:

An ideal inductor with no parasitic component (level1) is used in the simulation with an 847uH. The parameters of the inductor are explained below:

Table 3. 5: Table explaining the parameters of the inductor used in the EV-PV system [34].

PARAMETER	EXPLANATION
Model-level	The Level-1 model of the inductor is an ideal inductor with no parasitic components.
Inductance	Inductance, in H
Initial current	Initial inductor current, in A
Current flag	Flag for branch current output (1: current output; 0: no current output)

3.2.3.4 Diode parameters:

An ideal diode is used in the simulation with the parameters explained below:

Table 3. 6: Table explaining the parameters of the diode used in the EV-PV system [34].

PARAMETER	EXPLANATION
Model Level	Ideal
Forward voltage	Diode forward threshold voltage drop V_{th} , in V. The diode starts to conduct when the positive bias voltage is greater than V_{th} .
Resistance	Diode on-resistance, in Ohm, after it starts to conduct.
Initial position	Flag for initial diode position (0: open; 1: closed)
Current flag	Flag for current output (0: no output; 1: with output)

3.2.4 Maximum Power Point Tracking Command

In order to adjust the DC operating point to obtain the maximum power available from a PV array at any given time, the switch of DC/DC converters is commanded by an MPPT command. In the present simulation, the “perturb and observe” algorithm is used since it is the most commonly used in practice because of its ease of implementation [37].

The algorithm operates in these steps: first, the output current and voltage are measured using sensors, second, the power delivered by the solar panel is calculated ($P=V*I$) and it is compared at the previous power value, at the same time, the actual voltage value is compared to the last value. If the voltage and the power increase or decrease at the same time, a positive offset will be added to the previous value of the duty cycle, else a negative offset will be added to the previous value of the duty cycle. Finally, the duty cycle is compared to a triangular-wave voltage source to obtain the MPPT command (the state of the switch).

The model of perturb and observe algorithm in PSIM software is realized as follows:

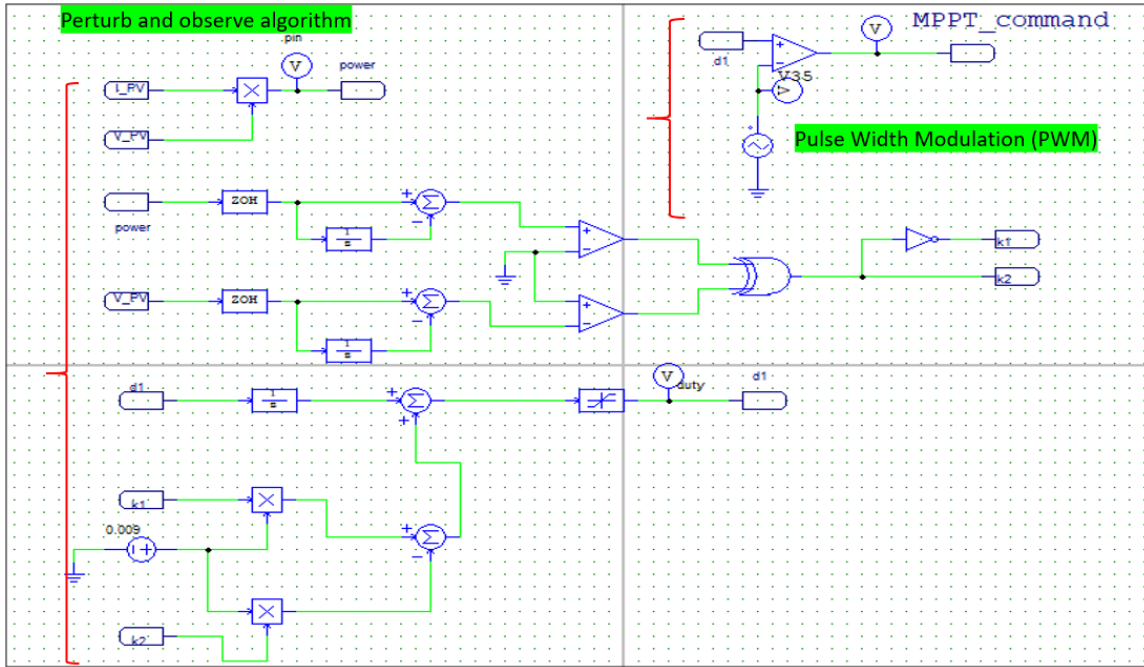


Fig 3. 7: Electric circuit of perturb and observe algorithm in PSIM software

The value of the perturbation applied to the duty cycle to approach or to move away from the maximal power-point must be well chosen. Once it is oversized, the maximal power-point will not be reached and the oscillations around this point will increase, which will cause many losses. The perturbation in the present work is selected using the trial and error method. The perturbation is fixed at 0.009, the time stability of the system and the oscillations of the extracted power are observed. The effected calculation is summarized in the table below:

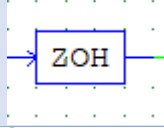
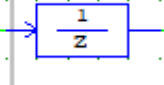
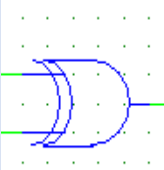
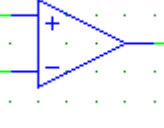
Table 3. 7: Table translating the effects of changing the perturbation value on the system time stability and the extracted power ripples

Perturbation value	Time stability of the system	Oscillation of the extracted power
0.02	$4.721 \cdot 10^{-3}$	16.00kW – 20kW
0.05	$3.035 \cdot 10^{-3}$	13.33kW – 20kW
0.009	$8.417 \cdot 10^{-3}$	17.70kW – 20kW
0.004	$1.680 \cdot 10^{-2}$	19.48kW – 20kW
0.002	$1.136 \cdot 10^{-2}$	19.80kW – 20kW

To have a compromise between the stability time and the oscillation rate, the chosen value is 0.009.

The components employed in the perturb and observe the algorithm model are:

Table 3. 8: Table explaining the different components of the MPPT system in PSIM Software [34].

Component	Symbol	Explanation
Zero-Order-Hold		Holds the sampled value until the next clock cycle.
Unit delay block		Delays the input by one sampling period.
XOR gate		Exclusive-OR gate: if the two inputs are the same (two 0 or two 1), then the output is 0 else the output is 1.
Comparator		If the non-inverting input is high than the inverting input, the output value is one. Else the output value is zero. If the two inputs are equal, the output will keep the previous value.

3.3 EV-PV Charging System Results

The EV-PV charging system is modeled and simulated under PSIM software with the conditions presented in the last section. In this section, the simulation results are presented and described.

The initial battery state of charge is 0% and the temperature of the solar panel is set at 25° for all the studied cases.

3.3.1 Case 1: Irradiation Equal to 1000 W/ m²

In this case, the radiation is continuously equal to 1000 W/ m². The curves translating the state of charge, the battery current and voltage, the solar panel voltage and current are presented below:

3.3.1.1 Battery Side Curves

The pace of the battery voltage as well as the battery current and the state of charge, are presented during the charging period.

As is illustrated, the battery current is around 47A for a state of charge less than 80% and started decreasing gradually until reaching 40A at the end of the charging period. Thus, the battery is charged in 60 min, as the maximum capacity of the battery is 45A/hour.

While the battery voltage increases gradually from 403V to 460V when the battery is fully charged, the power received from the battery is rippling around 20kW, as it can be seen in the fourth curve.

When the battery is fully charged, it becomes disconnected from the circuit. Hence, the current is canceled, and the voltage battery decrease until reaching 427V, which is the empty voltage battery for a state of charge equal to 100%.

The ripples for all the curves did not exceed the limits required by the IEEE 519-2014 standard [38].

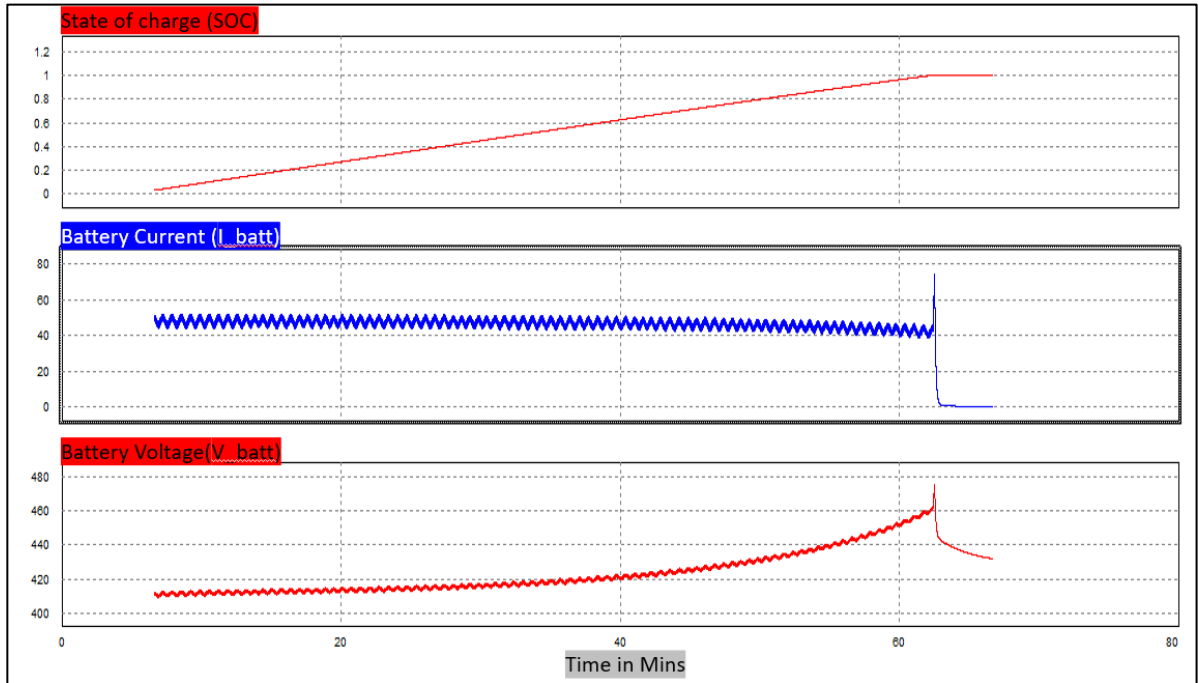


Fig 3. 8: Battery state of charge, current and voltage curves during the charging period in a PV-EV charging system for irradiation equal to 1000W/m^2

3.3.1.2 PV Side Curves

The solar panel used in the present system can produce 114V, 175A, and then 20kW. The PV voltage and current are constant with a small ripple that did not exceed 8% for the voltage and 5% for the current.

Once the state of charge reaches 100%, the DC/DC boost converter command is set at zero, the battery is disconnected and the MPPT no longer draws power from the solar panel. Therefore, the PV current vanishes as well as the extracted power as observed in the curves.

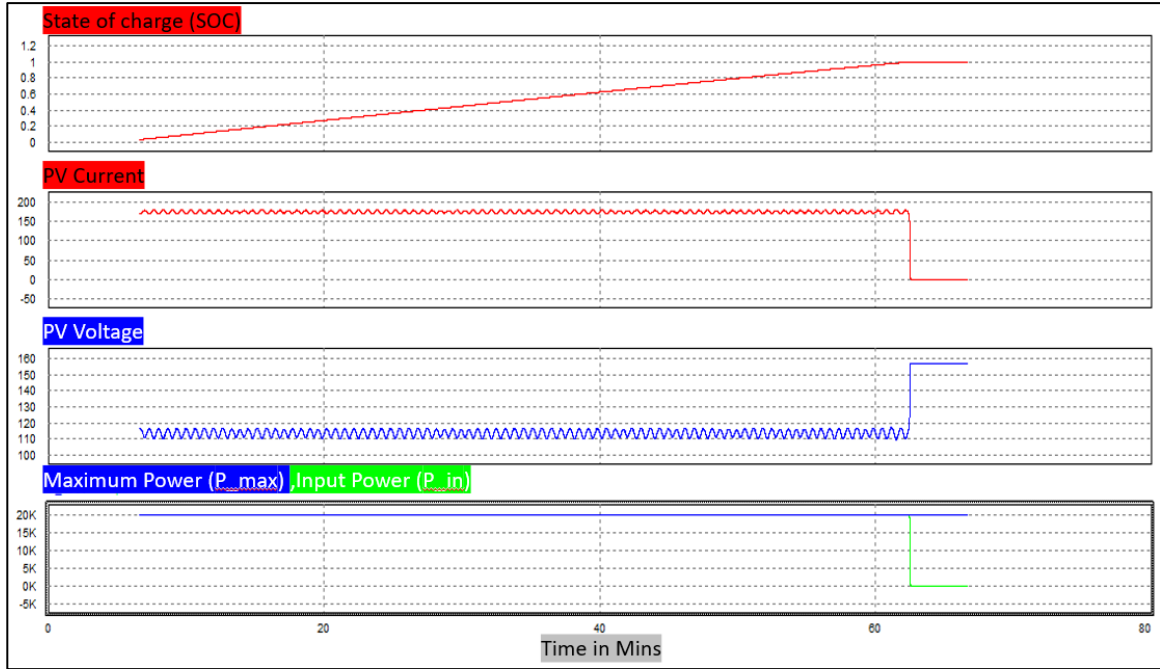


Fig 3. 9: The evolution of PV voltage, current, maximum power and extracted power during the charging period in a PV-EV charging system for irradiation equal to 1000W/m^2

The duty cycle is presented below in the first figure. Then it is compared to a triangular wave to obtain the DC/DC boost converter as detailed in the second figure.

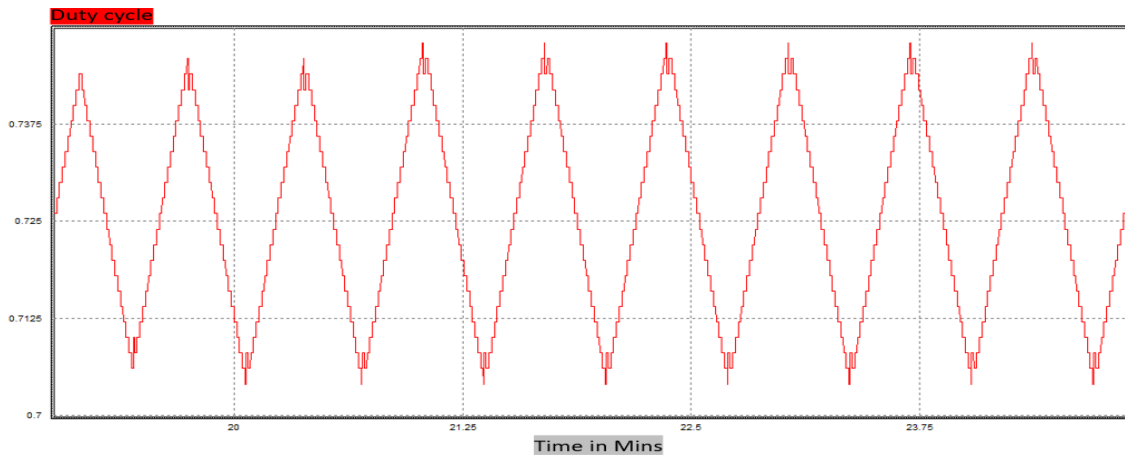


Fig 3. 10: The evolution of the duty cycle in perturb and observe algorithm employed in a PV-EV charging system for irradiation equal to 1000W/m^2

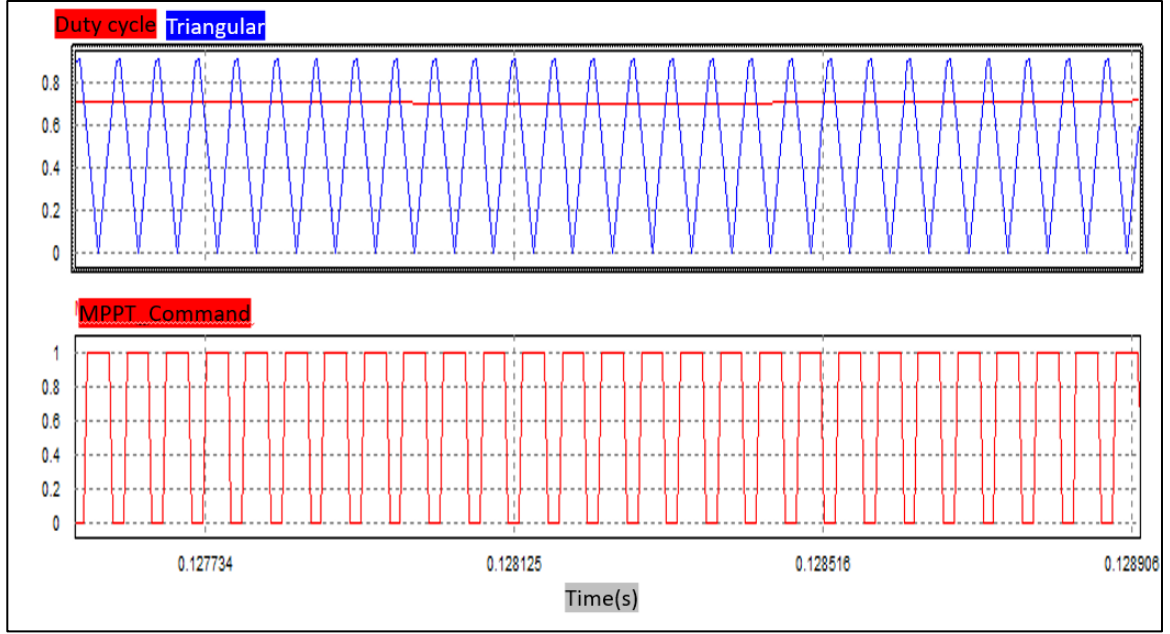


Fig 3. 11: Duty cycle, triangular wave and MPPT command curves translating the operating of PWM in a PV-EV charging system

3.3.2 Case 2: Irradiation equal to 700 W/m^2

In this case, the radiation is continuously equal to 700 W/m^2 . The curves translating the state of charge, the battery current and voltage, the solar panel voltage and current are presented below:

3.3.2.1 Battery Side Curve

As it is observed in the battery voltage, current and state of charge curves below, the current of the battery is equal to 35A, which is decreased with the decrease of the radiation. Moreover, the increase of the voltage battery is slower than the increase for radiation equal to 1000 W/m^2 . The consequence was that the charging period increased and reached 83min instead of 65min. It should be noted that the ripples still around the allowed percentage.

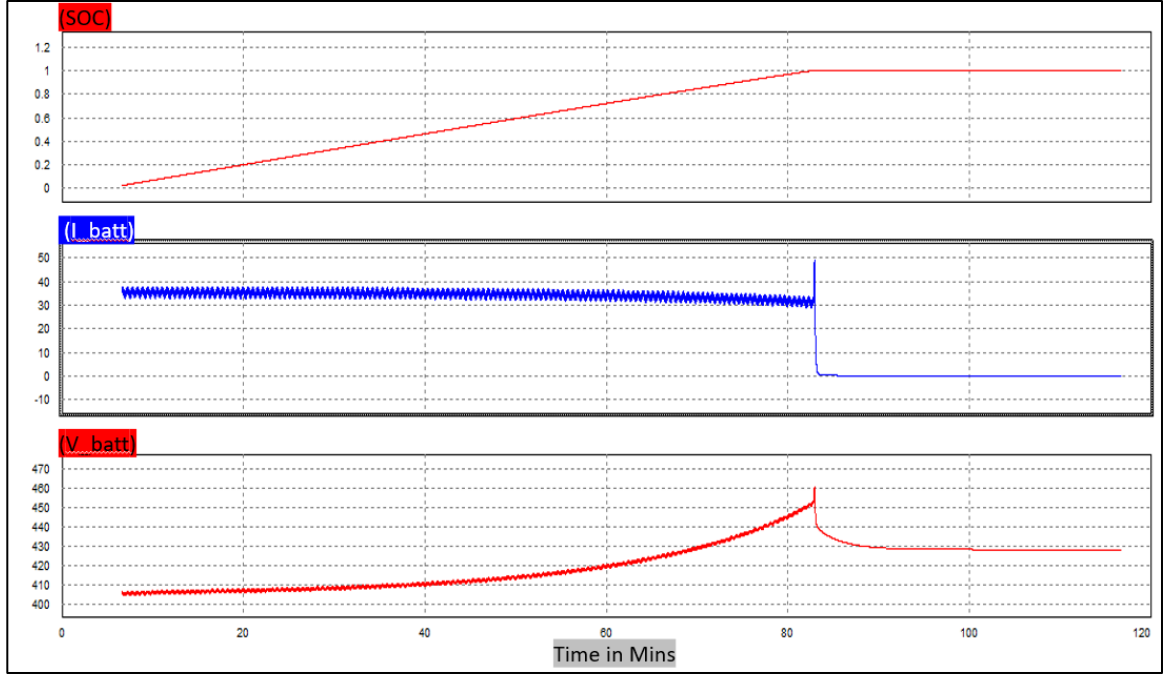


Fig 3. 12: Battery state of charge, current and voltage curves during the charging period in a PV-EV charging system for irradiation equal to $700\text{W}/\text{m}^2$

3.3.2.2 PV Side Curves

The decrease of the radiation from $1000\text{ W}/\text{m}^2$ to $700\text{ W}/\text{m}^2$ Influenced the delivered power. The solar panel current decreased from 175A to 125A and the voltage has undergone a slight increase from 114V to 117V. Hence, the power decreased from 20 kW to 15 kW.

When the battery is fully charged, the circuit is open, so the PV current becomes zero and the MPPT does not work anymore.

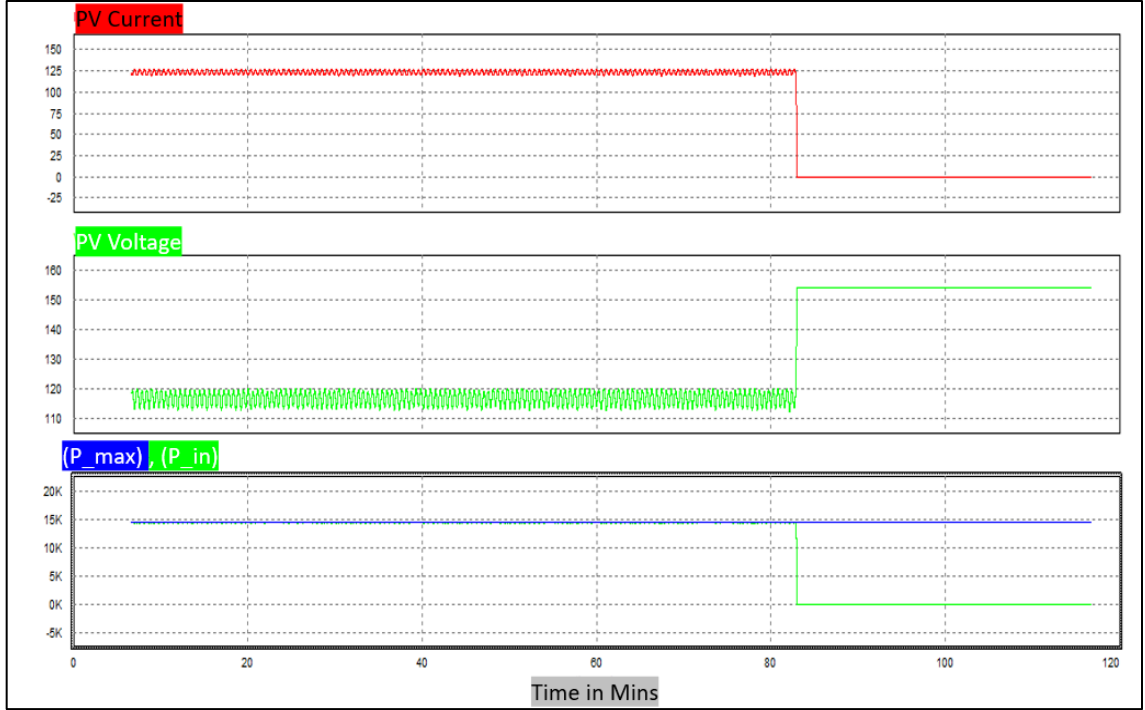


Fig 3. 13: The evolution of PV voltage, current, maximum power and extracted power during the charging period in a PV-EV charging system for irradiation equal to $700\text{W}/\text{m}^2$

As it is noticed, the duty cycle also decreased. For radiation equal to $1000\text{ W}/\text{m}^2$ the duty cycle reached 0.752 against 0.732 for radiation equal to $700\text{W}/\text{m}^2$.

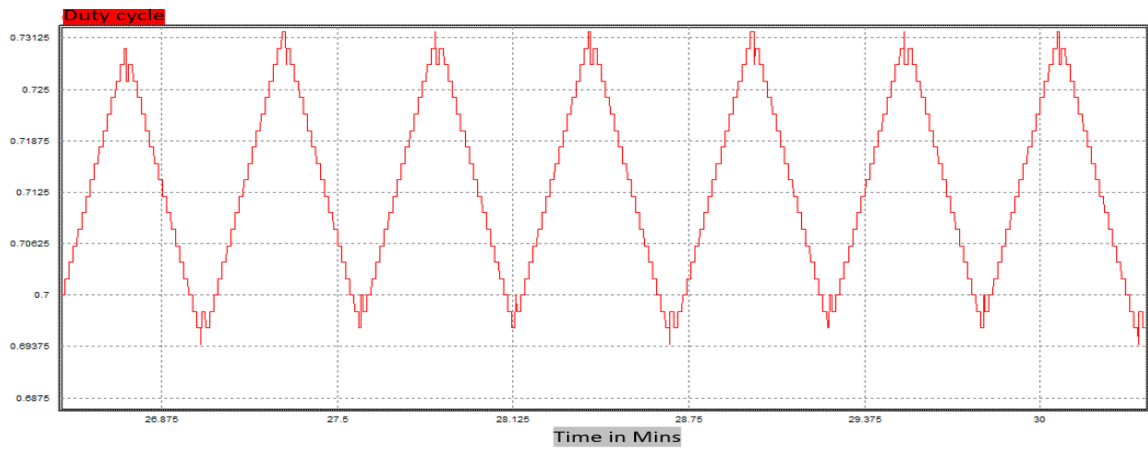


Fig 3. 14: The evolution of the duty cycle in perturb and observe algorithm employed in a PV-EV charging system for irradiation equal to $700\text{W}/\text{m}^2$

3.4 Conclusion

This chapter has addressed EV-PV charging system modeling and simulation under PSIM software. The different components were detailed as well as the simulation condition in the first section. In the second section, the simulation results were presented and discussed for different irradiation.

Chapter 4. EV-PV-Grid Charging System Design

4.1 Introduction:

Based on the comparison between different EV-PV-Grid systems established in the first chapter, the third architecture will be followed in our simulation. The purpose is to realize a design in PSIM software allowing the EV's battery charging from PV and Grid.

In the present chapter, the grid source is integrated into the previous chapter under PSIM software. In the first place, the EV-PV-Grid charging system structure is presented while explaining the simulation condition, charging method, energy management, converter employed, and their control associated. Then PSIM simulations results obtained are observed and analyzed.

4.2 EV-PV-Grid charging system structure in PSIM software:

In the same condition of the simulation realized in the second chapter, the grid source is integrated in order to charge the EV from the source in case the PV cannot satisfy the demand.

The block diagram of the realized system is presented below:

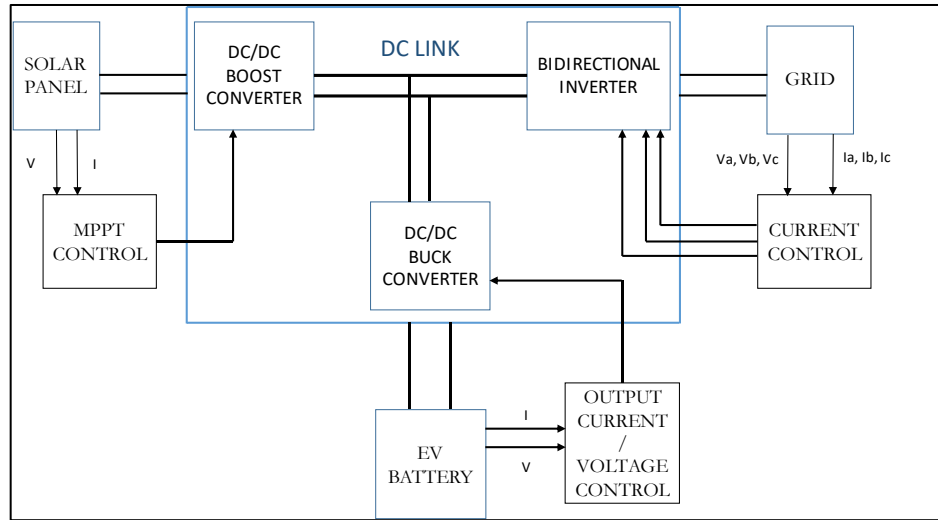


Fig 4. 1: Block diagram of EV-PV-Grid system

The electric circuit of the EV-PV-Grid system in PSIM software is presented below and Table 4.1 summarize all that used in the simulation.

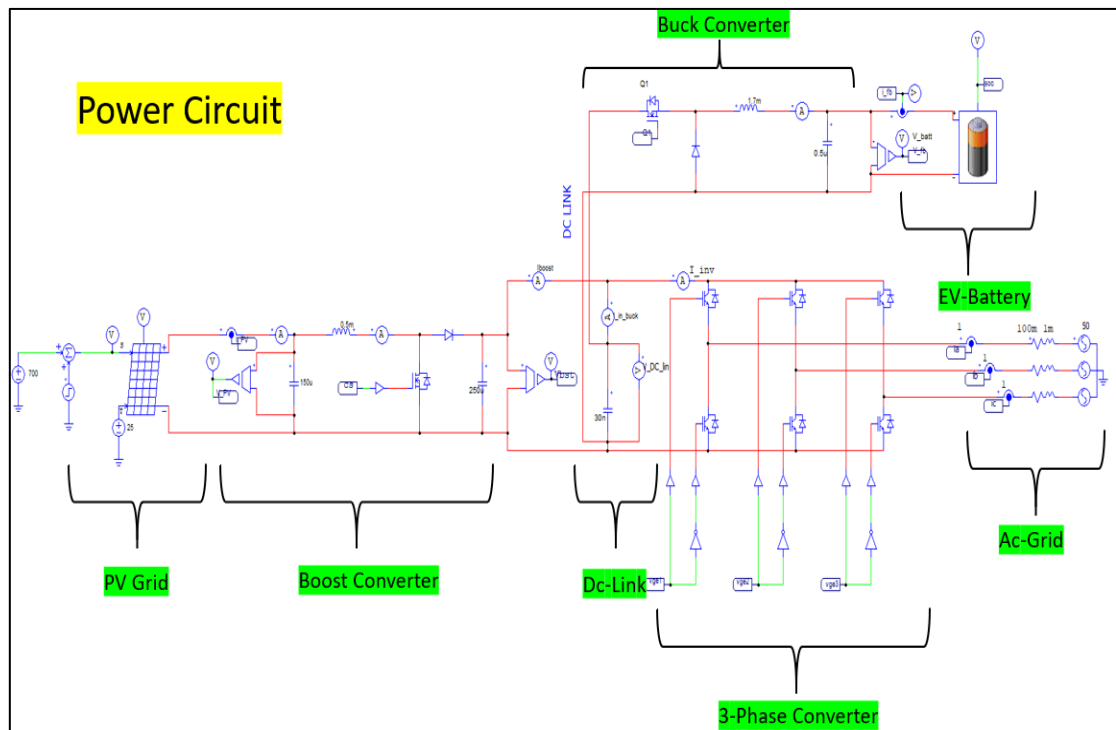


Fig 4. 2: Power circuit of EV-PV-Grid system in PSIM software

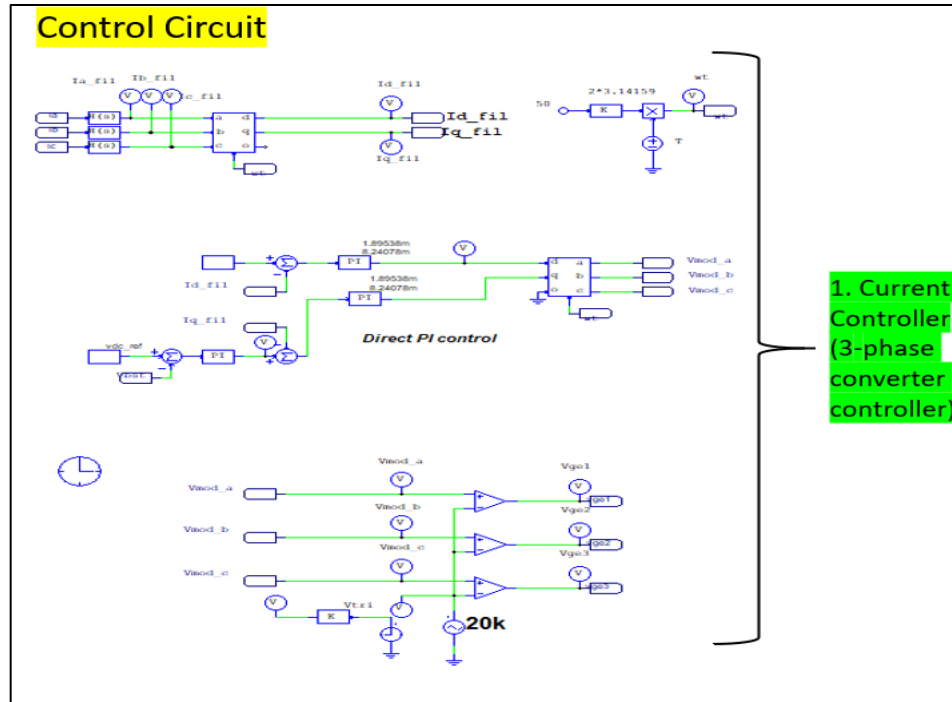


Fig 4. 3: Control circuit of EV-PV-Grid system in PSIM software (Current controller)

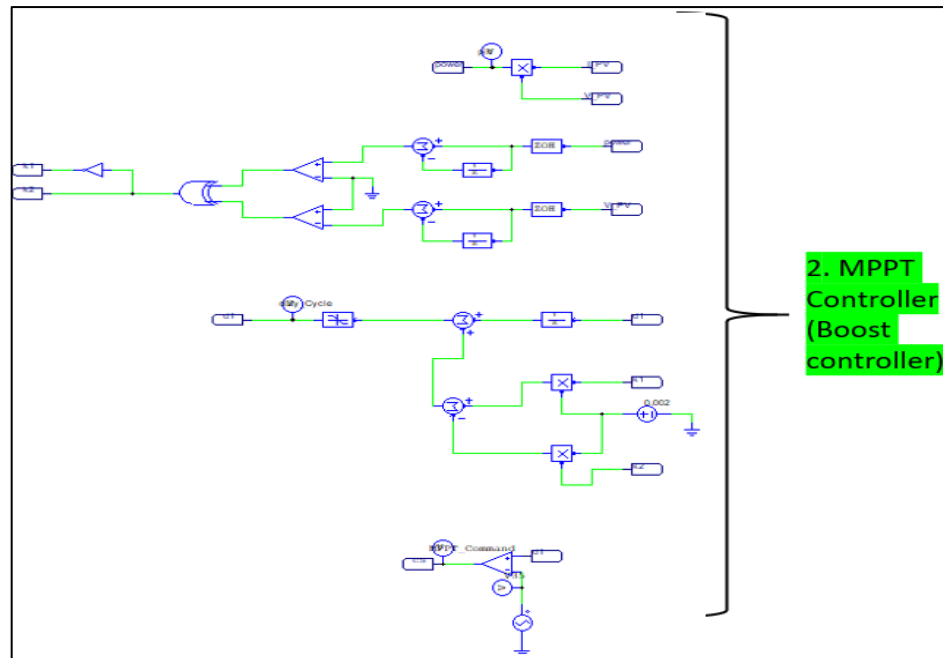


Fig 4. 4: Control circuit of EV-PV-Grid system in PSIM software (MPPT controller)

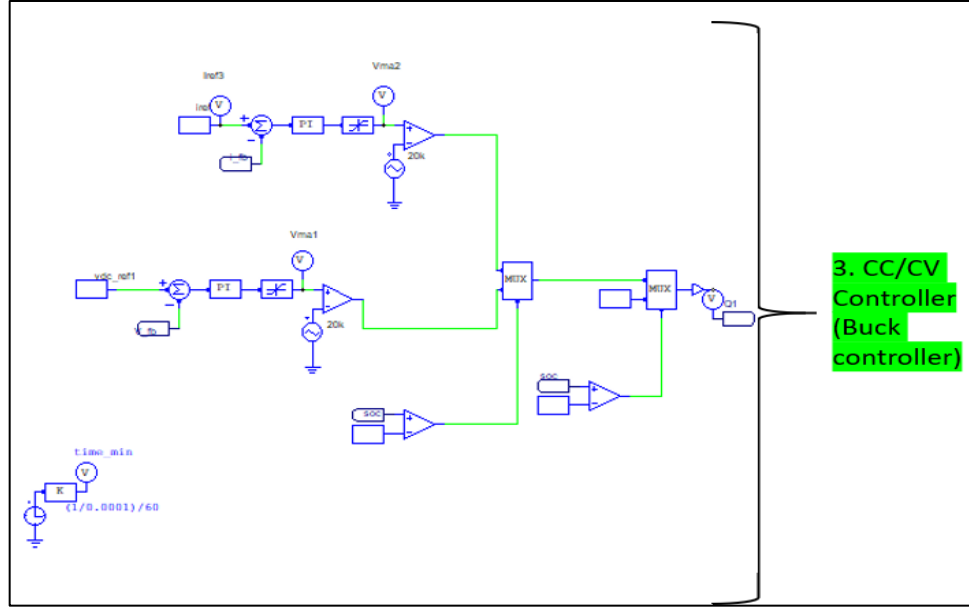


Fig 4. 5: Control circuit of EV-PV-Grid system in PSIM software (Constant Current/ Constant voltage controller).

Table 4. 1: Table explaining the simulation parameters in PSIM software.

PARAMETERS	VALUE
PV GRID	
P_{IN}	22.7kW
V_{PV}	128V
I_{PV}	175A
BOOST CONVERTER	
L_{B0}	0.5mH
C_{B0}	150 μ F
BUCK CONVERTER	
L_B	1.7mH
C_B	0.5 μ F
AC GRID	
V_g	208V
f	60hz
DC LINK	
V_{DC}	500V
C_{DC}	30nF
EV BATTERY	
P_{EV}	19.3kW
V_{BA}	427V
I_{BA}	45A

4.2.1 Simulation condition:

The solar panel, the DC/DC boost converter, MPPT algorithm and the battery are used and explained in chapter 1.

The model of the Grid used in PSIM software is a 3-phase Y-connected sinusoidal voltage source as shown in the figure below; the voltage is set at 208V line-to-line RMS and the frequency at 60Hz.

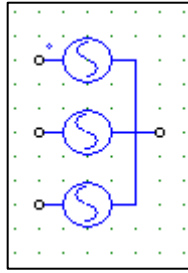


Fig 4. 6: A three-phase y-connected sinusoidal voltage source in PSIM software [34].

The characteristics of the three-phase Y-connected sinusoidal voltage source is detailed and explained in the following figure and table:

Table 4. 2: Table explaining the parameters of a three-phase y-connected sinusoidal voltage source in PSIM software [34].

PARAMETERS	EXPLANATION
V (line-line RMS)	Line-to-line RMS voltage amplitude of the 3-phase source, in V
Frequency	Frequency f , in Hz
Initial angle (phase A)	Initial phase angle for Phase A, in deg.
Series resistance	The series resistance of the source in each phase, in Ohm
Series inductance	The series inductance of the source in each phase, in H

4.2.2 Battery charging method:

The chosen charging method in this project is the constant current/constant voltage (CC/CV) to charge the battery quickly and to obtain a high-performance charging system[39].

First, the battery is charging in constant current mode until the batteries reach the maximum voltage. At that time, the state of charge of the battery is about 80% and the battery continues charging in constant voltage mode[40].

The two modes of constant current/ voltage current charging method are resumed in the following figure:

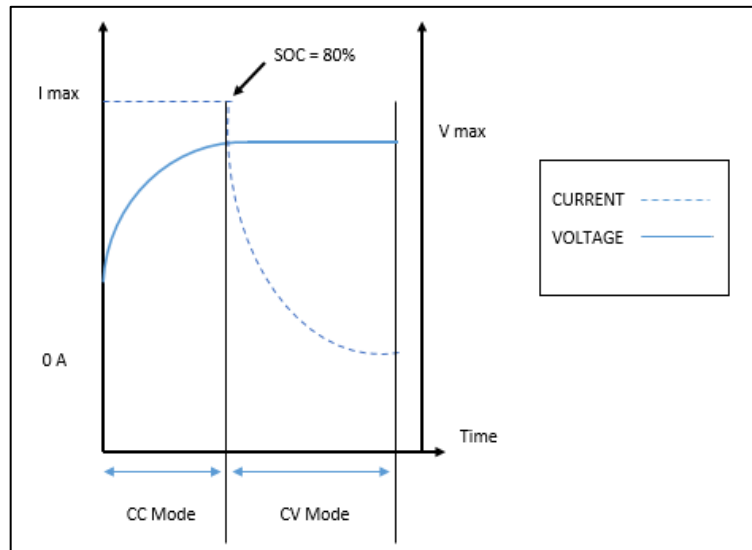


Fig 4. 7: Current-time and voltage-time curve during the charging method [39].

4.2.3 Energy management:

In order to manage the energy between the Grid, EV and PV, three controllers are used in our simulation:

The current control [41], with a voltage reference for the inverter side Grid: the purpose is to operate the inverter in a bidirectional way. In the first direction, the inverter operates as a rectifier (the power flow from the Grid to the DC link) in order to recover the demand of the battery if the PV cannot satisfy the demand. For the second direction the inverter operates as an inverter (the power flow from the DC link to the Grid) in order to feed the extra power provided by the PV to the Grid.

Therefore, the inverter act like a supervisor in our system, it extracts from or feeds to the DC link the necessary power which maintain his voltage at 500V, and which satisfy the demand of the battery.

The output current control for the buck converter of the battery side: the purpose is to control the input current of the battery during the first mode of charging (constant current).

The output current control with a voltage reference: the purpose is to control the battery voltage during the second mode (constant voltage).

The output current control and the output current control with a voltage reference allow drawing the necessary current from the DC link to charge the battery.

4.2.4 Dc link topology:

The PV converter that is responsible for maximum power point tracking, the EV converter controlling the EV charging power and the bidirectional inverter that is responsible for the power balance with the AC grid are connected using a central DC link, which allows exchanging energy between PV, EV and Grid [32].

The DC link act as a high voltage energy buffer between the ports and is preferred due to direct DC charging of EV from PV.

The choice of 500 voltage value across the DC link in the simulation is not made by chance; on the contrary, the DC link is chosen to be higher than the Grid peak voltage (325V).

4.2.5 Grid converter side:

The grid has an essential role in the EV-PV-Grid charging system; in fact, it is an available source at any temperature and any irradiation, which allows charging the EV battery in case the PV cannot provide the necessary power.

In order to transfer the electrical power from the grid to the DC link and vice versa, an AC/DC and DC/AC conversion are necessary. Those conversions are realized by connecting a bidirectional three-phase inverter on the grid side, as shown in the figure below:

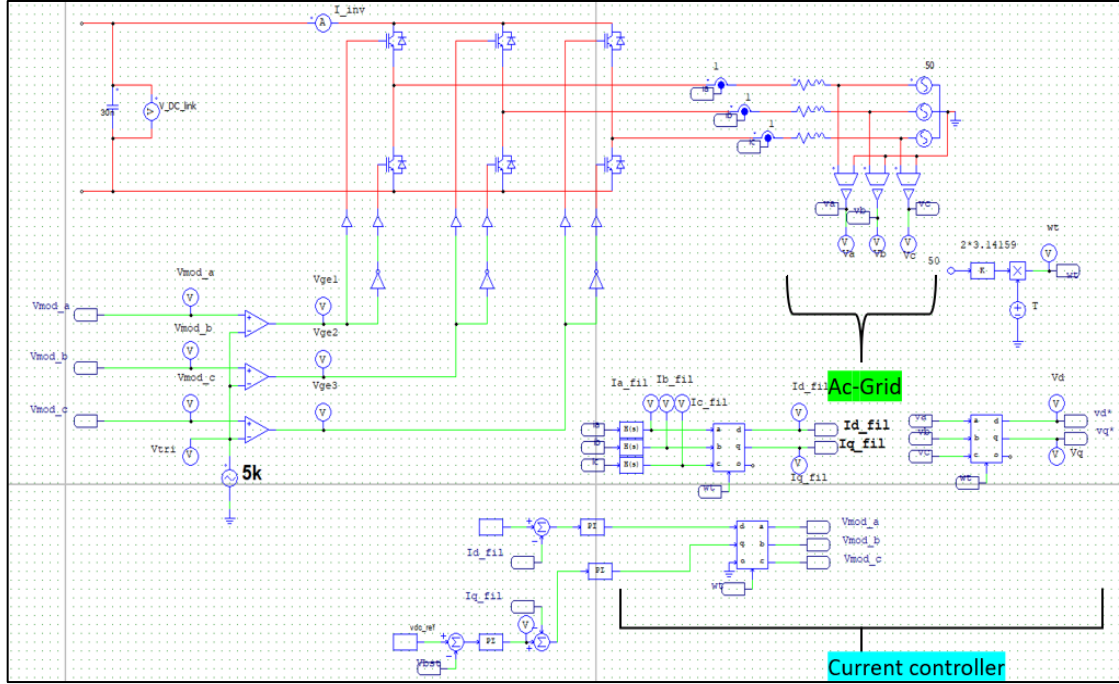


Fig 4. 8: Electric circuit of the grid converter side with a current control

The switches of the inverter are controlled by a current control so that the inverter ensures AC/DC conversion (in case the PV cannot satisfy the demand of the battery) or DC/AC conversion (in case the PV delivers more than the demand of the battery) to maintain the voltage across the DC link at 500V.

The current and voltage sensor measures the current and voltage of the three-phase Y-connected sinusoidal voltage source (Grid) and passes the value to the control circuit.

4.2.5.1 Control circuit operating:

- The grid voltages (V_a, V_b, V_c) are transformed into their dq components V_d and V_q using an abc/dq block.

- The grid-currents (I_a, I_b, I_c) are transformed into their dq components I_d and I_q using an abc/dq block which determines the real power and reactive power exchanged with the grid.
- Three PI controllers are adopted to regulate I_d and I_q : The first is employed to regulate the I_d at 0 amperes, the second is used to generate the reference I_q which regulates the DC voltage at 500V and the third is employed to adjust the I_q current at the I_q reference value.
- The output current of the PI controller I_d^* and I_q^* are transformed into a, b and c components using an abc/dq block to generate the three signal V_{mod_a} , V_{mod_b} , V_{mod_c} .
- The three signal V_{mod_a} , V_{mod_b} , V_{mod_c} are compared to a triangular signal (PWM techniques) in order to obtain the state of the switches.
- The abc/dq transformation block has the ' ωt ' as an input in order to be synchronized with the grid.

4.2.5.2 Control circuit components:

The electric circuit of the current control is presented and detailed below:

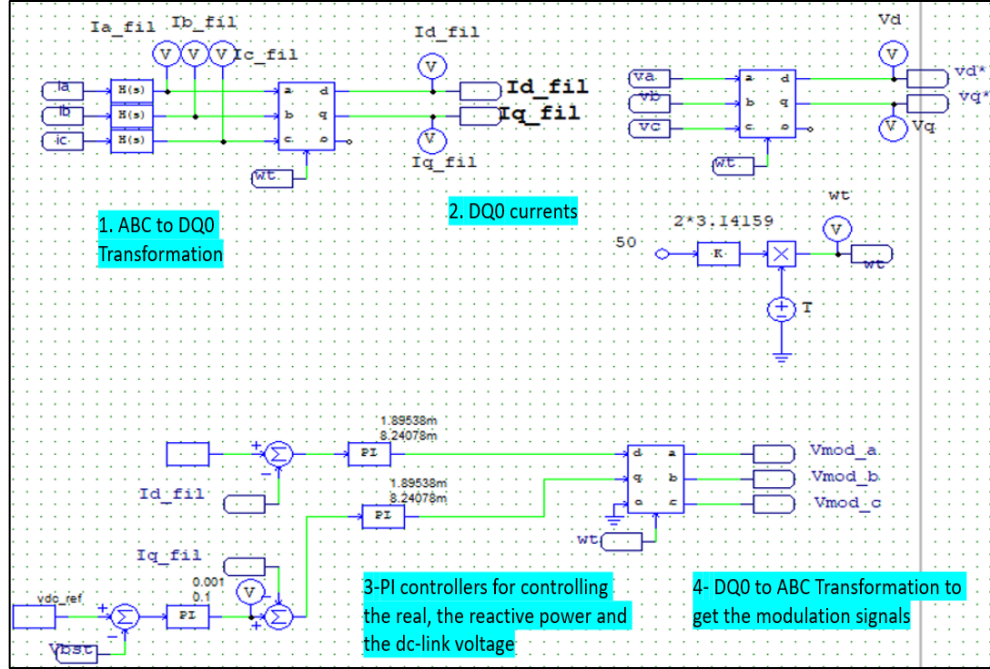


Fig 4. 9: Electric circuit of the current control

- **The abc/dq transformation block:**

Due to the ease of controlling one reference frame d or q instead of controlling three reference frame a, b and c, the current and voltage source are transformed to their dq component using an abc/dq transformation block as shown in the following figure:

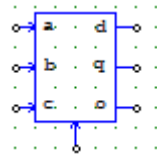


Fig 4. 10: abc/dq transformation block

Depending on the transformation flag, the transformation equations from abc to $dq0$ are as follows:

When the transformation flag is 0:

$$\begin{bmatrix} v_d \\ v_q \\ v_0 \end{bmatrix} = \frac{2}{3} * \begin{bmatrix} \cos\theta & \cos\left(\theta - \frac{2\pi}{3}\right) & \cos\left(\theta + \frac{2\pi}{3}\right) \\ -\sin\theta & -\sin\left(\theta - \frac{2\pi}{3}\right) & -\sin\left(\theta + \frac{2\pi}{3}\right) \\ \frac{1}{2} & \frac{1}{2} & \frac{1}{2} \end{bmatrix} * \begin{bmatrix} v_a \\ v_b \\ v_c \end{bmatrix} \quad (4.1)$$

When the transformation flag is 1:

$$\begin{bmatrix} v_d \\ v_q \\ v_0 \end{bmatrix} = \frac{2}{3} * \begin{bmatrix} \cos\theta & \cos\left(\theta - \frac{2\pi}{3}\right) & \cos\left(\theta + \frac{2\pi}{3}\right) \\ \sin\theta & \sin\left(\theta - \frac{2\pi}{3}\right) & \sin\left(\theta + \frac{2\pi}{3}\right) \\ \frac{1}{2} & \frac{1}{2} & \frac{1}{2} \end{bmatrix} * \begin{bmatrix} v_a \\ v_b \\ v_c \end{bmatrix} \quad (4.2)$$

- **PI controller:**

Three PI is used to control the inverter Grid side. One is employed to control the current d component and the others are employed to control the current q component.

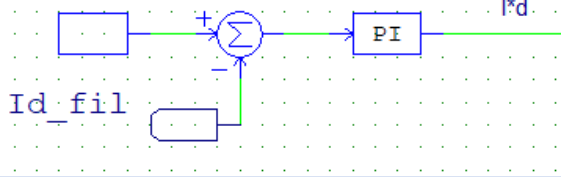
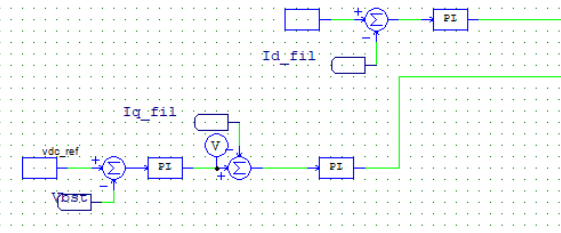
The transfer function of the PI controller is defined as:

$$G(s) = K * (1 + sT) / (sT) \quad (4.3)$$

with K: the gain of the PI controller

T: time constant of the PI controller

Table 4. 3: Table explaining the different control employed for the inverter

CONTROL	ELECTRIC CIRCUIT	EXPLANATION
I_d control		The I_d current value is controlled in order to be adjusted at 0V.
I_q control		The first PI is employed to obtain the necessary current that allows fixing the DC link voltage at 500V, and then this current is used as a reference in the second PI controller.

4.2.5.3 Control circuit design:

With the purpose of selecting the PI parameters, the trial and error method is used in the present system. First, the K is fixed, while increasing and decreasing T and measuring the overshoot and rise time. The choice of each PI parameters used in the control circuit is detailed in the tables below:

- **PI for DC-link control:**

Table 4. 4: The effect of the PI gain on the overshoot and time rise in DC-link controller

T= 0.001		
K	Overshoot	Time rise
0.005	786V	$3.03975 \cdot 10^{-2}s$
0.01	781V	$2.89945 \cdot 10^{-2}s$
0.05	750V	$2.56430 \cdot 10^{-2}s$

Because the third k has the minimum overshoot and time rise, it is selected for the PI controller.

Table 4. 5: The effect of the PI time constant on the overshoot and time rise in DC-link controller

K= 0.05		
T	Overshot	Time rise
0.0005	707V	$1.91836 \cdot 10^{-2} \text{s}$
0.0010	750V	$2.56430 \cdot 10^{-2} \text{s}$
0.0050	723V	$2.88386 \cdot 10^{-2} \text{s}$

Since the first value of T has the minimum overshoot and time rise, it is selected for the PI controller.

- **PI for I_d and I_q control:**

Table 4. 6: The effect of the PI gain on the overshoot and time rise in I_q and I_d controller

T= 0.0019		
K	Overshot	Time rise
0.0022	108A	$4.52065 \cdot 10^{-3}$
0.0082	114A	$2.52294 \cdot 10^{-3}$
0.01	116A	$2.35357 \cdot 10^{-3}$

Because K equal to 0.0082 has the best compromise between the overshoot and time rise, it is selected for the PI controller.

Table 4. 7: The effect of the PI time constant on the overshoot and time rise in I_q and I_d controller

K= 0.0082		
T	Overshot	Time rise
0.0009	118A	$3.67175 \cdot 10^{-3}$
0.0019	121A	$3.57429 \cdot 10^{-3}$
0.01	124A	$2.81741 \cdot 10^{-3}$

As the second value of K has the best compromise between the overshoot and time rise, it is selected for the PI controller.

4.2.6 Battery converter side:

The use of a DC/DC buck converter for the battery side has two essential reasons. On the one hand, it allows stepping down the voltage across the DC-link that is needed for charging the battery. On the other hand, it will enable controlling the battery-charging

mode by controlling the switches with an output current control and an output voltage control.

In this paragraph, the employed control is detailed and the electric circuit of a DC/DC buck converter for the battery side is presented below:

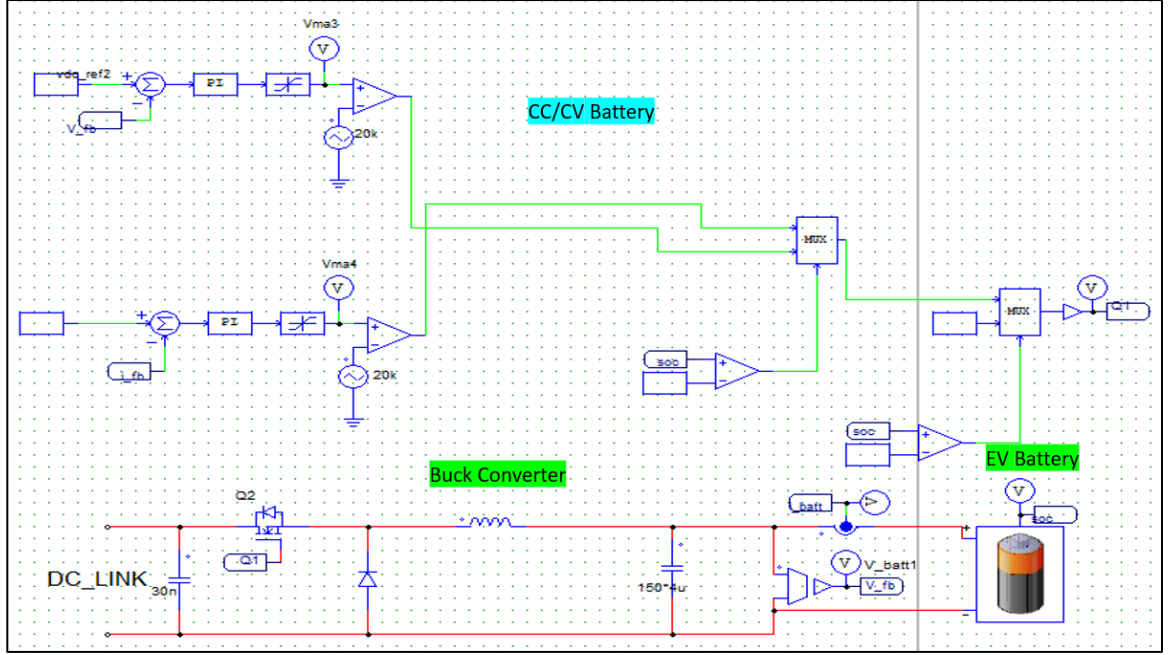


Fig 4. 11: Electric circuit of battery converter side

According to the IEEE 519 Standard, the ripples must not go beyond 8% in the voltage curve and 5% in the current curve[34]. Both values of the inductor and capacitor used in the buck converter are calculated to obtain the acceptable percentage of ripples[35]. The necessary calculation is explained below:

$$D = \frac{V_{out}}{V_{in}} \quad (4.4)$$

$$L = \frac{(V_{in} - V_{out}) * D * T_s}{2 \Delta i_L} \quad (4.5)$$

$$C = \frac{\Delta i_L * T_s}{8 \Delta v} \quad (4.6)$$

With: $2\Delta i_L$: The inductor current ripple peak to peak

$2\Delta V$: The capacitor voltage ripple peak to peak

D: the duty cycle of the buck converter

T_s : The inverse of the switching frequency

V_{in} : Voltage across the input

V_{out} : Voltage across the output

4.2.6.1 Control circuit operating:

While the state of charge of the battery is less than 80%, the charging mode is “constant current.” Once the state of charge exceeds 80%, the charging mode switch from “constant current” to “constant voltage.” Moreover, when the battery is fully charged (SOC=100%), the current is set at 0A.

In order to manage the charging mode of the battery, two controllers are employed: output current control and output voltage control which are explained below:

4.2.6.2 Control circuit components:

The electric circuit of the output current control and output voltage control is presented below:

4.3 EV-PV-Grid charging system simulation results under PSIM software:

The EV-PV-Grid charging system is realized and simulated under PSIM software. The simulation results are presented in this paragraph for different study cases: first, the system is simulated for constant radiation (1000 W/m^2) then for variable radiation.

The initial state of charge of the battery is considered as 0% and the temperature of the solar panel is set at 25 degrees for all the simulation.

4.3.1 Case 1: Constant Irradiation 1000 W/m^2

In this case, the radiation is constant and set at 1000 W/m^2 . The curves translating the variation of the battery voltage, the battery current, the state of charge, the solar panel voltage and current, the solar panel power, the DC-link voltage, the I_q and I_d current, the duty cycle and MPPT command are taken and presented as follow:

4.3.1.1 Battery side curves:

The following figure shows the evolution of the battery voltage, current and state of charge during the charging period.

This figure explains the charging method employed (constant current-constant voltage); when the SOC is less than 80%, the current is constant at 45A and the voltage grows gradually. Once the SOC reaches 80%, the voltage becomes constant at 431V and the current decreases until 0A for a SOC equal to 100%. After 80 minutes, when the battery is fully charged, the voltage decreases to 428V, which corresponds to the empty voltage across the battery for a SOC equal to 100%.

The curves shape and the values of the constant voltage and current ensure the proper functioning of the output current control and output voltage control used for the battery side converter.

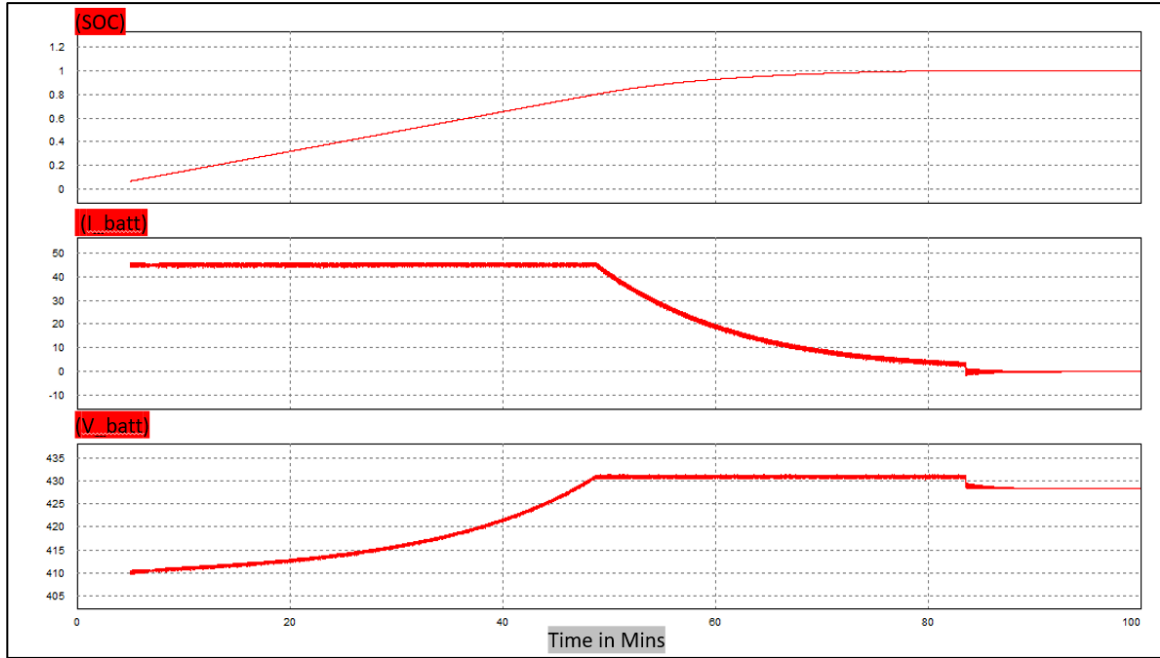


Fig 4. 13: Battery state of charge, current and voltage curves during the charging period in a PV-EV-Grid charging system for a constant irradiation

In order to calculate and check that the ripple did not exceed 8% for the voltage and 5% for the current, the current and voltage curves are zoomed as presented. For the battery current, the current ranges from 43.65A to 45.63A, so the ripples present 4.4% of the total value. While for the battery voltage, the voltage ranges from 430.555V to 431.4063V, which lead to a 0.2% ripple value.

Those ripples percentages are accepted. In addition, they confirm the optimal choice of the inductor and capacitor of the buck converter.

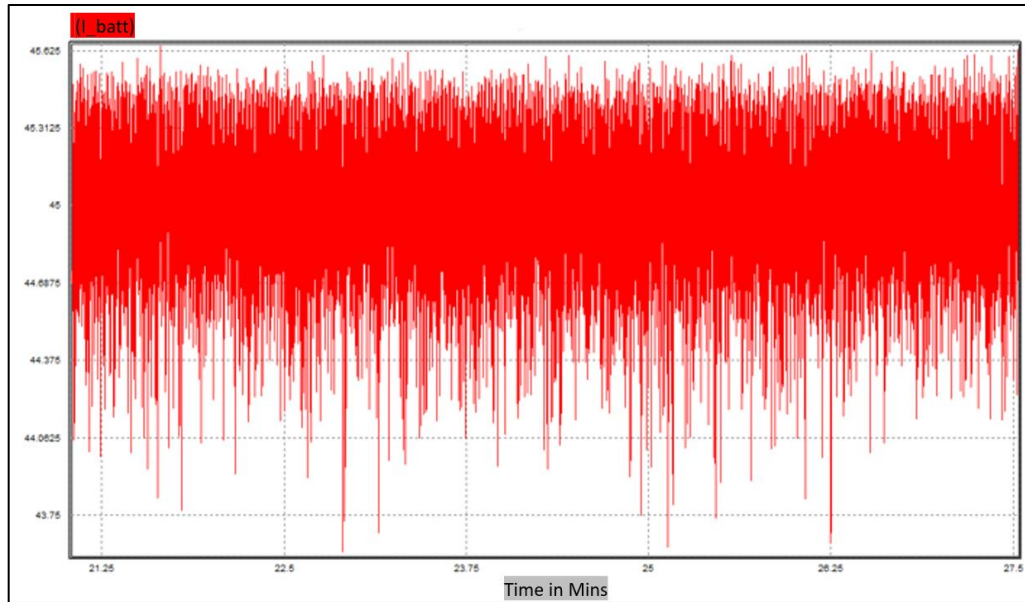


Fig 4. 14: Zoomed part of battery current in EV-PV-Grid system showing the ripple for a constant irradiation

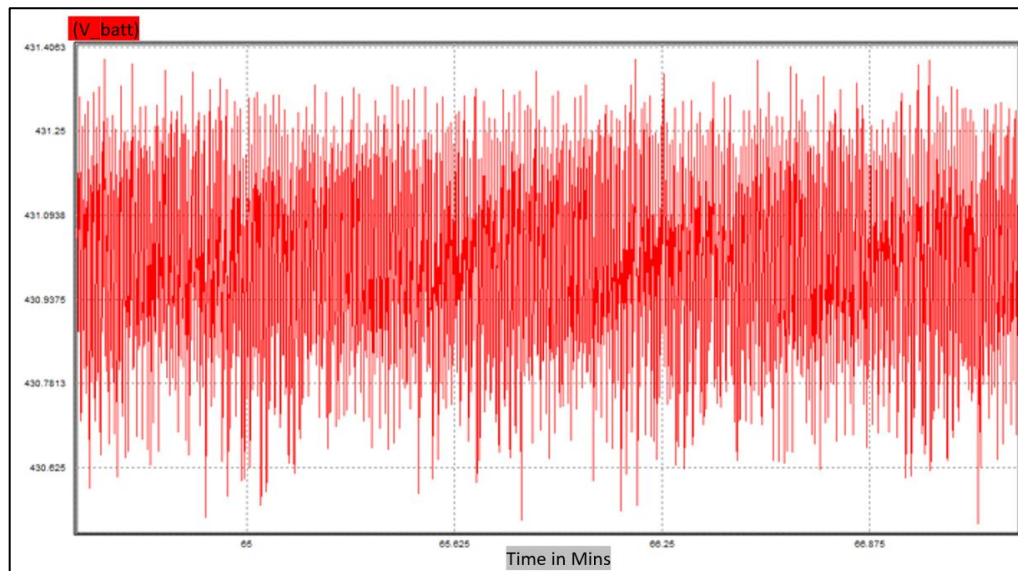


Fig 4. 15: Zoomed part of the battery voltage in EV-PV-Grid system showing the ripple for a constant irradiation

4.3.1.2 PV side curves:

From the curves obtained below, the solar panel used in the system simulation delivers a constant voltage with an average value worth 128V ranging from 115V to 135V, and a constant current with an average value worth 175 ranging from 169.75A to 181.05A.

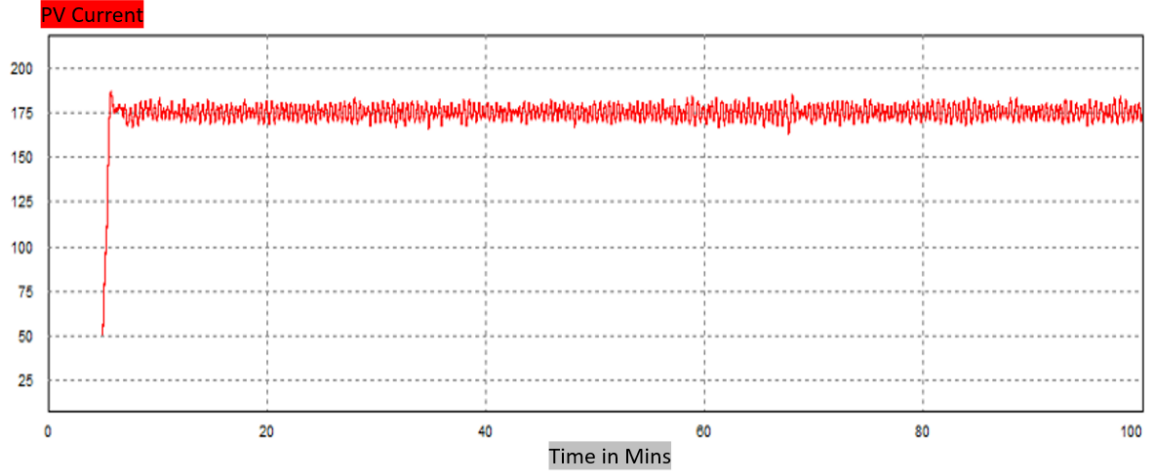


Fig 4. 16: The evolution of PV current during the charging period in a PV-EV-Grid charging system for a constant irradiation

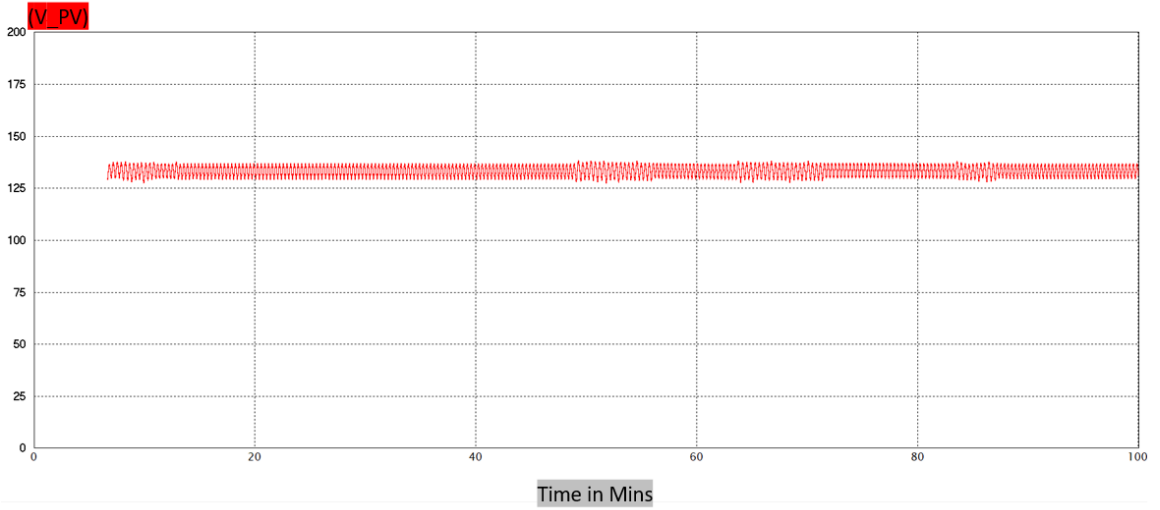


Fig 4. 17: The evolution of PV voltage during the charging period in a PV-EV-Grid charging system for a constant irradiation

The power P_{max} is the maximum power that can be provided by the solar panel, which is around 22700 W. As observed in the third figure, the exploited power P_{in} (the green curve) from the solar panel is nearly the same as the maximum power. This shows the smooth running of the MPPT employed.

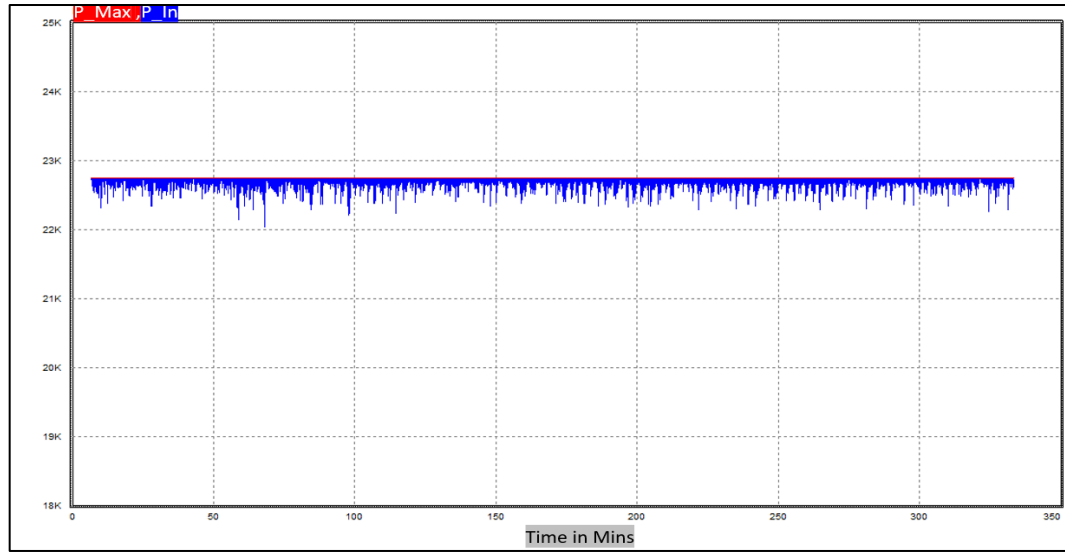


Fig 4. 18: The evolution of the maximum power delivered by the PV and the extracted power during the charging period in a PV-EV-Grid charging system for a constant irradiation

The following curves explain the operating of the maximum power tracker algorithm. The first curve translates the pace of the duty cycle, which is compared to a triangular-wave voltage source, as shown in the second curve. The third curve illustrates the command of DC/DC boost converter switches: if the duty cycle is higher than the triangular-wave voltage, then the state of the switch is one; else, the state of the switch is zero.

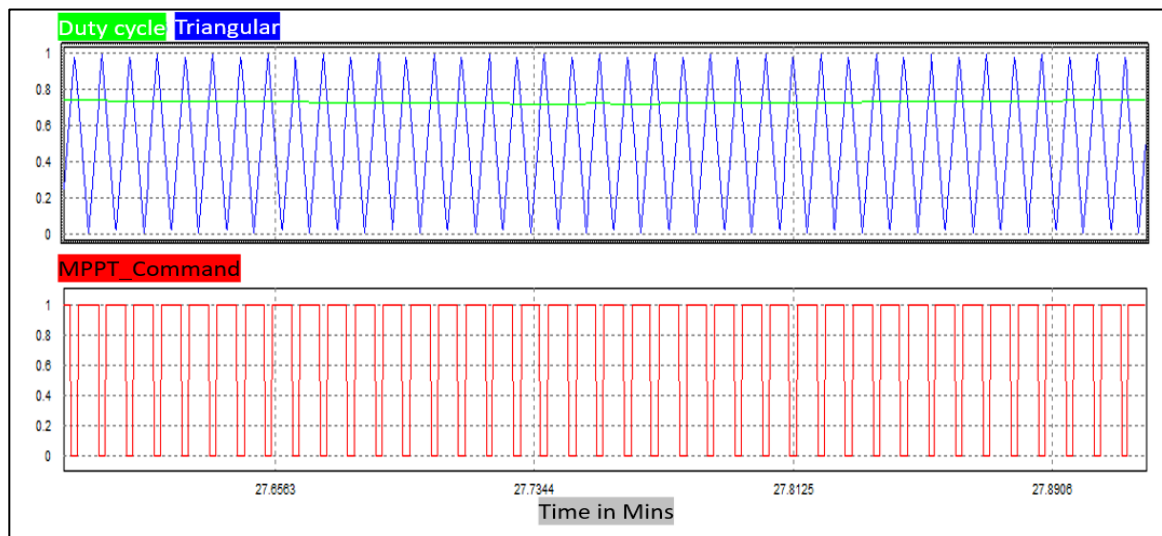


Fig 4. 19: Duty cycle, triangular wave and MPPT command curves translating the operating of PWM in a PV-EV-Grid charging system

4.3.1.3 Inverter curves side:

The sign of input inverter current allows knowing if the Grid is rewarding the needed power to charge the battery or extracting the extra power delivered from the solar panel. As noticed from the curves below, the current at the input of the inverter is positive, so the extra power delivered by the solar panel is fed to the Grid.

The current injected in the grid worth 8.18A and started increasing until reaching 44.7A. Once the SOC exceeds 80%, this evolution is explained by the evolution of the battery current. For a state of charge between 0% and 80%, the charging mode is ‘constant current’ and the needed current to charge the battery is 45A. So, the DC/DC boost converter's output current that is worth 44.7A is divided into two-part, the first for the battery (input buck converter current equal to 36.5A) and the rest is injected into the grid when the SOC exceeds 80%, the needed current to charge the battery decrease so the injected current to the grid increase.

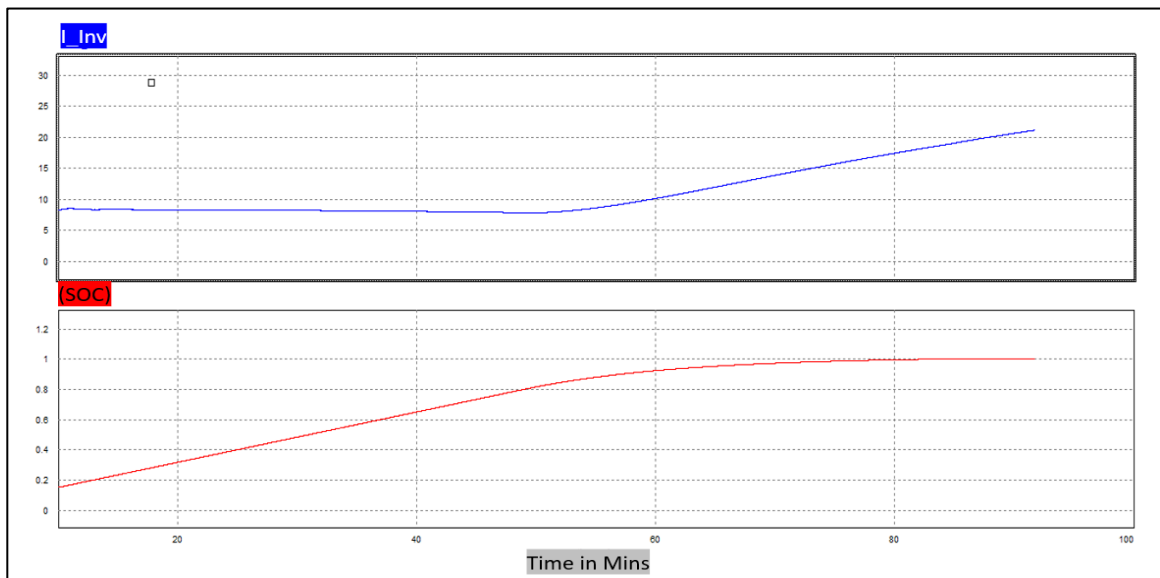


Fig 4. 20: Curve translating the inverter input current during the different state of charge in EV-PV-Grid charging system for a constant irradiation

The schema below details more the evolution of the input inverter current. For constant irradiation, the output boost current marked in blue is constant and the buck input current marked in green is less than the boost output current, so the extra is injected to the grid as marked in red. When the SOC reaches 80%, the buck input current decrease gradually and the input inverter current increase. The current fed to the grid continues increasing until reaching the value of the boost output current.

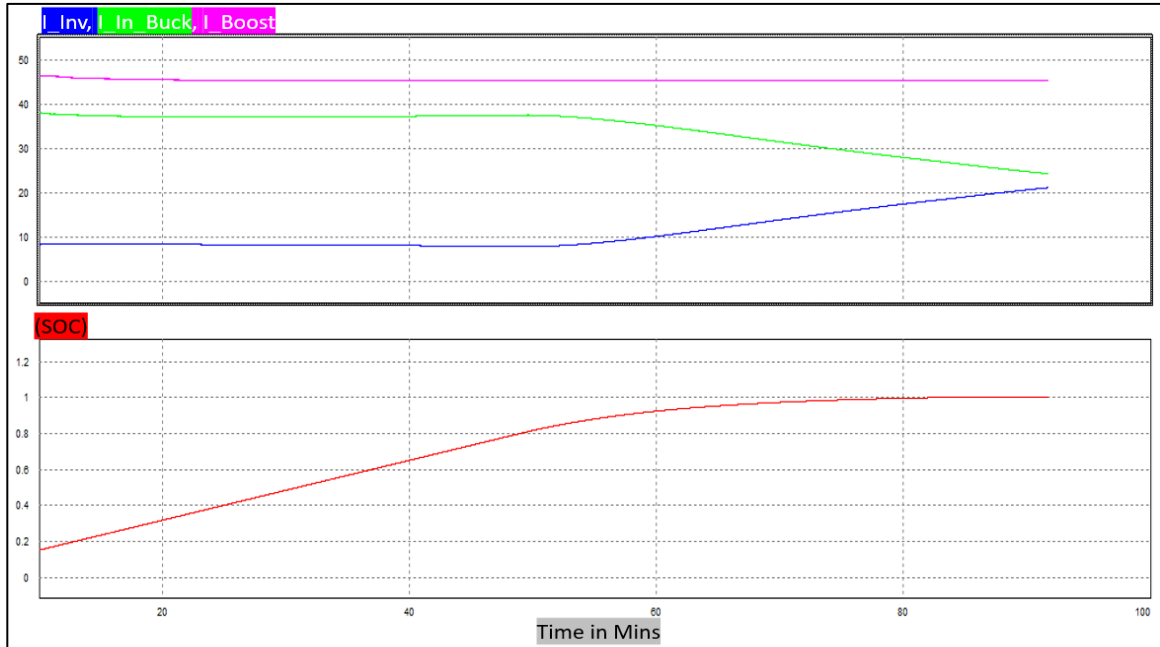


Fig 4. 21: Waveforms translating the input inverter, output boost and input buck current in EV-PV-Grid system for a constant irradiation

The inverter AC current waveforms are presented below. When the state of charge is less than 80%, the inverter AC current waveforms is a three-phase current with an amplitude around 12.5A. Once the state of charge exceeds 80%, the inverter AC three-phase current increase amplitude until reaching 75A with the increase of the inverter DC current.

The waveforms of the injected current prove the controller robustness and the low ripples prove the smooth choice of the current filter.

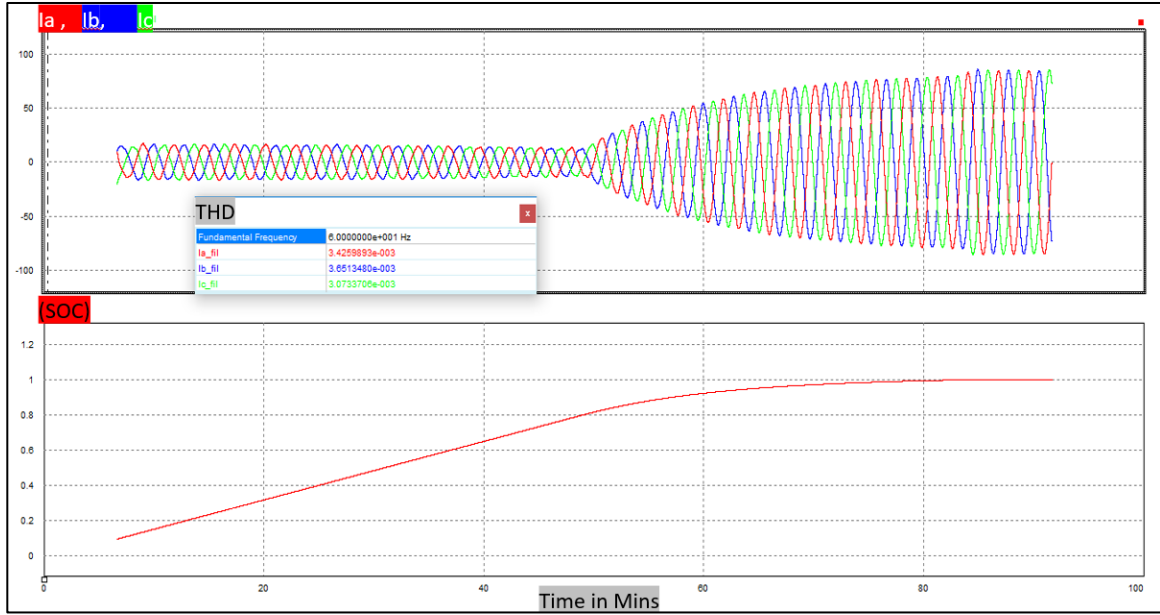


Fig 4. 22: The inverter AC current waveforms in EV-PV-Grid charging system for a constant irradiation

A zoomed-in for the inverter AC current was done to verify the synchronization and phase-shift. The first waveform was zoomed in for a state of charge less than 80% when the second waveform was zoomed in for a state of charge greater than 80%.

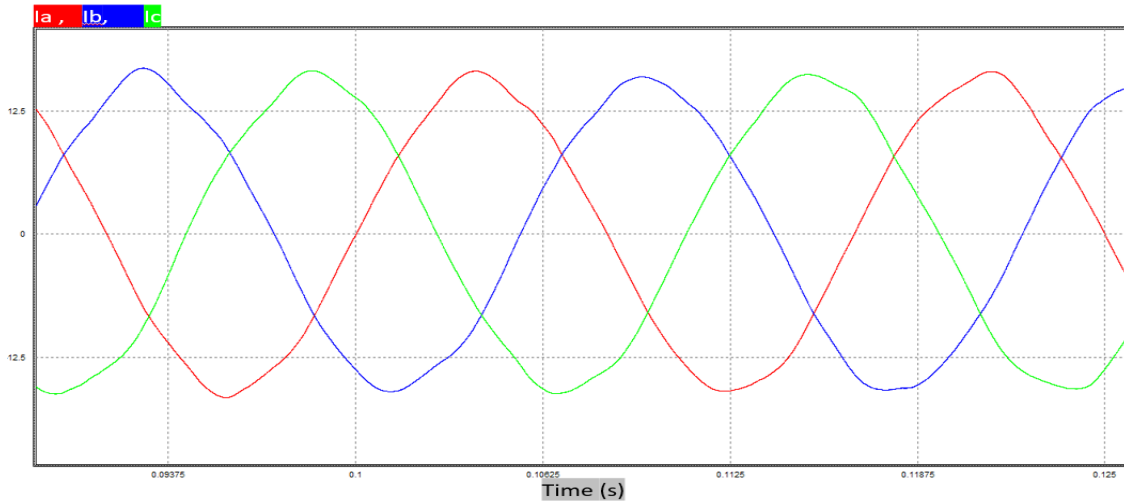


Fig 4. 23: Zoomed in for the inverter three-phase AC current during a SOC less than 80% in EV-PV-Grid charging system with a constant irradiation

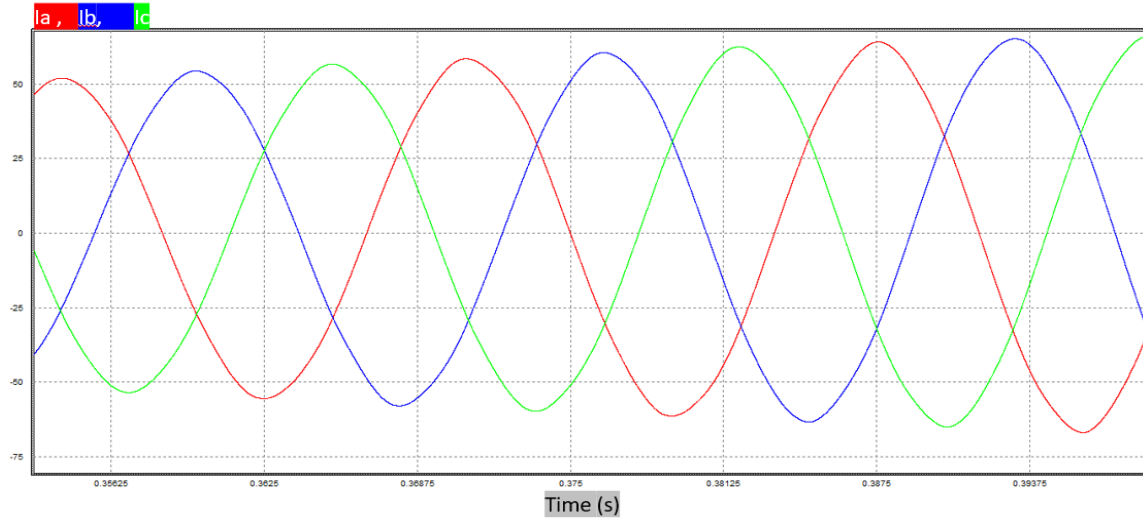


Fig 4. 24: Zoomed in for the inverter three-phase AC current during a SOC greater than 80% in EV-PV-Grid charging system with a constant irradiation

4.3.1.4 DC-link curve:

The voltage across the DC-link is presented as follows. As it can be observed, the voltage is constant during the system simulation around 500V, contains some ripples beyond the limits.

The DC-link voltage is maintained constant that confirms the adequate choice of the employed current control.

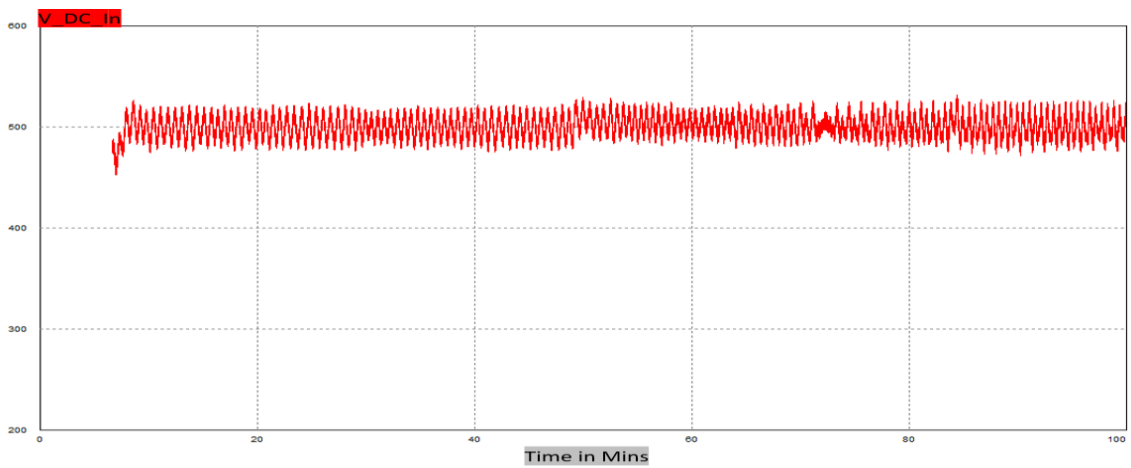


Fig 4. 25: Curve translating the voltage across the DC-link in a PV-EV-Grid system for a constant irradiation

4.3.2 Case 2: variable radiation:

In this case, the radiation is variable starting from 700 W/m^2 to 1000 W/m^2 as shown in the figure below:

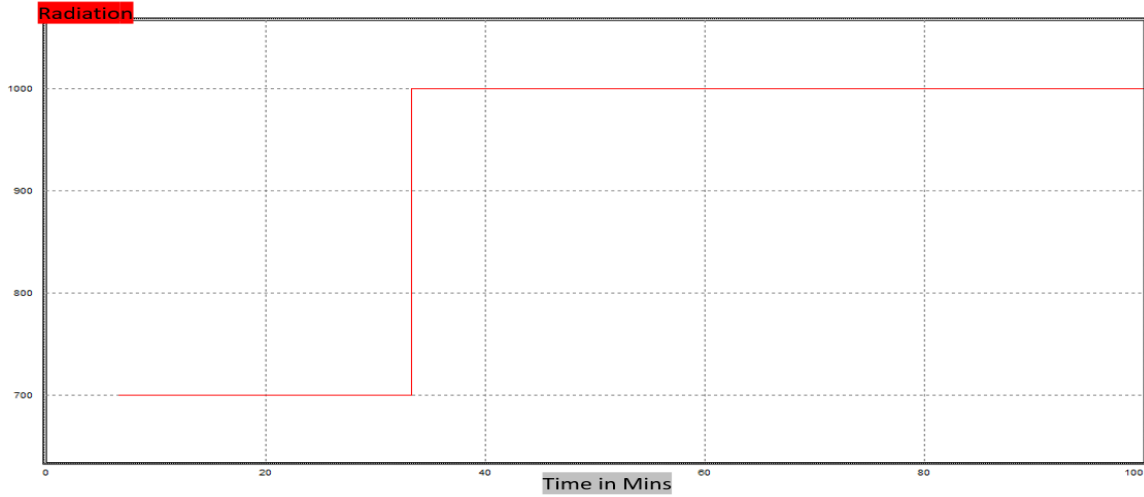


Fig 4. 26: Curve translating the variable irradiation in EV-PV-Grid charging system

The curves summarizing the variation of the radiation, the battery voltage, the battery current, the state of charge, the solar panel voltage and current, the solar panel power, the DC-link voltage, the I_q and I_d current, the duty cycle and MPPT command are taken and presented as follow:

4.3.2.1 Battery side curves:

The following figure shows the evolution of the battery voltage, current and state of charge.

As observed, the curves are the same as case number one studied above (constant radiation). For any radiation, the battery can be charged at the same time (80min) and with the same current and voltage. That means that the grid can supply the battery when the PV

cannot satisfy the demand. Thus, the current control employed in the system is doing the required energy management.

The ripple in the battery curve is less than 8%, and in the current curvet are less than 5%

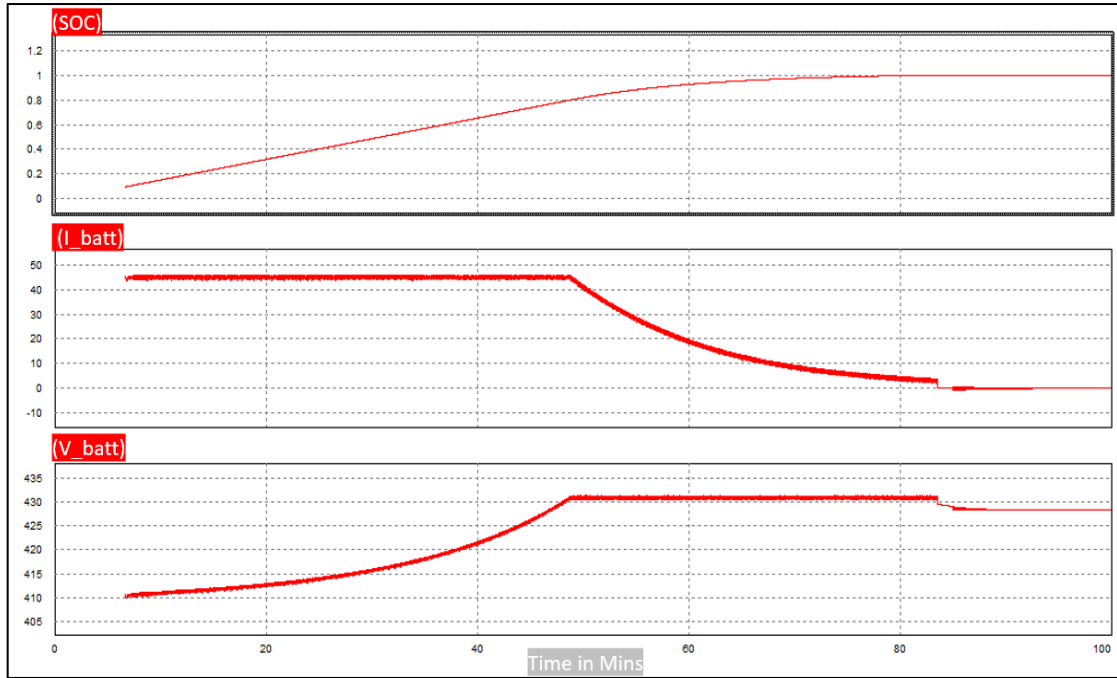


Fig 4. 27: Battery state of charge, current and voltage curves during the charging period in a PV-EV-Grid charging system for a variable irradiation

4.3.2.2 PV side curves:

From the PV side curves, it is evident that the current and maximum power provided by the solar panel increase with the increase of the radiation. By contrast, the voltage decrease.

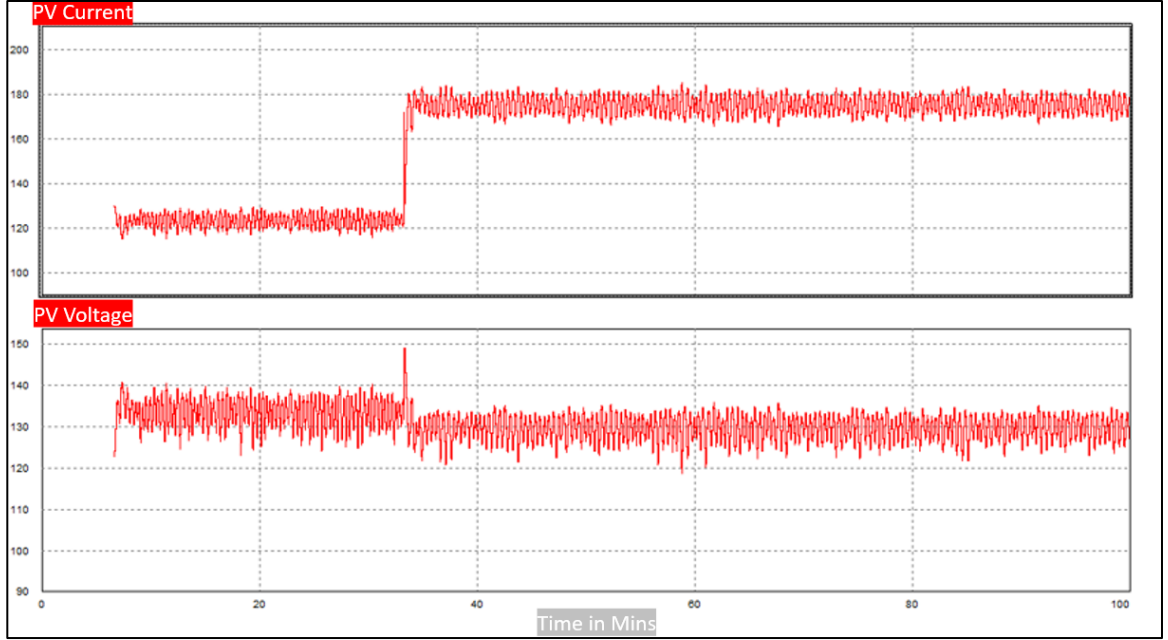


Fig 4. 28: The evolution of PV voltage and current during the charging period in a PV-EV-Grid charging system for a variable irradiation

During radiation equal to 700, the maximal power is 16.5Kw. On the other hand, for radiation equal to 1000, the maximal power reaches 22.7kW.

Always the MPPT allows extracting the maximum power from the PV, which is observable in the following figure.

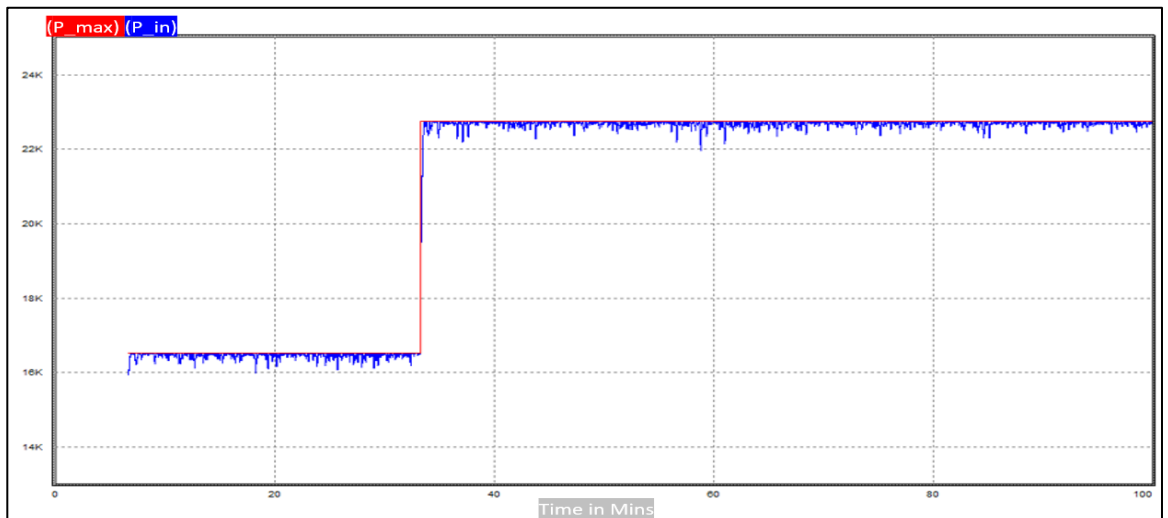


Fig 4. 29: The evolution of the power delivered by the PV and the extracted power in an EV-PV-Grid charging system for a variable irradiation

4.3.2.3 Inverter side curves:

It is noticed that when the radiation is equal to 700, the input of the inverter is negative. That means the PV cannot provide the needed power to charge the battery and the grid is supplying the lack of power. When the radiation is 1000, the solar panel can satisfy the demand of the battery and the extra delivered power is fed to the grid, which explains the positive sign of the inverter input current.

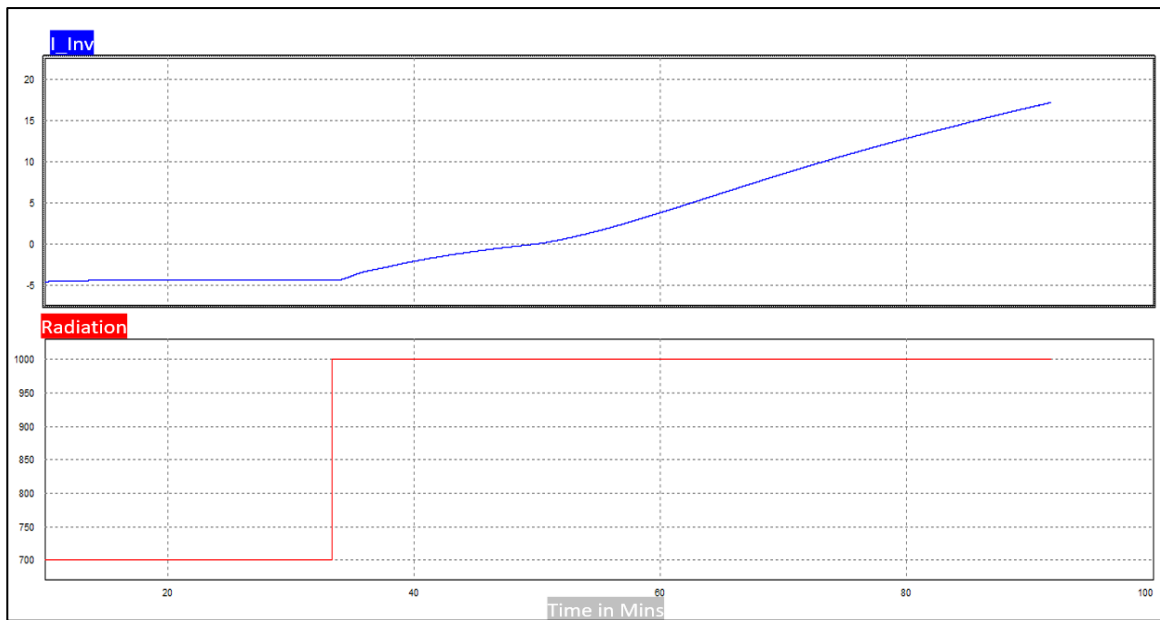


Fig 4. 30: Curve translating the inverter input current during the different state of charge in EV-PV-Grid system for a variable irradiation

The figure below translates the boost output current, the buck input current and the inverter input current. As it is seen, when the irradiation is worth $700\text{W}/\text{m}^2$ the grid is supplying the missing power to the battery. When the irradiation increase, the extra current is produced by the PV panel flow to the grid. When the battery is fully charged, the inverter input current continues increasing until reaching the same value of the output boost current value and the input buck converter continues decreasing until reaching 0A.

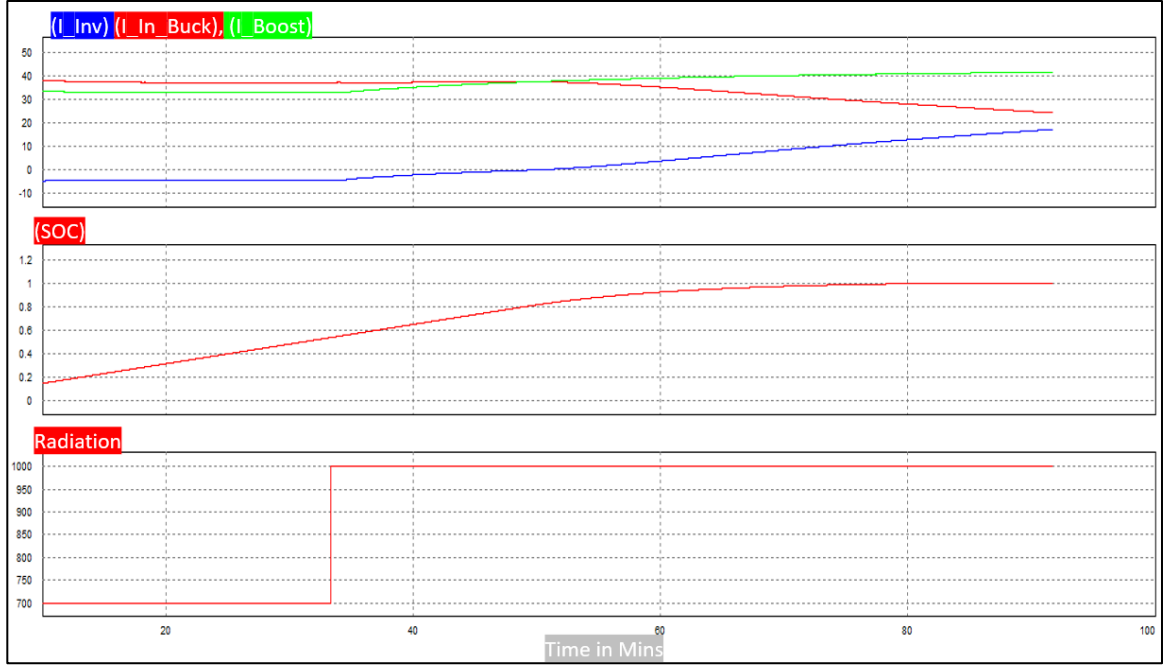


Fig 4. 31: Waveforms translating the input inverter, output boost and input buck current in EV-PV-Grid system for a variable irradiation

As observed in the following waveforms, for irradiation equal to $700W/m^2$. The grid supplies the missing power to charge the battery. The inverter AC three-phase current flow from the grid to the inverter with an amplitude equal to 8.7A. When the irradiation is equal to $1000W/m^2$. The solar panel can provide the needed power for the battery charging, so the inverter AC three-phase current flows from the inverter to the grid with an amplitude around 12.5A. Once the charging mode switch from the constant current mode to the constant voltage mode, the inverter AC three-phase current increases gradually and reaches 75A, which is justified by the rise of the inverter DC current.

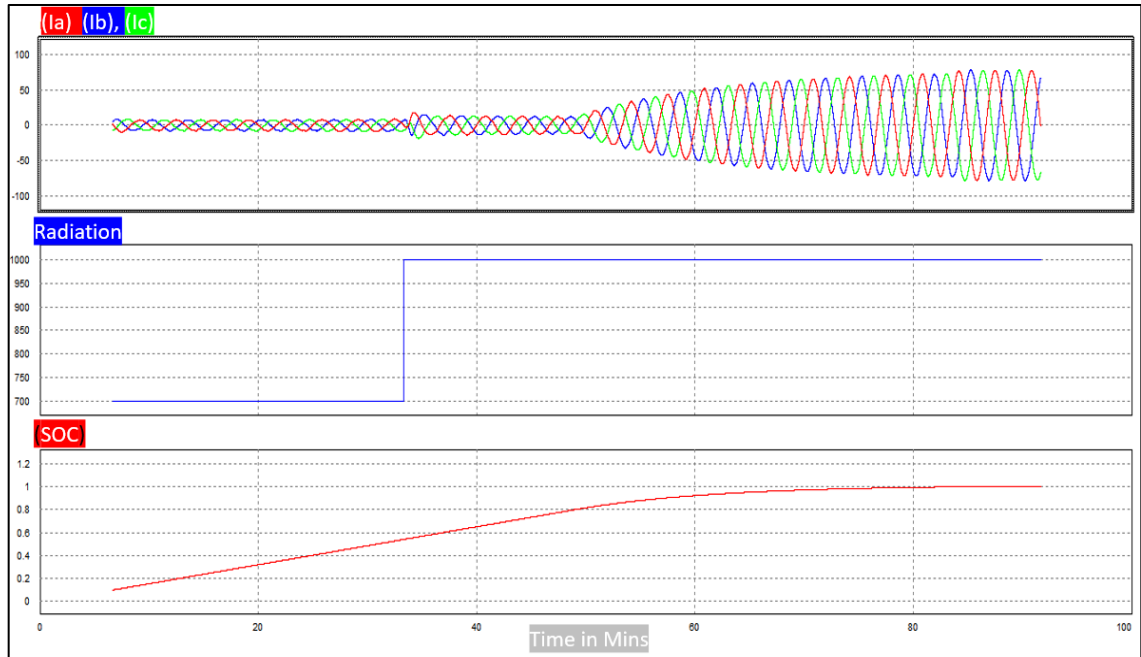


Fig 4. 32: The inverter AC three-phase current waveforms in an EV-PV-Grid charging system for a variable irradiation

4.3.2.4 DC-link curve:

For different radiation values, the DC link is constant around 500V. Also, the ripple has not exceeded the limits. The change of the radiation affects the stability of the DC-link voltage, but a few seconds later (0.027s), the voltage stabilizes again. This ensures the correct choice of the PI controller.

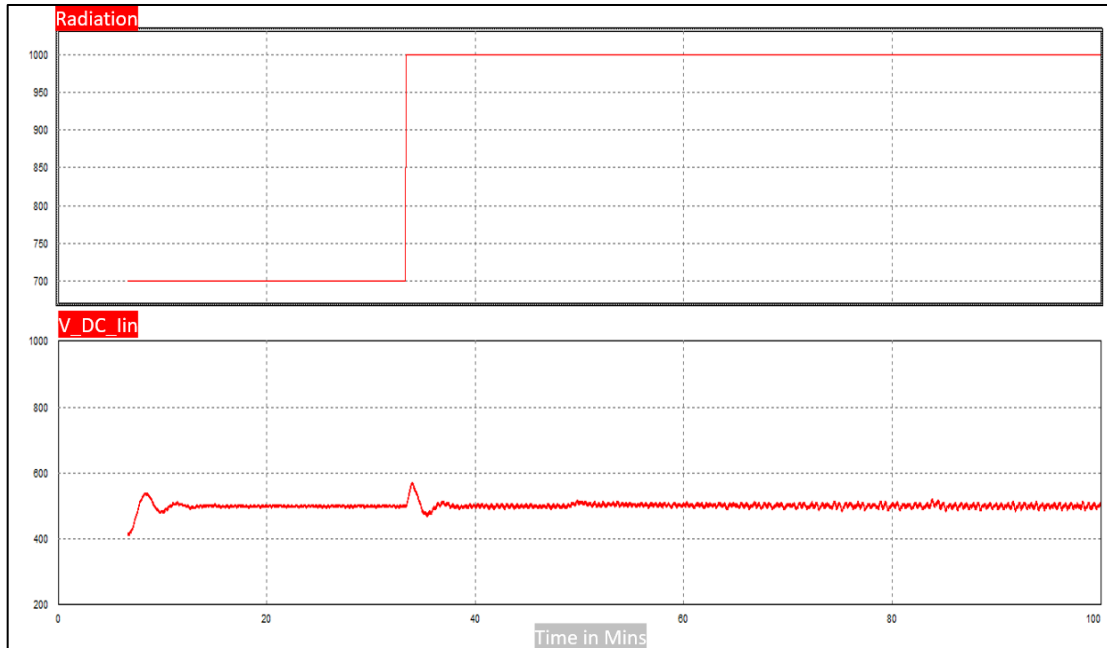


Fig 4. 33: Curve translating the voltage across the DC-link in a PV-EV-Grid system for a variable irradiation

4.3.3 Case 3: The Effect of Sudden Change of Grid voltage on the charger controller stability

On the off chance that any surprising change in the electric power gracefully may cause numerous issues in the enterprises, homes, workplaces. Voltage variances in the electrical power supply have a reduced impact on the associated load. These variances of over voltage and under voltage are created by numerous reasons which resemble voltage surges, restricting, over-burden and so on.

So that it is essential to study this case to understand what will happen to the system? and what is the response of the controller?

The voltage of the grid changes to 180V and 300V to simulate both Undervoltage and Overvoltage respectively.

The results show that there is no change on the battery side voltage and current which confirm that the controller is working very well to manage the increase or the decrease in power to maintain the stability of the charging process, as shown in Fig 4.32

The dc-link voltage remains constant at 500V and the ripple in the battery curve is less than 8%, and in the current curve is less than 5%

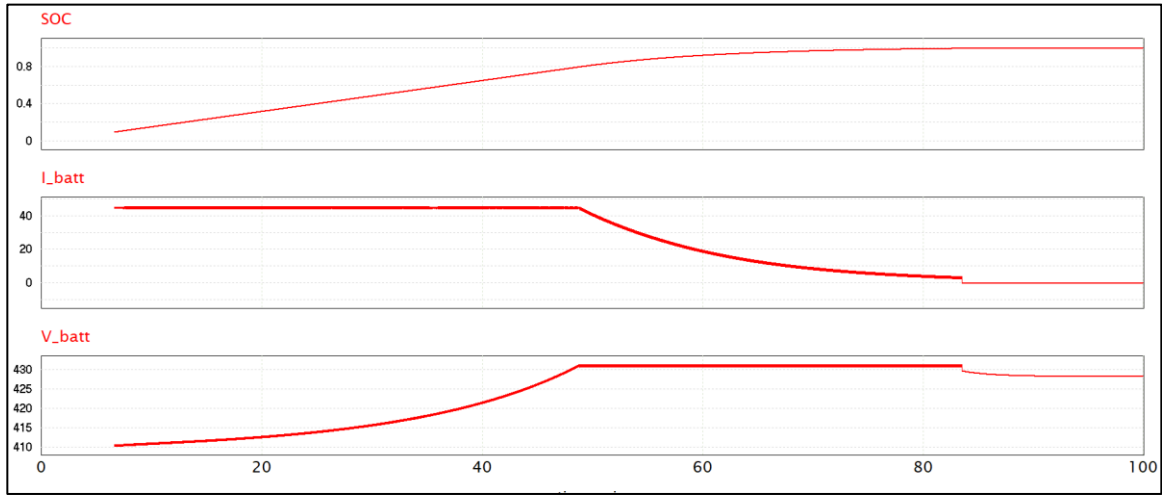


Fig 4. 34: Battery state of charge, current and voltage curves during the charging period in a PV-EV-Grid charging system for variable irradiation for Under/Overvoltage conditions

4.4 Conclusion

In this chapter, an EV-PV-Grid system was realized under PSIM software and simulated for different cases. In the first case, the solar panel was operating on constant irradiation that was able to charge the battery without the grid's intervention. In the second case, the irradiation was variable, and the PV was not always able to supply the battery, so the grid covered the missing power.

The simulation results showed the proper functioning of the energy management employed in the realized design

Chapter 5. The Experimental Test

5.1 The Experimental Setup

The experimental setup is shown in fig 4.33 was utilized to design an off-grid Photovoltaic Inverter for Residential Applications as the first stage of developing the whole charger and to do the comparison with the simulation results after that.

The test is consisting of two ports system was studied; the EV and the PV. The third port to complete the system is the grid.

However, there are extra conditions must be obtained to correctly connect the grid to the experimental setup such as: Verifying the synchronization and phase-shift for the grid fundamental components.

Unfortunately, due to COVID-19 situation, the work on the experimental setup stopped at this point, so in this Chapter, the results only represent the first part of the whole system (off-grid case study).

The following elements are used in the setup:

1. Oscilloscope.
2. Signal generator.
3. 12 V DC power supply
4. Multi-meter.

The specification of each component is presented in Table 4.8

Table 4. 9: The specification of each component in the experimental setup

	Model	Specification
Transformer	Hammond Manufacturing 166N12B-BULK	117V, 48VA, sec: 12V,4A.
Digital Oscilloscope	TBS 1052B-EDU	50 MHz,
Half Bridge	726-BTN7960B	8 V to 18 V
Buffers & Line Driver Buffer	595-SN74HC244APWR	3-State Outputs
2-Input NAND Gate	512-MM74HC00SJX	
Arduino Mega	2560 Rev 3	16 MHz
Inductors 47uH	-	47uH
Solder wire	-	-
12VDC 1A Power Supply	Aim TTI EX1810R	18 V 10 A
4 Channel Relay	MPN: MCS01584R	35V 2A
PCB Fabrication	ACS723	-

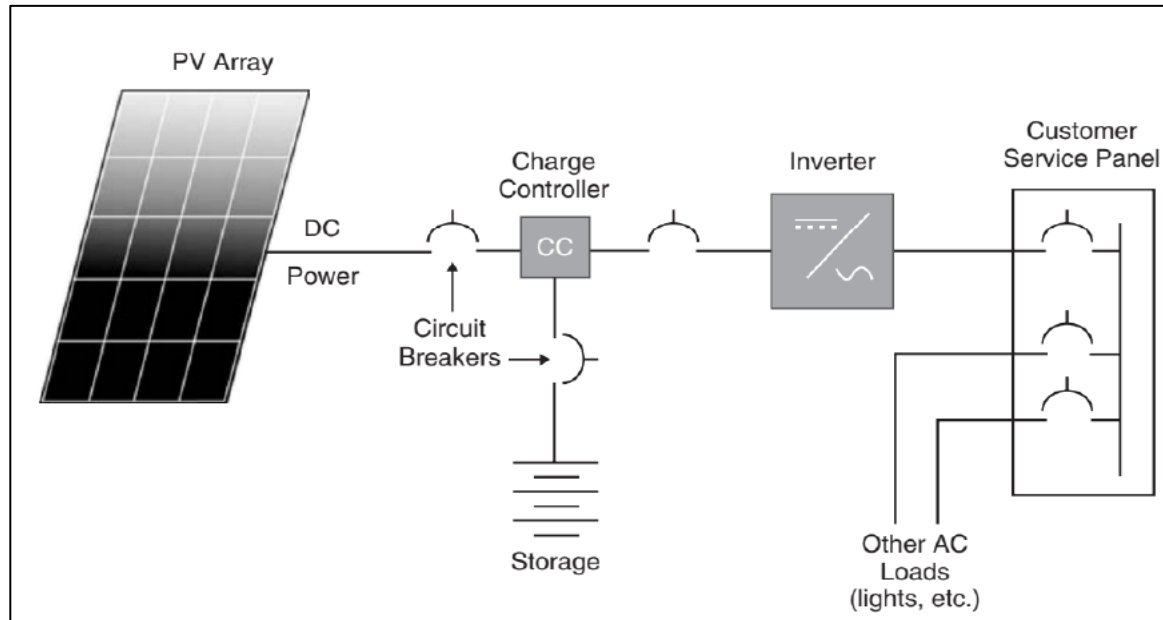


Fig 4. 35: Off-grid system simplified block diagram

The goal of a DC/AC power inverter is typically to take DC power provided by a battery, such as a 12 volt PV connected battery, and convert it into a 120 volt AC power source with a frequency of 60 Hz, emulating the power available at an ordinary household electrical socket.

The first stage of the inverter is typically a DC-DC converter that controls the PV panel to ensure that it operates at its MPP. Then, that PV power is delivered to an inverter stage that provides the PV power to the load. In the off-grid system, the inverter must independently create its output voltage signal in terms of amplitude and frequency.

Off-grid systems supply a local load and when the panel's generation exceeds the load demand the excess energy is usually stored in a battery system for later use.

5.2 Experimental Results

In the design process, all subsections of the design related to wires to inspect the correctness of the theoretical designs. In order to reach a functional result in the first step, the connection between Arduino, Full-bridge module, and transformer is made like Figure 4.34. The designed inverter generates the AC output with the predefined properties. The output of the circuit is depicted in Figure 4.35, which seems acceptable for a functional result. As the next step, a PCB must be designed to integrate the microcontroller and full-bridge sections. Also, the load effect on the circuit must be analyzed.

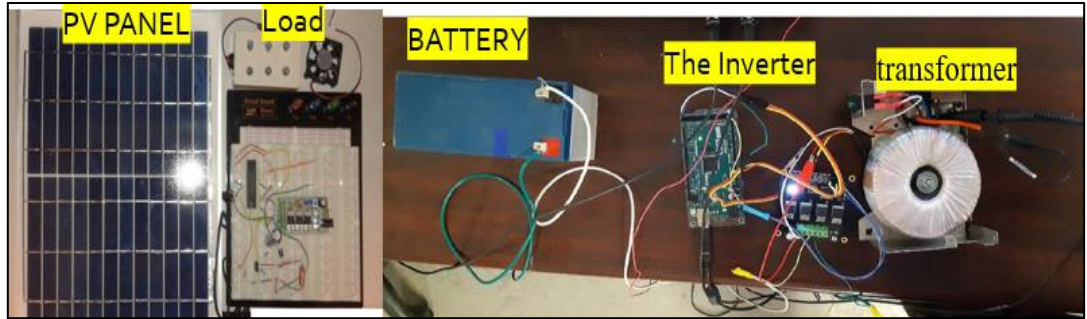


Fig 4. 36: Hardware implementation of single-phase inverter.

The inverter is designed to supply the output load with 120V.

The simulation results are compared to the practical one for the output voltage. In addition, the gating signal is shown in Fig 4.38.

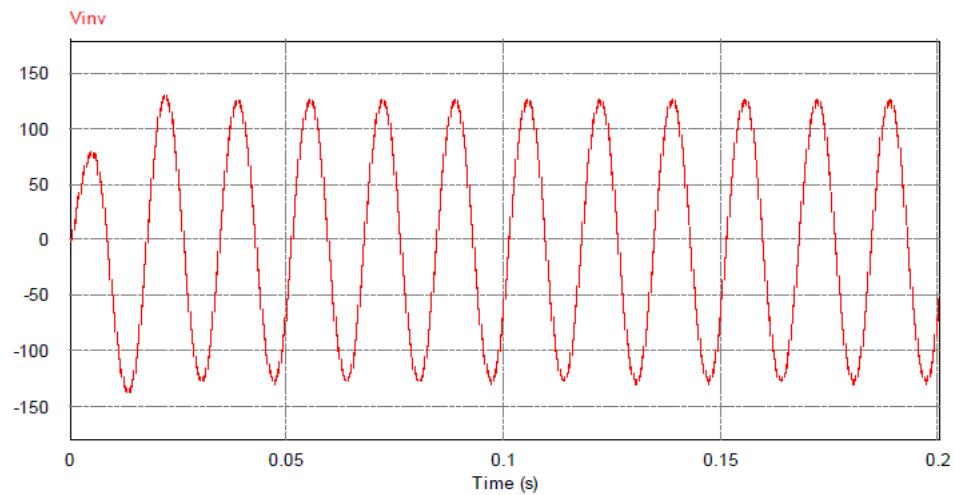


Fig 4. 37: The transient and steady-state behavior of the output voltages of the simulated circuit

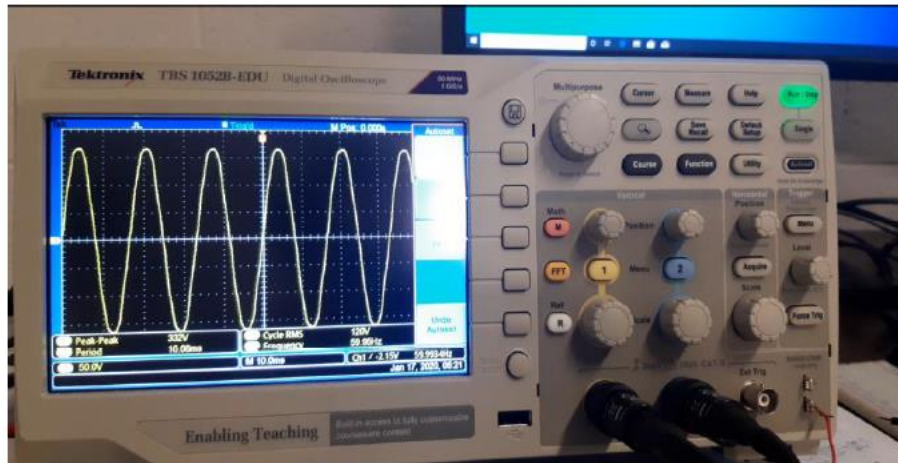


Fig 4. 38 Output of the implemented single-phase off-grid inverter on the oscilloscope.

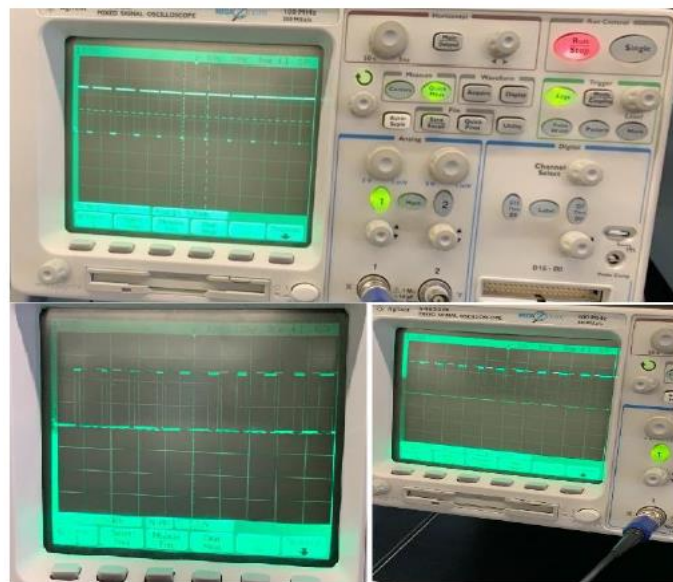


Fig 4. 39 Gate signals for the inverter switches on the oscilloscope.

Chapter 6. Conclusions

6.1 General Conclusion

This thesis proposed a novel structure of A Hybrid EV-Battery Charger Battery Charger for Optimum Grid Utilization, capable of supplying constant output power through different input sources with any Radiation variation. Chapter 1 of this thesis provided an introduction on all aspects of the work.

A literature review was done in chapter 2 on an overview of the photovoltaic system, of EV-PV-Grid charging system in the second part, and of EV-PV-GRID converter topology in the third part. While the last part was about detailing the thesis strategy and presenting the software used.

Chapter 3 has addressed to EV-PV charging system modeling and simulation under PSIM software. The different components were detailed as well as the simulation condition in the first section. In the second section, the simulation results were presented and discussed for different irradiation. In Chapter 4 an EV-PV-Grid system was realized under PSIM software and simulated for different cases. In the first case, the solar panel was operating on constant irradiation that was able to charge the battery without the grid's intervention. In the second case, the irradiation was variable, and the PV was not always able to supply the battery, so the grid covered the missing power.

The simulation and preliminary experimental results showed the proper functioning of the energy management employed in the realized design.

6.2 Research contributions

1. A new EV-charging station architecture: The new architecture combines the solar power with the grid and the EV; with flawless bidirectional energy flow.
2. A new supervisory control to determine the mode of operation.
3. This work integrated three controllers and their synchronization for the first time in a bidirectional energy flow mode. This has maintained that these components are off-the-shelf to achieve cost-effectiveness.
4. No additional components needed for: filtering, maintaining the synchronism, phase shift and reducing the harmonics.

6.3 Future Work

1. The topology was tested only with the PI controller. In the future, an advanced controlling method must be employed to get higher power efficiency, such as: LQR controlling method, Fuzzy LQR controller and nonlinear control.
2. The charger topology can be modified through two steps:
 - A. Step 1 can be designed to get better efficiency, control system and structure by reducing the number of components and implementing another optimized control algorithm like incremental conductance.
 - B. Step 2 can be designed to have more than two renewable energy sources (wind turbine and PV grid) and to be utilized for different applications at the same time depending on the renewable energy management methods.
3. Due to the COVID-19 situation, the hardware implementation stopped for six months. Further results for other operating conditions. It can be obtained in future work.

REFERENCES

- [1] R. Walker, L. E. Erickson, J. Cutsor, and H. Ford, "ELECTRIC VEHICLES_.pdf," pp. 11–22.
- [2] D. T. Hoang, P. Wang, D. Niyato, and E. Hossain, "Charging and discharging of plug-in electric vehicles (PEVs) in vehicle-to-grid (V2G) systems: A cyber insurance-based model," *IEEE Access*, vol. 5, pp. 732–754, 2017.
- [3] S. I. Vagropoulos, G. A. Balaskas, and A. G. Bakirtzis, "An investigation of plug-in electric vehicle charging impact on power systems scheduling and energy costs," *IEEE Trans. Power Syst.*, vol. 32, no. 3, pp. 1902–1912, 2017.
- [4] H. Chen, Z. Hu, H. Luo, J. Qin, R. Rajagopal, and H. Zhang, "Design and Planning of a Multiple-Charger Multiple-Port Charging System for PEV Charging Station," *IEEE Trans. Smart Grid*, vol. 10, no. 1, pp. 173–183, 2019.
- [5] I. Pavic, T. Capuder, and I. Kuzle, "A comprehensive approach for maximizing flexibility benefits of electric vehicles," *IEEE Syst. J.*, vol. 12, no. 3, pp. 2882–2893, 2018.
- [6] A. Dubey and S. Santoso, "Electric Vehicle Charging on Residential Distribution Systems: Impacts and Mitigations," *IEEE Access*, vol. 3, pp. 1871–1893, 2015.
- [7] S. Negarestani, M. Fotuhi-Firuzabad, M. Rastegar, and A. Rajabi-Ghahnavieh, "Optimal sizing of storage system in a fast charging station for plug-in hybrid electric vehicles," *IEEE Trans. Transp. Electrification*, vol. 2, no. 4, pp. 443–453, 2016.
- [8] Z. Wei, Y. Li, and L. Cai, "Electric vehicle charging scheme for a park-and-charge system considering battery degradation costs," *IEEE Trans. Intell. Veh.*, vol. 3, no. 3, pp. 361–373, 2018.
- [9] X. Wang, C. Yuen, N. U. Hassan, N. An, and W. Wu, "Electric Vehicle Charging Station Placement for Urban Public Bus Systems," *IEEE Trans. Intell. Transp. Syst.*, vol. 18, no. 1, pp. 128–139, 2017.
- [10] P. Shrivastava, M. S. Alam, and M. S. J. Asghar, "Design and techno-economic analysis of plug-in electric vehicle-integrated solar PV charging system for India," *IET Smart Grid*, vol. 2, no. 2, pp. 224–232, 2019.
- [11] S. M. Shariff, M. S. Alam, F. Ahmad, Y. Rafat, M. S. J. Asghar, and S. Khan, "System Design and Realization of a Solar-Powered Electric Vehicle Charging Station," *IEEE Syst. J.*, vol. 14, no. 2, pp. 2748–2758, 2020.
- [12] A. G. Cook, L. Billman, and R. Adcock, "Photovoltaic Fundamental," pp. 1–68, 1995.
- [13] K. Bisdom, Delft University of Technology Synthesis and evaluation of porous titanium scaffolds prepared with the space holder method for bone tissue engineering. 2016.
- [14] M. Kaltschmitt, W. Streicher, and A. Wiese, *Renewable energy: Technology, and*

environment economics. 2007.

- [15] A. F. Čotar, Andrej, "Photovoltaic Systems," Darko Jardas, dipl. ing. REA Kvarner Ltd, p. 1, 2012, [Online]. Available: http://www.irena-istra.hr/uploads/media/Photovoltaic_systems.pdf.
- [16] H. A. Wade, "Overview of Grid-Connected Solar PV," 2010.
- [17] S. C. Bhatia, "Solar photovoltaic systems," *Adv. Renew. Energy Syst.*, pp. 144–157, 2014.
- [18] N. A. Ahmed and M. Miyatake, "A stand-alone hybrid generation system combining solar photovoltaic and wind turbine with simple maximum power point tracking control," *Conf. Proc. - IPEMC 2006 CES/IEEE 5th Int. Power Electron. Motion Control Conf.*, vol. 1, pp. 242–248, 2007.
- [19] M. A. Eltawil and Z. Zhao, "MPPT techniques for photovoltaic applications," *Renew. Sustain. Energy Rev.*, vol. 25, pp. 793–813, 2013.
- [20] R. I. Putri, S. Wibowo, and M. Rifa'i, "Maximum power point tracking for photovoltaic using incremental conductance method," *Energy Procedia*, vol. 68, pp. 22–30, 2015.
- [21] C. M. Martinez, X. Hu, D. Cao, E. Velenis, B. Gao, and M. Wellers, "Energy Management in Plug-in Hybrid Electric Vehicles: Recent Progress and a Connected Vehicles Perspective," *IEEE Trans. Veh. Technol.*, vol. 66, no. 6, pp. 4534–4549, 2017.
- [22] J. Tang, B. Ye, Q. Lu, D. Wang, and J. Li, "Economic Analysis of Photovoltaic Electricity Supply for an Electric Vehicle Fleet in Shenzhen, China," *Int. J. Sustain. Transp.*, vol. 8, no. 3, pp. 202–224, 2014.
- [23] M. H. Tushar, "Comparative Study on Dc-Dc Converters," p. 10, 2001.
- [24] N. H. Baharudin, T. M. N. T. Mansur, F. A. Hamid, R. Ali, and M. I. Misrun, "Topologies of DC-DC converter in solar PV applications," *Indones. J. Electr. Eng. Comput. Sci.*, vol. 8, no. 2, pp. 368–374, 2017.
- [25] D. Cycle, K. Mathews, V. Three, A. A. Abu-aisheh, and M. G. Batarseh, "Buck Converter Learn more about Buck Converter Isolated converters have buck simplicity and performance DC – DC converters," 2015.
- [26] M. S. Ali, S. K. Kamarudin, M. S. Masdar, and A. Mohamed, "An overview of power electronics applications in fuel cell systems: DC and AC converters," *Sci. World J.*, vol. 2014, 2014.
- [27] I. Three, "Chapter 2 AC-DC Converter Operational Concepts," pp. 44–88.
- [28] J. Bauer, "Single-Phase Pulse Width Modulated Rectifier," *Acta Polytech.*, vol. 48, no. 3, pp. 84–87, 2008.
- [29] M. H. Rashid, *POWER ELECTRONICS HANDBOOK*. ACADEMIC PRESS.

- [30] M. Ünlü, S. Çamur, E. Beşer, and B. Arifoğlu, "A current-forced line-commutated inverter for single-phase grid-connected photovoltaic generation systems," *Adv. Electr. Comput. Eng.*, vol. 15, no. 2, pp. 85–92, 2015.
- [31] Y. Miao, P. Hynan, A. Von Jouanne, and A. Yokochi, "Current Li-Ion Battery Technologies in Electric Vehicles and Opportunities for Advancements," pp. 1–20, 2019.
- [32] M. Stunda and L. Ribickis, "Evaluation of Quasi-resonant DC Link Topologies for Soft Switching of Multiple DC-Inputs Three Phase Inverter," 2018 20th Eur. Conf. Power Electron. Appl. EPE 2018 ECCE Eur., pp. 1–10, 2018.
- [33] PSIM, "Solar Module Physical Model," no. October 2016, pp. 1–8, 2016, [Online]. Available: <https://powersimtech.com/drive/uploads/2016/12/Tutorial-Solar-Module-physical-model.pdf>.
- [34] IEEE Power and Energy Society, "IEEE Recommended Practice and Requirements for Harmonic Control in Electric Power Systems IEEE Power and Energy Society," ANSI/IEEE Std. 519, vol. 2014, pp. 5–9, 2014.
- [35] R. W. Erickson and Dragan Maksimovic, *Fundamentals of Power Electronics-Second Edition*. 2000.
- [36] I. M. Aq-ja, "PSIM User 's Manual ."
- [37] I. A. Sumalata and S. Nalini, "Simulation Analysis of MPPT Algorithm for a PV System Using a ZSI and Contrast with DC-DC Boosted VSI," no. June, pp. 318–323, 2017.
- [38] D. Committee, I. Power, and E. Society, "IEEE Recommended Practice and Requirements for Harmonic Control in Electric Power Systems IEEE Power and Energy Society Sponsored by the Transmission and Distribution Committee I," vol. 2014, 2014.
- [39] B. S. Dearborn, "" Charging Lithium-Ion Batteries : Not All Charging Systems Are Created Equal."
- [40] M. Elias, A. Arof, and K. Nor, "Design of high energy lithium-ion battery charger," *Australas. Univ. ...*, no. September, pp. 26–29, 2004.
- [41] M. P. Kazmierkowski and L. Malesani, "Current control techniques for three-phase voltage-source pwm converters: A survey," *IEEE Trans. Ind. Electron.*, vol. 45, no. 5, pp. 691–703, 1998.

Appendices

Appendices A: Characteristics of the solar panel in PSIM software

Solar Module (physical model) : SCP8

Parameters | Fixed-Point | Color

Solar module (physical model) Help

		Display
Name	SCP8	<input type="checkbox"/> ▾
Number of Cells Ns	36*8	<input type="checkbox"/> ▾
Standard Light Intensity S0	1000	<input type="checkbox"/> ▾
Ref. Temperature Tref	25	<input type="checkbox"/> ▾
Series Resistance Rs	0.008/15	<input type="checkbox"/> ▾
Shunt Resistance Rsh	15000	<input type="checkbox"/> ▾
Short Circuit Current Isc0	190	<input type="checkbox"/> ▾
Saturation Current Is0	32.4e-8	<input type="checkbox"/> ▾
Band Energy Eg	1.12	<input type="checkbox"/> ▾
Ideality Factor A	1.2	<input type="checkbox"/> ▾
Temperature Coefficient Ct	0.036	<input type="checkbox"/> ▾
Coefficient Ks	0	<input type="checkbox"/> ▾

Appendices B: Characteristics of Lithium-ion battery

Li-Ion Battery : S5

Parameters | Color

Li-Ion Battery Help

		Display
Name	S5	<input type="checkbox"/> ▾
No. of Cells in Series	7	<input type="checkbox"/> ▾
No. of Cells in Parallel	1	<input type="checkbox"/> ▾
Voltage Derating Factor	1	<input type="checkbox"/> ▾
Capacity Derating Factor	1	<input type="checkbox"/> ▾
Rated Voltage	51.2	<input type="checkbox"/> ▾
Discharge Cut-off Voltage	40	<input type="checkbox"/> ▾
Rated Capacity	45*0.0001	<input type="checkbox"/> ▾
Internal Resistance	0.06	<input type="checkbox"/> ▾
Discharge Current	45	<input type="checkbox"/> ▾
Capacity Factor	1.02	<input type="checkbox"/> ▾
Full Voltage	57.6	<input type="checkbox"/> ▾
Exponential Point Voltage	52	<input type="checkbox"/> ▾
Nominal Voltage	51.1	<input type="checkbox"/> ▾
Maximum Capacity	45*0.0001	<input type="checkbox"/> ▾
Exponential Point Capacity	34*0.0001	<input type="checkbox"/> ▾
Nominal Capacity	40*0.0001	<input type="checkbox"/> ▾
Initial State of Charge	0	<input type="checkbox"/> ▾

Appendices C: Characteristics of 3-phase resistor-inductor branch filter

RL3 : A

Parameters | Other Info | Color

3-phase resistor-inductor branch Help

		Display
Name	A	<input type="checkbox"/> ▾
Resistance	100m	<input checked="" type="checkbox"/> ▾
Inductance	1m	<input checked="" type="checkbox"/> ▾
Current Flag_A	1	<input type="checkbox"/> ▾
Current Flag_B	0	<input type="checkbox"/> ▾
Current Flag_C	0	<input type="checkbox"/> ▾